A CAUSAL ROLE OF ATM- AND NEMO-DEPENDENT NF-κB ACTIVATION IN DNA DAMAGE-INDUCED SENESCENCE AND AGING

by

Jing Zhao

M.D. Peking University, 2010

Submitted to the Graduate Faculty of

the School of Medicine in partial fulfillment

of the requirements for the degree of

Ph.D. in Immunology

University of Pittsburgh

2016

UNIVERSITY OF PITTSBURGH

SCHOOL OF MEDICINE

This dissertation was presented

by

Jing Zhao

It was defended on

December 4, 2015

and approved by

Laura J. Niedernhofer, M.D., Ph.D., Associate Professor

Lawrence P. Kane, Ph.D., Associate Professor

Jon D. Piganelli, Ph.D., Associate Professor

Abbe N. de Vallejo, Ph.D., Associate Professor

Dissertation Advisor: Paul D. Robbins, Ph.D., Professor

A CAUSAL ROLE OF ATM- AND NEMO-DEPENDENT NF-κB ACTIVATION IN DNA DAMAGE-INDUCED SENESCENCE AND AGING

Jing Zhao, Ph.D.

University of Pittsburgh, 2016

The accumulation of senescent cells induced by intracellular and extracellular stress contributes to multi-organ dysfunction and aging. Persistent DNA damage chronically accumulates with aging initiating a cellular stress response termed DNA damage response (DDR). Ataxia-telangiectasia mutated (ATM) kinase, a core component of DDR signaling, is involved in p53-p21 and p16-Rb senescent effector pathways, and is essential for senescence-associated secretory phenotype (SASP). In addition, ATM activates NEMO-dependent NF-κB pathway in response to genotoxic stress. However, the underlying molecular mechanisms through which DNA damage drives senescence and aging remain poorly characterized. Here we used the *Ercc1*$^{-/\Delta}$ mouse model of a human progeria that spontaneously develops osteoporosis, disc degeneration, glomerulonephropathy and neurodegeneration, to address the causal link between DDR-dependent NF-κB activation, cellular senescence and aging. In the first part, we demonstrated that DDR signaling, concomitant with NF-κB, was highly activated in *Ercc1*$^{-/\Delta}$ mice. A causal role of ATM in DNA damage-induced aging was demonstrated by genetic depletion of ATM in *Ercc1*$^{-/\Delta}$ mice, which extended health span as well as alleviated aging-related pathology. Moreover, ATM haploinsufficiency showed significantly reduced NF-κB activation and SASP. *In vitro* assays support an activation of ATM- and NEMO-dependent canonical NF-κB activation in response to oxidative stress. In the second part, we developed novel small molecule inhibitors to disrupt the interaction between IKKβ and NEMO/IKKγ. We demonstrated that novel NBD mimetics, in particular SR12343 and SR12460, efficiently inhibited both TNF-α and LPS-

induced NF-κB activation *in vitro*. Additionally, the chronic treatment with SR12343 and SR12460 reduced LPS-induced acute inflammation in lung and liver, and improved muscle pathology in *mdx* mice, a murine model of Duchenne muscular dystrophy. In the third part, we demonstrated that chronic treatment of *Ercc1*$^{-/\Delta}$ mice with SR12343 significantly improved aging symptoms and prolonged healthspan, as well as reduced the level of cellular senescence. Furthermore, suppression of IKK/NF-κB attenuated lipodystrophy and associated impaired glucose tolerance by reducing cellular senescence in fat. Taken together, these results suggest that NF-κB activation promotes cellular senescence and aging through an ATM-dependent pathway in *Ercc1*$^{-/\Delta}$ mice and the ATM-IKK-NF-κB pathway represents a key target for the development of novel approaches for healthy aging.

TABLE OF CONTENTS

LIST OF TABLES

LIST OF FIGURES

PREFACE

As five years of graduate school comes to an end, there are a lot of people that I would like to acknowledge. This work would not have been possible and I would not have gone this far without their support and help. First, I would like to thank my parents for their unconditional love, unwavering support and all the sacrifice they have made in my life. You have always been great role models, inspiring me to pursue my dream. It is your encouragement that helped me get through tough times and always be strong.

I would also like to thank my amazing husband, Brian. You have been the best present and surprise I got in graduate school. Thank you for your love and support during bad times and good times, which carried me to the end of this journey.

In addition, I would like to express my deepest gratitude to my mentor, Dr. Paul D. Robbins, for your great guidance throughout graduate school. Thank you for your patience and support these years and I learnt numerous lessons from you. I would also like to extend my greatest appreciation to Dr. Laura Niedernhofer, who has been our best collaborator as well as a female role model in science. I would like to thank my thesis committee members, Lawrence P. Kane, Jon D. Piganelli and Abbe N. Vallejo, for your insights and scientific suggestions to my research projects.

Finally, I would like to thank all my lab mates and friends: Rafael Flores, Xuesen Li, Heike Fuhrmann-Stroissnigg, Lana Corbo, Yuanyuan Ling, Chenjie Yang, Cori Booker,

Christina Bukata, Aditi Gurkar, Matthew Yousefzadeh, Sara Mcgowan, Diana Navarro, Tokio Sano and Amira Barghouthy. Thank you for the inspiring discussions and for all the fun we had in the lab. I especially thank Ralph for being my desk mate and for his tremendous help on preparing this thesis. To Matt who has provided great insights into my projects. To Chenjie Yang and Xuesen Li who taught me a lot of basic skills of research. To Heike and Lana for all the fun we had together.

Thank you all!

1.0 INTRODUCTION

1.1 NF-κB SIGNALING PATHWAY

1.1.1 Introduction to NF-κB

Nuclear factor-kappa B (NF-κB), a family of transcription factors, was first discovered in B lymphocytes by David Baltimore's lab in 1986 (1). Since then, extensive studies were performed revealing NF-κB as pleiotropic transcription factors. Our knowledge of stimuli that activate this pathway has expanded from lipopolysaccharide (LPS) and phorbol ester (e.g. PMA), to vast numbers of pro-inflammatory factors, oxidative stress and genotoxic stress (2-4). NF-κB was also unveiled to be not limited to B cells, but expressed in almost all cell types, regulating various essential biological events (5). To date, five NF-κB family members, three IKK complex subunits and nine IκB proteins were identified, along with their protein domains, crystal structures and biological function utilizing various techniques.

1.1.2 NF-κB family

In mammalian cells, the NF-κB family contains five members including RelA/p65, RelB, C-Rel, p50 (p105/NF-κB1) and p52 (p100/NF-κB2), all of which share a Rel homology domain (RHD) required for DNA binding and homo- or hetero-dimerization (6). RelA, RelB and C-Rel also

contain a transactivation domain (TAD) essential for transcriptional activity. The precursors of p50 and p52, p105 and p100 respectively, contain an ankyrin repeat-containing domain (ARD), which functions to sequester their NF-κB partners in the cytoplasm and prevent activation (3). To promote transcriptional activity, cleavage of precursors, p105 and p100, is required, mainly through co-translational processing and SCF-βTrCP-dependent or -independent degradation (7-9). RelA/p65:p50 is the most common heterodimeric combination involved in the canonical pathway, while RelB:p52 heterodimers predominate in non-canonical activation (Fig.1).

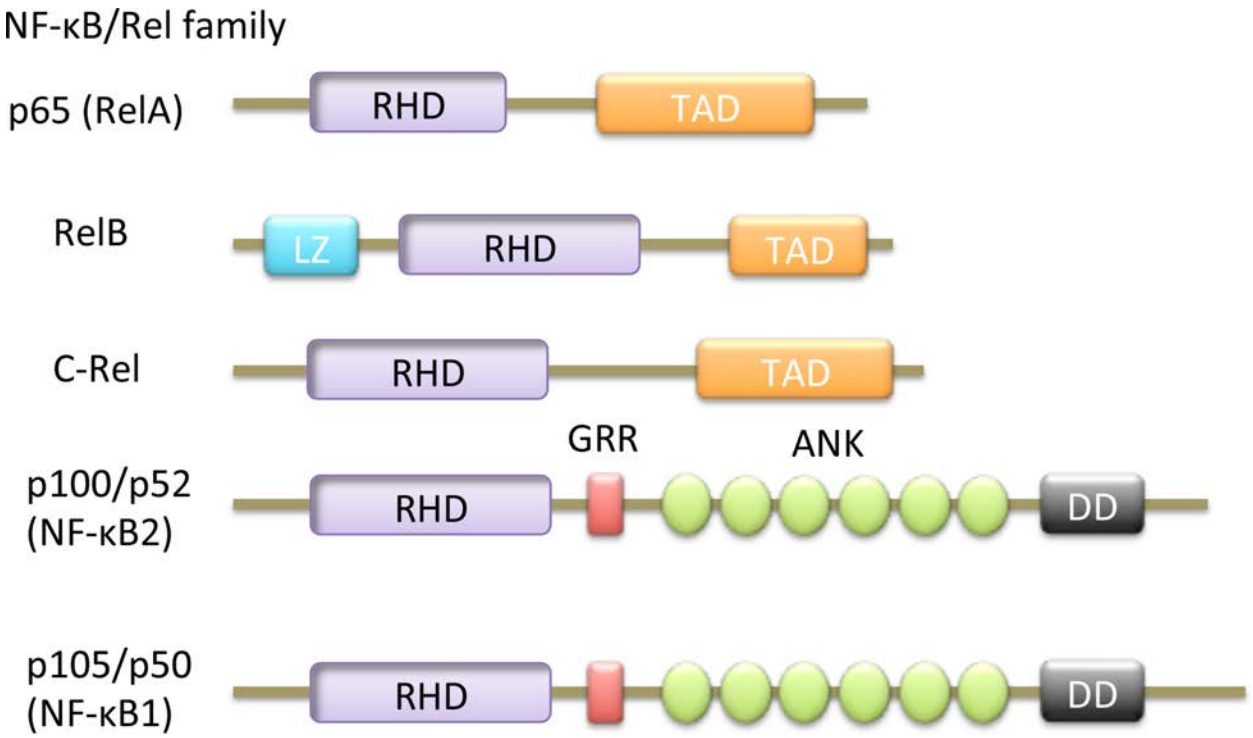

Figure 1: Members of NF-κB family. Structural motifs of NF-κB subunits are shown. RHD, Rel-homology domain; TAD, transactivation domain; LZ, leucine zipper; GRR, glycine-rich region; ANK, ankyrin-repeat motifs; DD, death domain. (Figure adapted from Perkins N.D. 2007 (3))

1.1.3 IκB kinase (IKK) complex

NF-κB is mainly activated by IκB kinase (IKK complex), which is the upstream of NF-κB. The IKK complex consists of three subunits, including two catalytic subunits, IKKα/IKK1 and IKKβ/IKK2, and one regulatory subunit IKKγ/NEMO. IKKα and IKKβ both contain a kinase domain, a leucine-zipper-like motif, a helix-loop-helix and a NEMO-binding domain (NBD), and are 52% identical to each other, with the kinase domain sharing 65% identity (10). NEMO contains two coiled-coil domains, one leucine-zipper domain and a zinc-finger (ZF) region (3). May et al. demonstrated that the NBD domain contained within the C-terminus of IKKβ/α is indispensible for the assembly and function of the IKK complex (11). In mammalian cells, the IKK complex exists as a high-molecular weight multiprotein complex with molecular size ranging between 600-900 kDa (10, 12) (Fig. 2).

Genetic evidence suggests that subunits of the IKK complexes are distinct, but related in function. IKKβ and NEMO knockout mice die on E12-E14 due to massive TNFα-induced apoptosis of hepatocytes, similar to RelA/p65 knockout mice (13, 14). This phenotype was later shown to be rescued in tumor necrosis factor receptor 1 (TNFR1) deficient mice, suggesting a protective role for IKKβ and NEMO in TNF-α-induced apoptosis (13, 15, 16). Of note, NEMO deficient cells exhibit a greater loss of NF-κB activity than IKKβ deficient cells (17-19). Surprisingly, IKKα knockout mice exhibit a distinct phenotype, including skeletal and epidermal abnormalities, rudimentary limbs and craniofacial deformities and die perinatally, suggesting that the function of IKKα is different from IKKβ (20-22).

In 2000, mutations in NEMO, were linked to two X-linked human genetic disorders, incontinential pigmenti (IP) and anhidrotic ectodermal dysplasia associated with immunodeficiency (EDA-ID) (23). NEMO is a 48 kDa protein encoded by the IKBKG gene

located on the X-chromosome (Xq28) (23). In humans, a loss-of-function mutation results in the production of a truncated protein, leading to antenatal lethality in males and incontinentia pigmenti (IP) in females (17, 23, 24). Female patients exhibit dermatosis, ophthalmologic, odontologic and nervous system abnormalities (23). Female mice heterozygous for NEMO exhibit keratinocyte hyper-proliferation, inflammatory infiltration and apoptosis in skin, similar to the manifestations in human IP patients (24, 25). EAD-ID results from hypomorphic mutation of NEMO. Affected males are able to survive, but suffer from EDA-ID due to reduced NF-κB activation, exhibiting fewer sweat glands, sparse scalp hair, absent teeth and recurrent infections (17, 23).

Although the exact mechanisms by which the IKK complex gets activated remain elusive, accumulating evidence suggests that ubiquitination of NEMO by E3 ubiquitin ligases plays a pivotal role in transducing signals and recruiting the IKK complex to upstream activators, such as transforming growth factor-β (TGFβ)-activated kinase-1 (TAK1) and MAPK-ERK kinase kinase (MEKK3) (3, 17, 26-28).

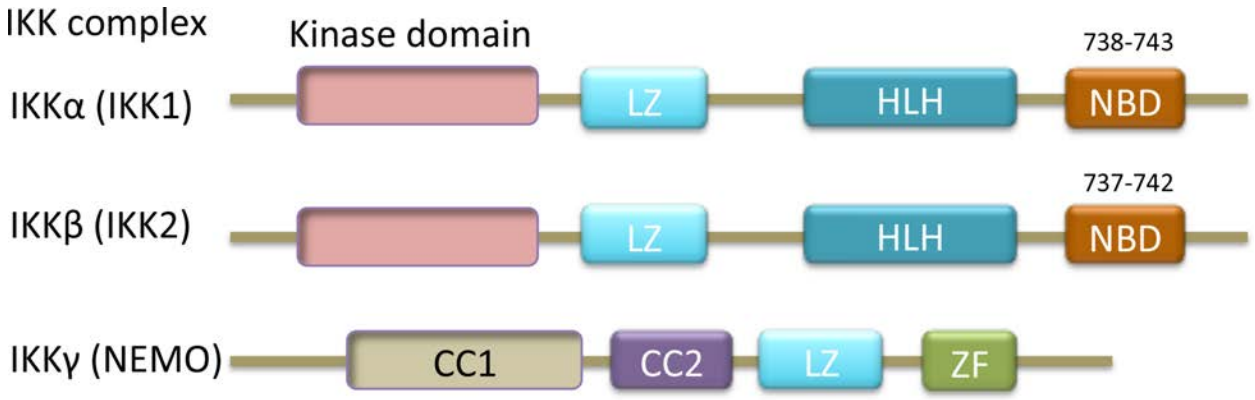

Figure 2: Structures of IKK subunits. Structural motifs of IKKα, IKKβ and NEMO are shown. CC, coiled-coil domain; LZ, leucine-zipper domain; HLH, helix-loop-helix domain; NBD, NEMO-binding domain; ZF, zinc-finger domain. (Figure adapted from Perkins N.D. 2007 (3))

1.1.4 IκB proteins

NF-κB activation and inactivation are tightly controlled by a group of inhibitory proteins IκBs, which function to mask the conserved nuclear localization sequence (NLS) on RelA/p65 and sequester NF-κB heterodimers in the cytoplasm in inactive condition (3). Nine IκB proteins have been identified and are divided into four groups: typical IκB proteins (IκBα, IκBβ, and IκBε), precursor proteins (p100 and p105), atypical IκB proteins (IκBζ, IκBNS and BCL-3) and an alternative transcript of IκBα (IκBγ) (3, 29, 30). All IκBs are characterized by the presence of five to seven ankyrin repeats that interact with the RHD in NF-κB subunits to mask the NLS and prevent nuclear translocation (29). Typical IκB proteins usually are present in the cytoplasm in an inactive state and go through degradation and resynthesis upon stimulation, whereas atypical IκB proteins are inducibly expressed in stimulated cells (29). In inactive conditions, IκBα masks the NLS of p65, exposing nuclear export sequence (NES) in IκBα, and sequesters NF-κB

heterodimers in the cytoplasm (30). The degradation of IκBα disrupts this balance and favors the nuclear localization of NF-κB. To establish a new balance, cytoplasmic localization of IκBα-NF-κB complexes is restored by NES in newly synthesized IκBα, which acts to shuttle NF-κB dimers back to the cytoplasm (30, 31) (Fig 3).

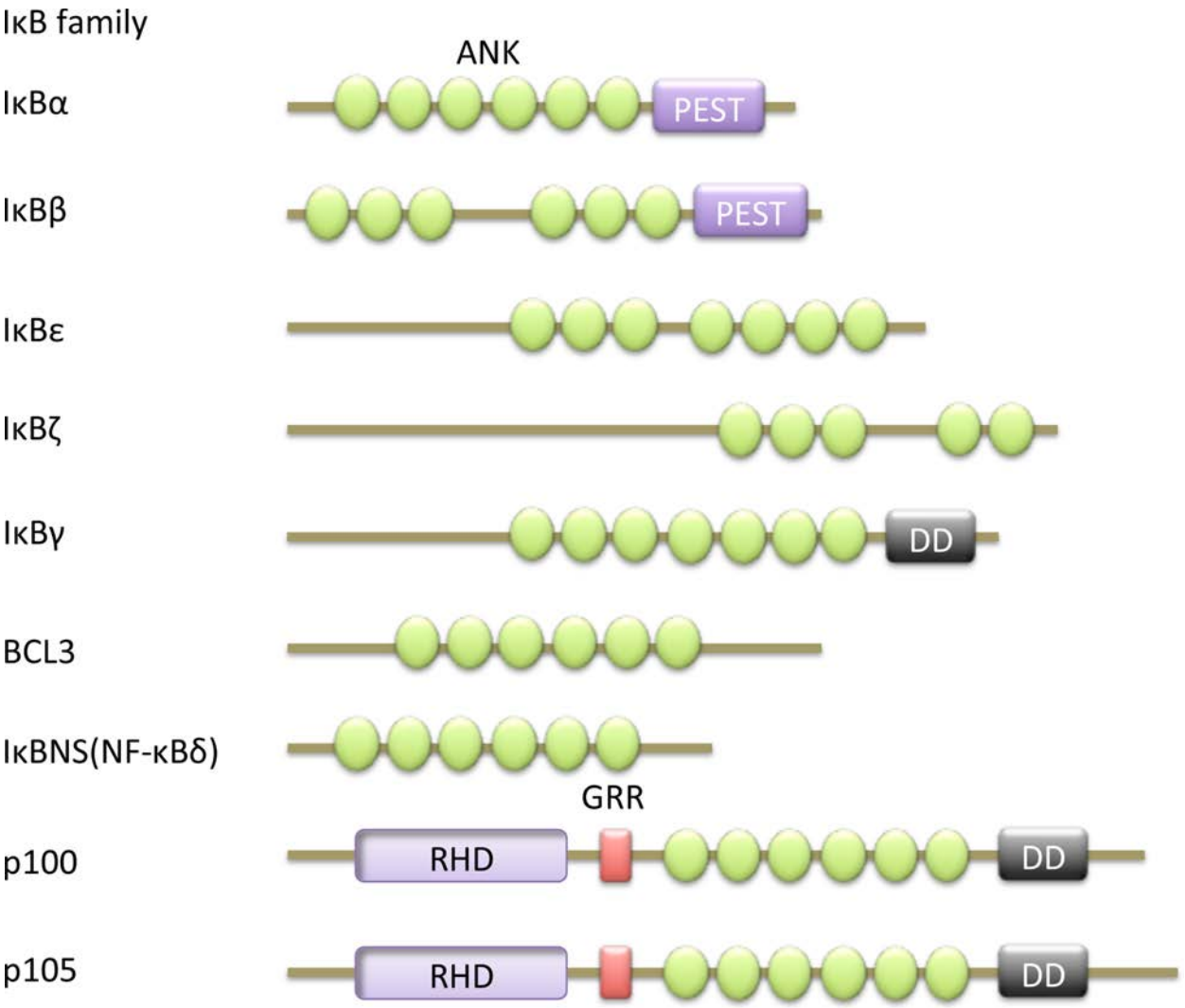

Figure 3: Members of IκB family. Structural motifs of nine IκB proteins are shown. ANK, ankyrin-repeat motifs; PEST, domain rich in proline (P), glutamate (E), serine (S) and threonine (T); RHD, Rel-homology domain; GRR, glycine-rich region; DD, death domain. (Figure adapted from Perkins N.D. 2007 (3))

1.1.5 Activation of NF-κB

A wide variety of stimuli can lead to the activation of NF-κB. Depending on the involvement of specific IKK components, NF-κB subunits and upstream activators, NF-κB activation is divided into the canonical pathway and non-canonical pathway (IKK complex-independent pathway). As a result, distinct subsets of target genes are transcriptionally regulated in respond to intracellular and extracellular stresses.

1.1.5.1 Canonical NF-κB pathway Extensive effort has been devoted to the characterization of the canonical NF-κB pathway during the past two decades. Various pro-inflammatory factors are able to activate NF-κB via binding to transmembrane receptors, such as tumor necrosis factor receptor (TNFR), interleukin-1 receptor (IL-1R), toll like receptor (TLR) and T-cell receptor (TCR) (32-34). All these distinct pathways eventually converge on activated IKK complexes, which induce phosphorylation of IκBα at Ser 32 and 36, followed by the polyubiquitination and degradation of IκBα in the 26S proteasome. The liberated NF-κB heterodimer then translocates into nuclei where it binds to the κB DNA response elements to regulate transcription (3) (Fig. 4).

In addition, genotoxic stress has been shown to induce the activation of NF-κB through a complex of ataxia telangiectasia mutated (ATM) and NEMO (3, 4). Nuclear DNA damage rapidly leads to the activation of the checkpoint kinase ATM, which in turn phosphorylates and facilitates the sumoylation and mono-ubiquitination of NEMO in the nucleus (3, 4). Mono-ubiquitination of NEMO then leads to the nuclear export of ATM-NEMO complex to the cytoplasm where it mediates the activation of the IKK complex and NF-κB (3) (Fig. 4).

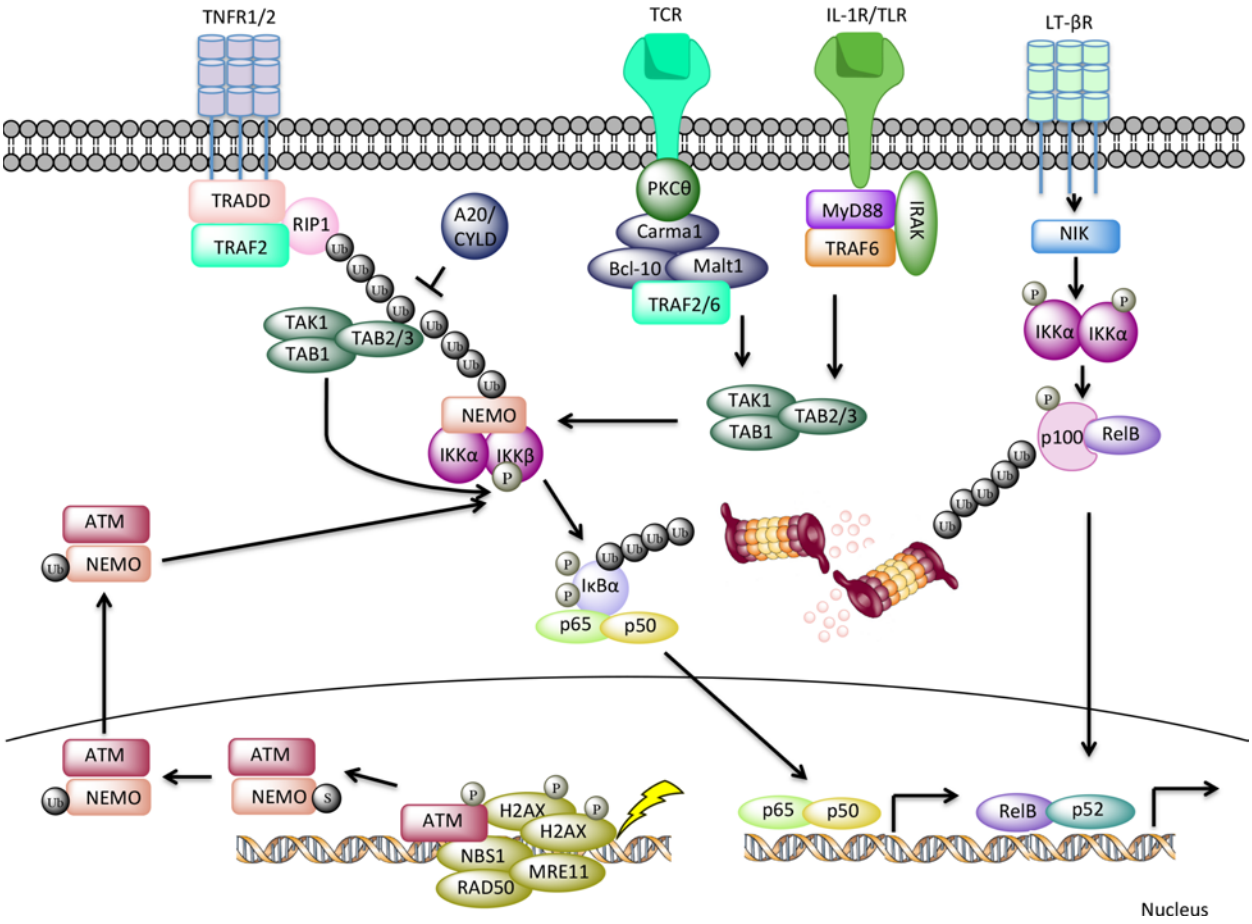

Figure 4: The activation of canonical and non-canonical NF-κB pathways. The canonical NF-κB pathway is induced by TNF-α, IL-1, LPS, TCR ligands and genotoxic stress. TNF-α-induced NF-κB activation requires adaptor proteins, TRADD and TRAFs (also act as E3 ubiquitin ligases), as well as RIP1, the polyubiquitination of which is required for the recruitment of IKK complexes to TAK1 kinase. TAK1 kinase is responsible for the phosphorylation of IKKβ, which in turn leads to the phosphorylation and degradation of IκBα. The liberated p65/p50 heterodimers then translocate into the nucleus regulating target gene expression. IL-1 and LPS activate the canonical NF-κB pathway through IL-1R and TLR-4 respectively, resulting in the recruitment of MyD88, IRAK and TRAF6, which are essential for the activation of TAK1. Activated TAK1 then phosphorylates the IKK complex, leading to NF-κB activation. TCR

ligation induces an activation of the PKCθ kinase, which further activates the Carma1-Bcl-10-Malt1 complex, leading to the activation of TAK1 via TRAF2/6. In response to DNA damage, activated ATM phosphorylates nuclear NEMO at Ser 85. Phosphorylated NEMO then undergoes sumoylation and monoubiquitination. Mono-ubiquitinated NEMO in turn translocates to the cytoplasm with ATM, activating the IKK complex and NF-κB. Notably, A20 and CYLD, both of which are de-ubiquitinating enzymes (DUBs), negatively regulate NF-κB activation by disassembling the K63-linked ubiquitin chains on NEMO. (Figures were adapted from (3, 29, 32-35))

1.1.5.2 Non-canonical NF-κB pathway The non-canonical NF-κB pathway is distinct given it is IKK complex-independent. Genetic evidence indicates an essential role of this pathway in lymphoid organogenesis, B-cell survival, dendritic cell activation, and osteoclastogenesis (36, 37). The non-canonical pathway can be initiated by lymphotoxin beta (LTβ), B-cell activating factor (BAFF), CD40 and RANKL, which activate NF-κB-inducing kinase (NIK). NIK in turn activates the homodimeric IKKα complex, which results in the phosphorylation and proteasome-dependent processing of p100 to p52. This is followed by the release of p52-RelB complex into the nucleus, which binds to specific κB elements (3).

Another IKK complex-independent NF-κB pathway is mediated by tyrosine kinases and casein kinase-II (CK2) in response to oxidative stress (hypoxia and hydrogen peroxide), and genotoxic stress (UV) and oncogene *HER2*, respectively. These kinases directly phosphorylate IκBα, releasing p50-RelA dimers into nucleus where NF-κB exerts its transcriptional activity (3).

1.1.6 NEMO-binding domain (NBD) peptide

NEMO was identified in 1998 by Karin and Israel, who reported a direct and stable association of NEMO to IKKβ, but not to IKKα (38, 39). Further studies demonstrated an essential role of NEMO in the activation of the canonical NF-κB pathway induced by TNF-α, LPS and IL-1, by acting as a regulatory adaptor protein (20, 40). May et al. hypothesized that prevention of the association of NEMO and IKKs may inhibit NF-κB activation. They further demonstrated that this protein-protein interaction requires the C-terminus of IKKβ and the N-terminus of NEMO (41). They identified the α_2-region in the C-terminus of IKKβ (IKKβ 735-745) as the NEMO-binding domain (NBD), which contains six core amino acids (LDWSWL) that are conserved between IKKα and IKKβ (41). Site directed mutagenesis revealed an essential role of D738, W739 and W741 in mediating the binding of NEMO and IKKα/β, which was further confirmed by crystallography studies (11, 42). May and colleagues thus developed a cell-permeable peptide (FTALDWSWLQT), based on the eleven amino acids derived from the NEMO-binding domain in the C-terminus of IKKβ, termed NBD peptide (41). The peptide selectively inhibits the kinase activity of the IKK complex by disrupting the association between IKKβ and NEMO without affecting basal NF-κB activity (41). NBD peptide also blocks the association of NEMO and IKKα, although with a significantly lower affinity (18, 43-45).

Although kinase inhibitors targeting IKKβ strongly inhibit NF-κB activity *in vitro*, effects *in vivo* are less than optimal due to reasons unknown. In contrast, NBD peptide potently inhibits NF-κB *in vivo* and has therapeutic effects in various murine disease models. In 2004, Ghosh et al. showed that NBD peptide not only attenuated RANKL-mediated osteoclastogenesis but also reduced the severity of collagen-induced arthritis *in vivo*, suggesting that NBD peptide could be a clinical tool for the management of chronic joint swelling or destruction of bone and

cartilage (46). Plevy et al. in 2007 reported that the NBD peptide blocked LPS-mediated NF-κB activation in the mouse intestine and, more importantly, ameliorated established chronic colitis in *IL-10*$^{-/-}$ mice, by reducing the production of inflammatory cytokines by mucosal macrophages (47). In addition, Guttridge and colleagues showed a significant therapeutic effect of NBD peptide in *mdx* mice, a murine model of Duchenne muscular dystrophy (DMD). Macrophage-mediated inflammation and necrosis were reduced and muscle regeneration were improved by chronic treatment of NBD peptide (48). The therapeutic effects of the NBD peptide were also established in murine models of Parkinson's disease, Type 1 diabetes, as well as other diseases mediated by NF-κB activation (49, 50). Moreover, a phase 1 clinical trial testing the safety and efficacy of NBD peptide was conducted in a canine model of activated B-cell (ABC) diffuse large B-cell lymphoma (DLBCL), where increased apoptosis and a reduction in tumor burden were demonstrated post-treatment, indicating the possible utility of NBD peptide in clinical treatment (51). Additionally, another trial in the golder retriever muscular dystrophy (GRMD) model of DMD showed improved pelvic limb muscle force as well as attenuated histopathology (52).

Thus, the NBD peptide is of potentially great utility for clinical interventions for the following reasons: 1) strong inhibitory and therapeutic effects in various animal models across different species; 2) selective inhibition of IKK/NF-κB activation in response to stress without influencing its basal activity, which should minimize potential side effects, such as infection or immunosuppression; 3) inhibition of the IKK complex activity by disrupting the association between NEMO and IKKα/β, which should limit off-target effects, in particular limiting crossreaction with other kinases as kinase inhibitors do; and 4) ability to block established chronic NF-κB activation by disrupting the association of preformed IKK complexes. However,

one obstacle to the application of NBD peptide as a therapeutic is that the NBD peptide is technically difficult to synthesize, making it expensive to conduct clinical trials in human. Thus, developing small molecules mimicking the NBD peptide would be advantageous, which will be discussed in the following chapters.

1.2 ATAXIA TELANGIECTASIA MUTATED (ATM) IN DNA DAMAGE RESPONSE

1.2.1 Ataxia Telangiectasia mutated (ATM)

Ataxia telangiectasia mutated (ATM) is a Serine/Threonine protein kinase that belongs to the phosphatidylinositol 3 kinase-like kinase (PIKK) family (53). Other PIKK Ser/Thr protein kinases include ataxia-telangiectasia and RAD3-related (ATR) and DNA-dependent protein kinase catalytic subunit (DNA-PKcs), both of which are also involved in the DNA damage response (53). ATM kinase is primarily activated by DNA double-strand breaks (DSBs) and functions to regulate cell-cycle checkpoints and DNA repair machinery to maintain genome stability. Patients deficient in ATM have increased radiosensitivity, chromosome aberrations and neurodegeneration (54). Inactive ATM resides in the nucleus as homodimers or higher-order multimers, which dissociate and obtain kinase activity upon autophosphorylation at Ser1981 (55, 56). ATR is activated by single-stranded DNA damage that occurs during DNA replication and is recruited to preserve the stability of replication forks (57). DNA-PKcs, the catalytic subunit of DNA-PK, is indispensible for the non-homologous end-joining (NHEJ) repair of DSBs, where sequence homology is not required (58).

1.2.2 DNA damage response (DDR)

DNA damage can be triggered by endogenous insults, including replication error and fork collapse, and exogenous genotoxins such as ultraviolet (UV), ionizing radiation and chemotherapeutic drugs (59). In response to double-strand breaks, MRE11-RAD50-NBS1 (MRN) complex is recruited to the DNA lesion site to initiate the DNA damage response, which in turn attracts and activates ATM kinase (53, 56, 60). Activated ATM phosphorylates a histone H2A variant (γH2AX), which is a key step to amplify DDR signaling (53, 56, 60) (Fig. 4). γH2AX helps attract multiple DNA repair proteins, leading to the formation of detectable DNA damage foci. Another pivotal consequence of ATM activation is the engagement of cell cycle checkpoint kinase 2 (CHK2), which functions away from the lesion site (53, 56, 60). CHK2 activation results in the activation of a tumor suppressor p53, which further leads to the transcription of a cyclin-dependent kinase inhibitor p21, thus initiating cell-cycle arrest (53, 56, 60). Collectively, these processes are termed the DNA damage response (DDR). Cell-fate decisions are made depending on the extent and types of DNA damage. Mild DNA damage results in transient cell-cycle arrest and DNA damage foci will be eventually disassembled. In contrast, severe DNA damage may enhance DDR signaling, forming persistent, enlarged nuclear foci including γH2AX and 53BP1, which leads to permanent cell cycle arrest and cellular senescence. An additional outcome of extensive DNA damage is apoptosis (53, 56, 60).

Similar to DSBs, single-strand DNA breaks, including those that occur at stalled replication forks, attract a different serine/threonine protein kinase, ATR to the lesion site. γH2AX is also a core component of this ATR-mediated DDR signaling. However, ATR recruits a different subset of DDR mediators, including replication protein A (RPA), heterotrimeric 9-1-1 complex (RAD9-RAD1-HUS1) and topoisomerase-II-binding protein1 (TOPBP1) (57, 61-63).

To halt the cell cycle progression, checkpoint kinase 1 (CHK1) and downstream effector cell-division cycle 25 (CDC25) phosphatases are modified, leading to a rapid cell-cycle arrest (57, 61-63).

1.2.3 Ataxia-telangiectasia (A-T): a rare autosomal recessive disorder

Ataxia-telangiectasia (A-T) was first reported in 1926 by Syllaba and Henner and was described as a distinct syndrome by Boder and Sedgewick in 1957 (64, 65). A-T is a very rare autosomal recessive disease, caused predominantly by frameshift or nonsense mutations (80-90%) in *ATM*, which lead to a truncated form of ATM (53, 66, 67). A-T patients exhibit neurodegeneration, immunodeficiency, growth retardation, radiation sensitivity and cancer predisposition (68). A-T carriers, comprising around 1% of the general population, do not appear to have neurodegeneration or a cancer predisposition (69, 70). Mouse models of A-T, where no ATM protein is expressed, have been reported to recapitulate most human A-T symptoms, with the exception of progressive neurodegeneration (71). Interestingly, mice bearing a loss-of-function mutation of ATM (D2880A/N2885K, D2899A or Q2740P) exhibit disrupted kinase activity and are embryonic lethal, likely due to an enhanced inhibition on homologous recombination (72, 73). Evidence also suggests that ATM inhibitors targeting the kinase domain can cause a more severe phenotype in cell culture than in ATM-null cells (74).

1.2.4 Cytoplasmic function of ATM

Increasing evidence indicates that ATM, in addition to its nuclear functions regulating DNA repair machinery, also plays an important role in the cytoplasm, revealing the long-time

unknown mechanisms underlying the metabolic syndrome and neurological pathology in A-T patients (75). Cytoplasmic functions of ATM have been identified in response to hypoxia, insulin and reactive oxygen species (ROS), unveiling its versatile roles as a protein kinase (76, 77). Emerging evidence has linked ATM to redox balance by suggesting that oxidative stress, in the absence of DSBs, could activate dimeric ATM in a manner independent of Mre11-Rad50-Nbs1 (MRN) complex and ATM autophosphorylation (78). Recent studies further revealed that ATM negatively regulates the mTOR complex 1 (mTORC1), and thus promotes autophagy and limits cell growth in response to ROS (75, 79). Collectively, oxidative stress activates cytoplasmic ATM, which in turn induces the phosphorylation and activation of AMPK (AMP-activated protein kinase) at Thr172 through LKB1 (liver kinase B1). Activated AMPK subsequently activates the Tuberous sclerosis complex 2 (TSC2), which negatively regulates mTORC1 (53, 75, 79). Further studies demonstrated that ATM-null cells have increased mitochondrial number due to impaired destruction (mitophagy), rather than increased mitochondrial biogenesis, linking ATM protein to mitophagy (53, 80). Additionally, a fraction of ATM protein has also been found in centrosomes, peroxisomes and vesicles (81-83).

1.3 CELLULAR SENESCENCE AND AGING

Aging refers to a state of gradual decline in physical activity and organ function over time. With progress in modern medicine over the past few decades, more people are living longer and aging is rapidly becoming an emerging problem that brings new challenges to the healthcare system as well as economy. The population aged 65 or older is projected to outnumber children under age 5 in 2020 and reach 1.5 billion worldwide in 2050 (84) (Fig. 5). Thus a major shift of leading

diseases, from communicable to noncommunicable diseases, is expected, such as heart disease, hypertension, diabetes, cancer, lung disease and mobility impairment. The incidence of these chronic diseases increases exponentially with age, thus are termed aging-related diseases. As aging-associated diseases tend to occur in combination, understanding the underlying mechanisms of aging would be of great help to better prevent and manage frailty and comorbidities in the elderly.

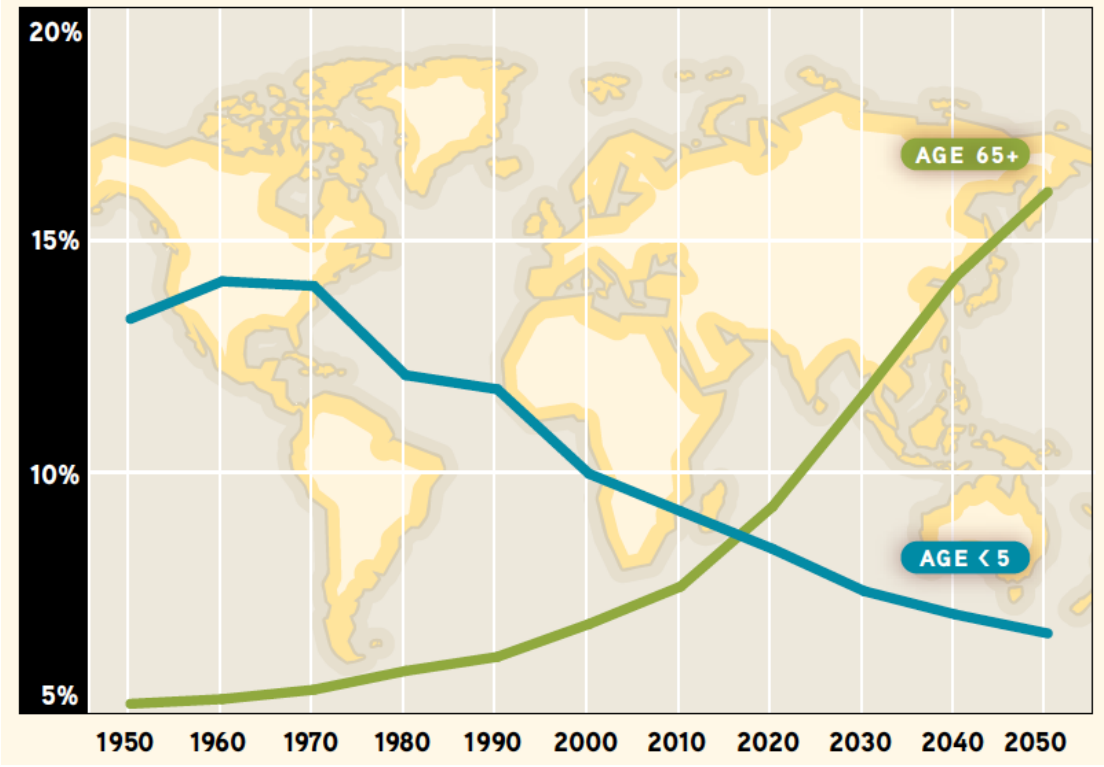

Figure 5: Global population older than 65 and under age 5. Data were collected by United Nations Department of Economic and Social Affairs, Population Division. (Reprinted from "why population aging matters: A global perspective" (84).)

Senescent cells are metabolically active yet irreversiblely held in G1/G2 phase in response to intrinsic and extrinsic cellular stresses. Cellular senescence, in particular replicative senescence, was first described more than 50 years ago by Hayflick and Moorhead, who

demonstrated that human cells in culture could undergo a finite number of cell divisions (85). Senescent cells are known to accumulate in mammals as they age (86) and are found to be associated with many age-related degenerative diseases, such as atherosclerosis, osteoarthritis, sarcopenia, gastrointestinal ulcers, and Alzheimer's disease (87). Furthermore, cellular senescence facilitates tissue remodeling by promoting embryogenesis and wound healing (88). A recent study in transgenic mice clearly demonstrated that removal of even a fraction of senescent cells attenuates many age-related symptoms in mice with accelerated aging (89). Moreover, a new class of drugs that induce apoptosis of senescent cells, termed senolytics, is able to enhance cardiovascular function in chronologically aged mice, restore treadmill endurance in radiation-exposed mice, and decrease frailty, neurologic dysfunction and bone loss in progeroid mice (90). Thus cellular senescence is a physiologically important process in aging, a process that needs to be further studied in both animal models and in patients.

1.3.1 Senescence-inducing stimuli

1.3.1.1 Telomere attrition Telomere refers to the repetitive DNA sequences located at the termini of linear DNA in eukaryotic cells to protect end to end fusion of chromosomes (91). Telomerase functions to elongate the telomeric repeats on chromosomes. Telomere shortening occurs with each cell division, thus leading to a finite doubling capacity (replicative senescence) especially in human somatic cells, where telomerase activity is undetectable (91, 92). Human cells overexpressing telomerase exhibit reduced senescence as well as extended proliferative capacity (93). Telomere deficient mice exhibit premature aging similar to other progeria mouse models and the reintroduction of telomerase is able to attenuate tissue atrophy and stem cell depletion (94).

The inability of the DNA replication machinery to copy the lagging ends of chromosomes directly leads to telomere shortening, which can be recognized as double-strand breaks by DNA repair proteins (95, 96). As a result, DDR proteins, including the tumor suppressor p53-binding protein 1 (53BP1), γH2AX, ATM, Mre11, Rad50, NBS1 and checkpoint kinase 2 (CHK2), are recruited to the telomeric DNA, forming telomere dysfunction-induced foci (TIFs), which triggers a cell-cycle arrest (95, 97). Notably, TIF-induced senescence can be attenuated by caffeine and wortmannin, which are ATM inhibitors, as well as in A-T cells where ATM is depleted, suggesting a requirement for persistent DDR signaling to maintain replicative senescence (95, 98).

Telomere shortening-induced senescence is of great importance in human aging, as human somatic cells don’t express telomerase. Therefore, understanding telomere shortening-

mediated senescence and aging will provide great insights into human aging development and progression.

1.3.1.2 DNA damage-induced senescence When DNA damage occurs, repairable DNA lesions will lead to a transient DDR response, while irreparable DNA damage will result in apoptosis or a sustained DDR signaling that eventually leads to cellular senescence. Persistent DNA damage response chronically activates p53 and p21, inducing and maintaining irreversible cell-cycle arrest. Additionally, persistent DNA damage signaling has been demonstrated to be indispensable for the senescence-associated secretory phenotype (99). ATM knockdown *in vitro* using shRNA/siRNA reduces cellular senescence and the production of IL-6, suggesting a central role of DDR signaling in senescence and SASP (99).

1.3.1.3 Oncogene-induced senescence (OIS) Oncogenic Ras provokes permanent G1 cell cycle arrest in primary cells, which is termed oncogene-induced senescence (100). Ras acts as a sustained mitogenic stimulus in cells, leading to aberrant DNA replication, which in turn results in the accumulation of DNA damage and persistent DDR signaling (101). The arrested cell growth in Ras-induced replicative senescence is achieved by engaging cell-cycle regulators p53/p21 and p16 (100). Notably, oncogene activation of E2F3 and c-Myc triggers cell growth arrest via a DDR-independent pathway (102, 103). BRAF(V600E), a dominant mutation in melanoma, induces senescence by upregulating mitochondrial pyruvate dehydrogenase (PDH), highlighting a role of bioenergetics in driving senescence (87). Of note, one common mechanism mediating OIS is the engagement of p53-p21 and/or $p16^{INK4a}$-Rb to initiate and maintain cell cycle arrest. Similarly, inactivation of tumor suppressors, such as PTEN, Rb and NF1, also

induces senescence (104, 105). Oncogene-induced senescence prevents precancerous cells from unlimited proliferation, thereby has an important impact on combating tumorigenesis. Studying the underlying mechanisms of OIS will provide insights into the development of pro-senescence therapy for cancer treatment (104).

1.3.1.4 Reactive oxygen species (ROS) The free radical theory of aging was first raised in 1954 by Harman, who postulated that free radical reactions that are largely of mitochondrial origin, drive aging (106). Moreover, it was predicted that antioxidants, caloric restriction and the reduction of temperature would elongate life expectancy, all of which proved correct 60 years later (106). Parrinello et al. demonstrated that primary mouse embryonic fibroblasts with long telomeres undergo cellular senescence in ambient oxygen (20%), possibly due to the increased oxidative damage. Senescence could be delayed by physiological oxygen tension (3%) and was later suggested to be associated with mitochondrial production of ROS (107, 108). Furthermore, sublethal doses of hydrogen peroxide, endogenous superoxides and hydroxyl radicals are implicated in p53/p21-dependent G1 cell cycle arrest (109, 110). Notably, scavengers of free radicals, such as N-acetylcysteine (NAC), rescue p53 and/or p21 mediated growth arrest (111). Moreover, oncogene activation, such as Ras, increases mitochondrial mass, ROS and oxidative DNA damage in human fibroblasts, suggeting a central role of mitochondrial dysfunction in cellular senescence (108).

Multiple causes of senescence, such as telomere shortening, oncogene activation and oxidative stress, induce DNA damage and persistent DDR signaling. Thus understanding the role of DDR signaling will greatly advance our understanding of cellular senescence.

1.3.2 Biomarkers of senescence

Senescent cells exhibit cell markers that make them distinguishable from other cell populations, especially quiescent cells, which are arrested in G0 (59). Morphological changes, including a flattened and enlarged appearance, increased vacuolization and stress granules are observed in senescent cells in *vitro*.

1.3.2.1 Senescence-associated β-galactosidase (SA-βgal) Senescence-associated β-galactosidase (SA-βgal) staining is one of the best-characterized and most convenient single-cell based methods to measure senescence *in vitro* and *in vivo*. SA-βgal staining measures the activity of lysosomal-origin β-galactosidase at a suboptimal pH of 6.0 instead of acidic pH of 4.0 (112). It was demonstrated that senescent cells exhibit increased lysosomal biogenesis which results in abundant lysosomal enzyme activity as well as increased lysosomal mass (113). Replicative senescence, genotoxic or oxidative stress-mediated senescence *in vitro*, as well as aged tissues such as skin, liver, kidney and pancreas, all stain blue by SA-βgal assays (114, 115). Notably, increased senescence-associated β-galactosidase activity is a consequence of senescence rather than its cause, as cells deficient in lysosomal β-gal still undergo senescence (116). Moreover, although SA-βgal is a biomarker of senescence, it hasn't been connected with any specific pathways identified yet in senescent cells and is not required to reach the cellular senescent state (115).

1.3.2.2 Tumor suppressors: $p16^{Ink4a}$ and $p21^{CIP1}$ $p16^{Ink4a}$, a G1 cyclin-dependent kinase (CDK) inhibitor targeting CDK4 and CDK6, negatively regulates the phosphorylation of

retinoblastoma protein (Rb), thus blocking cell-cycle progression from G1 to S phase. CDKN2A, also named the INK4a-ARF locus, encodes $p16^{Ink4a}$ as well as $p14^{ARF}$ (human) and $p19^{ARF}$ (mouse) proteins. $p14^{ARF}$ and $p19^{ARF}$, which are translated in an alternative reading frame (ARF), are distinct tumor suppressors from $p16^{INK4a}$ (117-119). Evidence suggests that $p14^{ARF}$ stabilizes p53 by promoting the degradation of MDM2 (117-119). Deletion of the ARF-INK4a locus disrupts both tumor suppressor pathways: p16-Rb and p53-p19/p14.

$p16^{Ink4a}$ is upregulated in senescent cells and aged tissues, but absent in healthy and young tissues. Inducible depletion of $p16^{Ink4a}$ positive cells reduces cellular senescence in tissues and extends the healthspan of $BubR1^{H/H}$ mice (120-122). In addition, increased expression of $p19^{ARF}$ has been linked to aging in rodent and human tissues, mirroring $p16^{Ink4a}$ (121). However, the exact role of $p19^{ARF}$ in senescence remains controversial.

$p21^{Cip1}$, encoded by CDKN1A (CIP1/WAF1), is another cyclin-dependent kinase inhibitor regulating cell cycle progression through G1-, G2- and S-phase (123). In response to DNA damage, p21 is upregulated transcriptionally by the tumor suppressor p53, which is a major effector in cellular senescence (124). $p21^{Cip1}$ accumulates in senescent cells, which correlates with G1 phase cell-cycle arrest (125). Deletion of $p21^{Cip1}$ improves the function of progenitor cells and hematopoietic stem cells in telomerase knockout mice, suggesting that telomere shortening-induced senescence is mediated by p53/p21 (126). Moreover, oncogenic activation of Ras can transcriptionally regulate $p21^{Cip1}$ in a p53-independent way (127).

Cellular stress that induces the DNA damage response, primarily engages the p53/p21 pathway via ATM/ATR kinase to halt cell-cycle progression, whereas certain oncogenic activation is associated with p16/Rb signaling. However, the two effector pathways likely converge in late phase of senescence through an undefined mechanism.

1.3.2.3 Loss of Lamin B1 In senescent cells, the overall nuclear morphology, including nuclear lamina, nucleoli, nuclear matrix and nuclear bodies, are altered and multi-nucleation can often be seen as a consequence of defects in nuclear envelope breakdown (128). Nuclear lamins contribute to the size, shape and stability of the nucleus and are divided into type A (A and C) or type B (B1 and B2). Several reports suggest that lamin B1 is a biomarker for senescent cells with loss of lamin B1 observed in senescent cells, but not in quiescent cells. Additionally, inhibition of lamin B1 drives proliferating cells to a senescent state. Downregulation of lamin B1 also leads to major chromatin remodeling, leading to senescence and the production of SASP.

1.3.2.4 Senescence-associated secretory phenotype (SASP) Senescent cells undergo widespread changes in protein expression and secretion, including the acquisition of the senescence-associated secretory phenotype (SASP) (87). Among more than 40 identified SASP factors are proteins involved in cellular signaling, such as growth factors (e.g. transforming growth factor-β (TGF-β)), inflammatory cytokines such as interleukins (IL-6) and chemokines (IL-8), and proteases (129). Senescence-activated transcription factors (such as NF-κB or C/EBPβ), DDR signaling molecules and certain microRNAs must be expressed to promote SASP (130, 131). SASP not only is a marker of senescent cells, but also can induce senescence through a non-cell autonomous mechanism (129, 132).

1.3.3 NF-κB activation in cellular senescence and aging

NF-κB pathway is a conserved signaling pathway that responds to multiple cellular stresses, including pro-inflammatory stress, oxidative stress and genotoxic stress, which are all implicated as factors in aging. NF-κB activity is elevated in numerous aged tissues, such as skin, cerebellum

and kidney (133-135). A genome-wide motif study by Adler et al. identified NF-κB as the most strongly activated transcription factor in natural aging in humans and mice, as well as premature aging in mice(136). Moreover, they reported that inducible genetic depletion of NF-κB rejuvenated aged skin and reverted the transcriptome of skin to that of younger mice (136).

A causal role of NF-κB in cellular senescence and aging was established by pharmacologic and genetic reduction of NF-κB in two progeria mouse models. Our group demonstrated an elevated NF-κB level in multiple tissues in *Ercc1*$^{-/\Delta}$ mice, a mouse model of XPF progeroid syndrome, including kidney, muscle, pancreas and liver (137). Reducing NF-κB activity genetically (*p65*$^{+/-}$) or pharmacologically (NBD peptide) significantly ameliorated the aging symptoms as well as aging-associated pathology (137). Increased NF-κB activity was also reported in *Zmpste24*$^{-/-}$ mice, a model of Hutchinson-Gilford progeria syndrome (HGPS), where prelamin A is not processed properly to lamin A (138). RelA/p65 haploinsufficiency was shown to extend the lifespan and attenuate aging-associated pathology in skin, spleen and thymus in *Zmpste24*$^{-/-}$ mice (138). Notably, this study implied an activation of ATM and NEMO-dependent NF-κB pathway in response to nuclear lamina defects, which would indicate that ATM and NEMO may be essential mediators transducing signals from nuclear to cytoplasm (138). Interestingly, tissue specific knockout of IKKβ in brain and hypothalamic microglia ameliorates aging-associated neurodegeration and extends longevity by regulating gonadotropin-releasing hormone (GnRH) (139). This suggests that the hypothalamus plays a role in programming aging, in addition to its well known roles in growth, development and metabolism (139). NF-κB has also been linked to a variety of aging-related chronic diseases, such as Alzheimer's disease, Parkinson's disease, Type 2 diabetes, osteoporosis and atherosclerosis (140).

Increased chronic low-grade inflammation has been noted in *Nfkb1/p50*$^{-/-}$ mice, thus a premature aging phenotype in these mice would further back a causative role of NF-κB in driving aging (141, 142). Two recent studies showed that mice lacking the p50 subunit of NF-κB exhibited accelerated aging features such as kyphosis and osteoporosis, as well as significantly shortened lifespan, approximately around 90 weeks (141, 143). Furthermore, these results suggest chronic inflammation as an inducer of cellular senescence and premature aging (143).

It is important to note that pro-inflammatory SASP factors produced by senescent cells are transcriptionally regulated by NF-κB. SASP factors relay stress signals in cell-intrinsic and cell-extrinsic fashions, to enhance cell cycle arrest, amplify the inflammatory cascade and alter the tissue microenvironment (144-147). The most prominent SASP components, IL-6 and TNFα, are implicated in cell-autonomous and cell-nonautonomous pathways to extend senescent signals to neighboring cells via transmembrane receptors, such as interleukin-1 receptor (IL-1R) and tumor necrosis factor receptor 1/2 (TNFR1/2) (129) (145).

Notably, IKK and NF-κB-inducing kinase (NIK) protein levels are unchanged in tissues of old rodents where NF-κB nuclear-translocation is increased (148). Moreover, the transcriptional activity of a parallel pro-inflammatory pathway, activation protein 1 (AP-1), remains unchanged or even decreased in old livers (149).

1.4 *Ercc1*$^{-/\Delta}$ PROGERIA MOUSE MODEL

1.4.1 ERCC1-XPF endonuclease

ERCC1 (excision repair cross-complementation group 1) forms a heterodimeric complex with XPF (xeroderma pigmentosum group F), acting as a structure-specific endonuclease essential for the repair of nucleotide excisions (NER), DNA interstrand crosslinks (ICLs) and double-strand breaks (DSBs) (150). XPF contains the nuclease activity and ERCC1 facilitates DNA binding and the stabilization of XPF (150, 151). Several inherited human diseases are linked to mutations in ERCC1-XPF, such as xeroderma pigmentosum (XP), cerebro-oculo-facioskeletal syndrome (COFS), Cockayne syndrome, Fanconi anemia and XFE progeroid syndrome (152). Only two cases of *Ercc1* mutation in humans have been reported and were diagnosed with COFS syndrome and Cockayne syndrome respectively (153, 154). Most reported cases of XPF deficiency in human are characterized by UV sensitivity, freckling of skin and late-onset of skin cancer, as well as neurodegeneration and premature aging in very rare cases (150). Thus murine models deficient in ERCC1-XPF were generated to understand its biological role and the link to diverse syndromes associated with impaired DNA repair. Interestingly, evidence suggests that mouse models deficient in ERCC1 or XPF have identical phenotypes and both exhibit accelerated aging (155, 156)

1.4.2 *Ercc1* hypomorphic mice (*Ercc1*$^{-/\Delta}$)

Ercc1 hypomorphic mice (*Ercc1*$^{-/\Delta}$), in which 5% of normal levels of ERCC1 is expressed, are considered a murine model of XPF progeroid syndrome. The normal lifespan of wild type mice

is around 3 years, while *Ercc1*$^{-/\Delta}$ mice have a shorter lifespan of 7 months that allows a time window for phenotyping aging-associated symptoms as well as testing pharmacological interventions (157). *Ercc1*$^{-/\Delta}$ mice are smaller in size compared to wild-type controls, but there is no evidence yet supporting developmental defects in *Ercc1*$^{-/\Delta}$ mice (158, 159). *Ercc1* hypomorphic mice grow normally until 8 weeks, then gradually develop aging-associated phenotypes that progress rapidly (158, 159). Similar to *Ercc1* mutation in human, *Ercc1*$^{-/\Delta}$ mice exhibit severe neurological symptoms (ataxia, gait disorder and dystonia), kyphosis, tremor and muscle wasting, which resemble symptoms in old WT (158, 159). Notably, *Ercc1* hypomorphic mice spontaneously develop numerous aging-associated diseases over time, including osteoporosis, intervertebral disc degeneration, sarcopenia, renal and liver dysfunction, neurodegeneration and muscle wasting (152, 160-163).

2.0 CELLULAR SENESCENCE IS INDUCED IN AN ATM-NF-κB-DEPENDENT MANNER IN A DNA DAMAGE-INDUCED PROGERIA MOUSE MODEL

2.1 INTRODUCTION

Aging, a process associated with accumulation of cellular senescence, loss of organ homeostasis and decline of stem cell function, has been implicated in various aging-related diseases, including osteoporosis, intervertebral disc degeneration, liver and kidney dysfunction, diabetes, neurodegeneration and cancer (164). Cellular senescence, characterized by cell cycle arrest, has been demonstrated to cause aging-related phenotype, based on the finding that depletion of $p16^{INK4a}$ positive cells in *BubR1*$^{H/H}$ progeroid mice led to an extended healthspan (122). Senescent cells produce a distinct group of secretion factors, including cytokines, chemokines, growth factors and proteases, termed senescence-associated secretory phenotype (SASP) (129, 132). Pro-inflammatory SASP components, such as IL-6, IL-1α and TNF-α, were shown to extend senescence to neighboring cells by transducing stress signals in both cell-autonomous and cell-nonautonomous fashions (129, 165, 166).

DNA damage response (DDR) is a critical pathway required for faithful replication and genome stability by recruiting and forming a multiprotein complex at the site of DNA double-strand breaks (DSBs) (78, 167-169). Ataxia-telangiectasia mutated (ATM) kinase is a central mediator required for the initiation and amplification of DDR signaling. Upon DNA damage, the

MRE11-RAD50-NBS1 (MRN) complex is recruited to the lesion sites as the first sensor, which in turn facilitates the recruitment, retention and activation of nuclear ATM (53). Autophosphorylated ATM kinase subsequently leads to the phosphorylation and activation of a histone H2A variant (γH2AX), which acts to further amplify DDR cascade by attracting more ATM protein, as well as recruiting more DDR effectors to the DNA lesions. Multiple DDR proteins, such as KRAB-associated protein-1 (KAP1), p53 and checkpoint kinase 2 (CHK2), are phosphorylated by ATM kinase once recruited, which further promotes cell-cycle arrest, DNA repair, apoptosis or senescence (61, 170).

The nuclear factor κB (NF-κB) family of transcription factors consists of five members in mammalian cells, including RelA/p65, RelB, c-Rel, p50/p105 and p52/p100. All NF-κB proteins contain a Rel-homology domain (RHD), which is essential for DNA binding activity and dimerization. NF-κB functions to regulate innate and adaptive immune responses, development, proliferation, apoptosis, oncogenesis and senescence (3). The canonical NF-κB pathway is activated by inflammatory stimuli, such as TNF-α, IL-1α, IL-1β and LPS, which activate the IκB kinase (IKK) complex. The IKK complex in turn phosphorylates and facilitates the degradation of the inhibitory protein IκBα in 26S proteosome, which leads to the release of NF-κB dimers into the nucleus where it can regulate the transcription of target genes (3). The IKK complex is composed of two catalytic subunits, IKKα and IKKβ, and one regulatory subunit, NF-κB essential modifier (NEMO/IKKγ). Miyamoto et al. demonstrated a role for genotoxic stress in the activation of TNF-α-independent NF-κB pathway, which is absent in ataxia-telangiectasia (AT) cells (4, 171). Upon DNA damage, activated ATM mediates a series of post-translational modifications on NEMO, including phosphorylation at Ser85 and sumoylation and mono-ubiquitination at Lys 277 and 309 (172). This in turns triggers the nuclear

export of ATM-NEMO complex to the cytoplasm, where it converges on the IKK complex to initiate NF-κB activation (4).

Elevated NF-κB activity has been found in multiple aged tissues, such as skin, cerebellum and kidney (133-135). Mounting evidence suggests that NF-κB activation plays a causal role in cellular senescence and aging (137, 138, 146). This is supported by our previous study that genetic reduction of the RelA/p65 subunit of NF-κB delayed the onset of aging symptoms in *Ercc1*$^{-/\Delta}$ mice (137). In addition, *Zmpste24*$^{-/-}$ mice heterozygous for p65/RelA exhibited attenuated aging pathology and a prolonged lifespan, which was linked to a reduced systemic inflammatory response and a reduction in ATM- and NEMO-mediated NF-κB activation (138). Moreover, *Nfkb1*$^{-/-}$ mice, where increased low-grade inflammation was noted, showed signs of premature aging, exhibited by neural degeneration, impaired regeneration and declined overall lifespan (141, 143, 173, 174). In addition, NF-κB was associated with multiple aging-related chronic diseases, including Alzheimer's disease, Parkinson's disease, Type II diabetes, osteoporosis and atherosclerosis (140). This could be largely attributed to the systemic inflammation mediated by chronic NF-κB activation (175). Moreover, NF-κB is considered as a master regulator of SASP factors, which can be transcriptional regulated by NF-κB.

Persistent DDR signaling mediated by accumulative DNA damage, particularly ATM activation, has been demonstrated to be essential for cellular senescence and the SASP phenotype (99). Genotoxic stress induced by DNA damage, oxidative stress, telomere shortening or oncogene activation, could trigger an upregulation of p53/p21 pathway, leading to cell-cycle arrest. Senescence that developed independent of DNA damage, such as $p16^{Ink4a}$ overexpression, was also shown to trigger cell growth arrest, but failed to induce the secretion of SASP components due to the lack the persistent DNA damage response (87, 99, 176). Moreover, a

previous study reported unresolved DNA damage foci and elevated ATM at the transcriptional level in ap2-*Ercc1*$^{F/-}$ mice, where a DNA repair protein was specifically knocked out in adipose tissue, again implicating a central role of ATM and DDR in aging (177). However, it remains elusive whether ATM or DDR signaling plays a causal role in senescence and aging.

Here we used an *Ercc1*$^{-/\Delta}$ mouse model, where only 5% of ERCC1-XPF was expressed, to address the causal role of DDR signaling in senescence and aging. The *Ercc1* hypomorphic (*Ercc1*$^{-/\Delta}$) mice exhibit defects in nucleotide excision repair, interstrand crosslink repair and DSB repair, and spontaneously develop osteoporosis, sarcopenia, intervertebral disc degeneration, glomerulonephropathy, neurodegeneration, peripheral neuropathy, incontinence and loss of vision, hearing and cognition. We found that NF-κB level was persistently elevated in both chronological and accelerated aging, concomitant with a hyperactive DDR signaling. Repressing ATM in the presence of persistent DNA lesions reduced cellular senescence and downregulated ATM- and NEMO-mediated NF-κB activation *in vitro*. *Ercc1*$^{-/\Delta}$ mice heterozygous for *Atm* exhibited significantly reduced NF-κB activity, as well as extended healthspan. Our findings suggest that the DSB-mediated DDR response, especially ATM kinase activation, may directly lead to NF-κB activation through NEMO shuttling, resulting in intensified senescence and aging. Furthermore, we showed that the reduction of ATM activity could attenuate a premature aging phenotype, suggesting ATM as a potential therapeutic target for delaying or improving frailty and aging-related diseases.

2.2 MATERIALS AND METHODS

2.2.1 Cells and mice

Primary mouse embryonic fibroblasts (MEFs) were isolated on embryonic day 12.5-13.5. In brief, mouse embryos were isolated from yolk sac followed by complete removal of viscera, lung and heart. Embryos were then minced into fine chunks, fed with MEFs medium, cultured under 3% oxygen to reduce stresses and split till confluence. MEFs were grown in 1:1 of Dulbecco's Modification of Eagles Medium (with 4.5g/L glucose and L-glutamine) and Ham's F10 medium, supplemented with 10% fetal bovine serum, penicillin, streptomycin and non-essential amino acid. To induce oxidative stress-induced DNA damage in *Ercc1*$^{-/-}$ MEFs, MEFs were transferred to 20% oxygen for further incubation starting from passage 3.

Ercc1$^{+/-}$ and *Ercc1*$^{+/\Delta}$ mice from C57BL/6J and FVB/n backgrounds were crossed to generate *Ercc1*$^{-/\Delta}$ F1 hybrid mice to prevent potential strain-specific pathology. *Atm*$^{+/-}$ mice were crossed to *Ercc1*$^{+/-}$ from C57BL/6J background to generate *Atm*$^{+/-}$;*Ercc1*$^{+/-}$ mice, which were then bred with *Ercc1*$^{+/\Delta}$ mice from FVB/n background to generate *Atm*$^{+/-}$;*Ercc1*$^{-/\Delta}$ mice. Mice were backcrossed for 10 generations to achieve genetic identity. Animal protocols used in this study were approved by Scripps Florida Institutional Animal Care and Use Committees.

2.2.2 Immunoblotting

MEFs were treated with KU-55933 (Selleckchem) or vehicle control for 72 hours. Cells lysate were prepared in RIPA buffer (20 mM Tris-HCl (pH 7.5), 150 mM NaCl, 1 mM Na_2EDTA, 1 mM EGTA, 1% NP-40, 1% sodium deoxycholate, 2.5 mM sodium pyrophosphate, 1 mM β-

glycerophosphate, 1 mM Na_3VO_4, 1 µg/ml leupeptin, 1X protease inhibitor cocktails (sigma) and 1X Halt phosphatase inhibitor cocktail (Thermo)). Snap frozen liver and kidney were homogenized in RIPA buffer described above using FastPrep-24 instrument. 40-50 ug protein was resolved by MINI-PROTEAN TGX 4-15% SDS-PAGE. Blots were blocked in 5% non-fat milk. Primary antibodies were incubated at 4^oC overnight and secondary antibodies were incubated at room temperature for 1 hour. Anti-p-ATM (1:1000, Rockland), anti-ATM (1:1000 CST), anti p-KAP1 (1:1000 Abcam), anti-KAP1 (1:2000 Abcam), anti-γ-H2AX (1:5000 Novus), and anti-PARP1 (1:1000 CST) were employed to detect DDR proteins. Anti-p-p65 (1:1000 CST), anti-p65 (1:2000 CST), anti-p-IκBα (1:1000 CST), anti-IκBα (1:2000 CST) and anti-NEMO (1:1000, CST) were used to assess NF-κB activation. Anti-p16 (1:1000, Santa Cruz) and anti-p21 (1:1000 Santa Cruz) were used to detect the expression of senescent markers. Anti-laminA/C (1:5000 Santa Cruz), anti-tubulin (1:2000 CST), anti-GAPDH (1:5000 CST) and anti-actin (1:5000 Santa Cruz) were used as loading controls.

2.2.3 Nuclear extraction

Cytoplasmic and nuclear fractions were extracted using the NE-PER nuclear and cytoplasmic extraction reagents (ThermoFisher) according to the manufacturer's instructions. Briefly, $1x10^6$ cells were suspended and lysed in CERI and CERII reagents consecutively on ice. The supernatant of centrifugation was collected as cytoplasmic fraction, and the pellet was suspended in NER reagent and collected as nuclear fraction.

2.2.4 Quantitative reverse transcription-polymerase chain reaction

Snap frozen tissues were preserved in RNAlater RNA stabilization solution (ThermoFisher). Total RNA was extracted using TRIZOL reagent (Life Technologies) and 1.5 μg of RNA was subjected to synthesize complementary DNA (cDNA) using SuperScript VILO cDNA synthesis kit. qRT-PCR was performed in a StepOnePlus Real-Time PCR system using Platinum SYBR Green qPCR SuperMix-UDG (ThermoFisher). Target gene expression was calculated using the comparative C_T method ($\Delta\Delta C_T$) and normalized to an internal control gene Actb (β-actin). Primers used are as follows: *Cdkn1a* (p21) forward: GTCAGGCTGGTCTGCCTCCG; *Cdkn1a* (p21) reverse: CGGTCCCGTGGACAGTGAGCAG; *Cdkn2a* (p16) forward: CCCAACGCCCCGAACT; *Cdkn2a* (p16) reverse: GCAGAAGAGCTGCTACGTGAA; *Tnf* (TNF) forward: CTATGTCTCAGCCTCTTCTC; *Tnf* (TNF) reverse: CATTTGGGAACTTCTCATCC; *Il6* (IL-6) forward: AAGAAATGATGGATGCTACC; *Il6* (IL-6) reverse: GAGTTTCTGTATCTCTCTGAAG; *Actb* (β-actin) forward: GATGTATGAAGGCTTTGGTC; *Actb* (β-actin) reverse: TGTGCACTTTTATTGGTCTC.

2.2.5 Immunofluorescent staining

MEFs were seeded onto chamber slides and allowed to attach in 20% oxygen overnight. Cells were fixed in 4% paraformaldehyde (PFA) for 10 min, permeabilized with 0.3% Triton X-100 and blocked with 3% BSA for 1 hour in room temperature. Primary antibody incubation was performed overnight at 4^{o}C and secondary antibody incubation for 1 hour at room temperature. Cell nuclei were counterstained with Vectashield mounting medium with DAPI. Five images of

each cell type were acquired using an Olympus confocal microscopy at 40x magnification. Primary antibodies used are as follows: anti-p65 (Santa Cruz) and anti-NEMO (Santa Cruz).

2.2.6 Senescence-associated β-galactosidase staining *in vivo* and *in vitro*

MEFs were seeded into a 6-well plate at $3x10^4$ cells per well, allowed to attach overnight and treated by vehicle control or KU-55933 at 10 uM for 72 hours. Cells and fresh fat tissues were fixed in 2% formaldehyde and 0.2% glutaraldehyde in PBS for 10 minutes and then stained with SA-βgal staining (pH 5.8 for MEFs and pH 6.0 for fat) solution (40 mM citric acid in sodium phosphate buffer, 5 mM $K_4[Fe(CN)_6]$ $3H_2O$, 5 mM $K_3[Fe(CN)_6]$, 150 mM sodium chloride, 2 mM magnesium chloride and 1 mg/ml X-gal dissolved in N,N-dimethylformamide) for 16-20 hours in a 37^{o}C incubator without CO_2 injector. To quantify, ten images were acquired randomly using a bright-field microscopy at 20x maginification. Total SA-βgal$^+$ cells was normalized to the total cell number (DAPI). Fresh liver tissues were fixed in 10% neutral buffered formalin (NBF) for 3-4 hours and then transfered to 30% sucrosed overnight to replace water. Tissues were then imbeded in OCT and stored at -80^{o}C. Cryosection at 5μM was performed and slides were stained in SA-βgal staining solution (pH 5.8) at 37^{o}C for 16-24 hours. To quantify, ten random images were captured using a bright-field microscopy at 20x magnification and the number of SA-βgal$^+$ cells was counted. The quantification was shown as mean+/- SD.

2.2.7 Health Evaluation

Health assessment was conducted weekly to assess body weight, general conditions, neurodegeneration and muscle wasting. Kyphosis, body condition and coat condition were

assessed as general conditions. Ataxia, dystonia, gait disorder and tremor are used as indicators for neurodegeneration. Muscle wasting was studies by evaluating hindlimb paralysis and forelimb grip strength. All aging symptoms were scored based on a scale of 0, 0.5 and 1, except dystonia with a scale from 0 to 5. The sum of aging scores for each genotype group was used to determine the overall aging conditions.

2.2.8 Cell proliferation assay

Passage 3 MEFs were seeded in a 10-cm plate at $5x10^5$ cells and allowed to grow for 72-96 hours in 20% oxygen. Cells were then trypsinized. Harvested cells were counted using a Moxi Z Mini automated cell counter and then seeded at the same density until passage 5. Log cell number was plotted versus each passage.

2.2.9 Histology analysis

Tissues fixed in 10% neutral buffered formalin (NBF) overnight were imbedded in paraffin. Tissue was sectioned at 5 μm using a microtome. Hematoxylin and eosin (H&E) staining was conducted following a standard protocol.

2.2.10 Glycosaminoglycan (GAG) analysis

Snap frozen lumber spines were harvested from 12-week-old *Ercc1*$^{-/\Delta}$ and *Atm*$^{+/-}$;*Ercc1*$^{-/\Delta}$ mice. Nucleus pulposus (NP) tissue was isolated under microscope and six lumbar intervertebral discs were pooled together for analysis. GAG was isolated by papain digestion at 60^{o}C for 2 hr. GAG

concentration was measured by following DMB procedure (Sigma) and DNA concentration was measured using PicoGreen assay (Molecular Probes), which was used for normalization.

2.2.11 Statistical analysis

All values were presented as mean+/-S.E.M. Microsoft Excel and Graphpad Prism 6 were used for statistical analysis. Two-tailed Student's *t*-test was performed to determine differences between two groups. When comparing difference in more than two groups, one-way ANOVA (Dunnett test) was conducted. A value of $p < 0.05$ was considered as statistically significant, shown as $*p < 0.05$, $**p < 0.01$, and $***p < 0.001$.

2.3 RESULTS

2.3.1 NF-κB and DDR signaling are highly activated in cellular senescence and in accelerated and natural aging

Multiple age-related chronic diseases, including Type 2 diabetes, osteoporosis, disc degeneration and cancer, are associated with elevated NF-κB activity (140). Blockade of NF-κB activity in epidermis in chronologically aged transgenic mice rejuvenated skin aging, suggesting that NF-κB may be one of the driving forces in aging. Our previous study demonstrated an increased NF-κB activation in the liver, kidney, skeletal muscle and pancreas of *Ercc1*$^{-/\Delta}$ mice by using an NF-κB^{EGFP} knock-in mouse model. Here we found that the level of p-p65 (Ser 536) was increased in the liver of 16-week-old *Ercc1*$^{-/\Delta}$ mice, while wild type (WT) mice at the same age only showed

a minimal activation (Fig. 6A). To determine if NF-κB hyperactivation correlates with DNA damage-induced DDR signaling, we measured the total expression of ATM and its downstream substrates. In *Ercc1*$^{-/\Delta}$ liver, we also found elevated level of p21 protein, which is a main downstream effector of p53 and a biomarker of senescence (Fig. 6B). The level of γH2AX, a substrate of ATM and a marker of senescence reflecting persistent DNA damage, was also increased, consistent with our previous findings that *Ercc1*$^{-/\Delta}$ mouse liver bear more oxidative DNA damage than WT littermates (Fig. 6B) (137). Old mice have more irreparable DSBs in liver, kidney, lung, brain and testes, as measured by γH2AX foci, compared to young animals (178). Thus to test if *Ercc1*$^{-/\Delta}$ mice mirror natural aging, we tested liver from WT mice at different ages. Higher p-p65 level was detected in 2-year-old WT livers (with lifespan of 3 years) compared to livers from 3 and 12 months old animals where only minimal p65 activation was observed (Fig6. C&D). Consistently, activation of IκBα was slightly increased in 2-year-old liver, as represented by p-IκBα. We then tested primary mouse embryonic fibroblasts (MEFs) isolated from *Ercc1*$^{-/-}$ embryos, where no ERCC1-XPF was expressed. We discovered a higher level of p-p65 in passage 5 *Ercc1*$^{-/-}$ MEFs grown at ambient oxygen levels (20%), compared to WT MEFs (Fig. 6F). Phosphorylation of ATM and KAP1, an ATM effector, were increased in *Ercc1*$^{-/-}$ MEFs compared to WT MEFs (Fig 6E). Immunofluorescent staining of p65 and NEMO in *Ercc1*$^{-/-}$ and WT MEFs revealed increased nuclear-localized p65 and NEMO, suggesting upregulated p65 activation (Fig 6G). Although NEMO is mainly a cytoplasmic protein, its shuttling between nucleus and cytoplasm has been shown required for bridging ATM and NF-κB upon genotoxic stress (4). Taken together, our results suggest an activation of NF-κB pathway in DNA damage-induced senescence and aging, which is likely ATM- and NEMO-dependent.

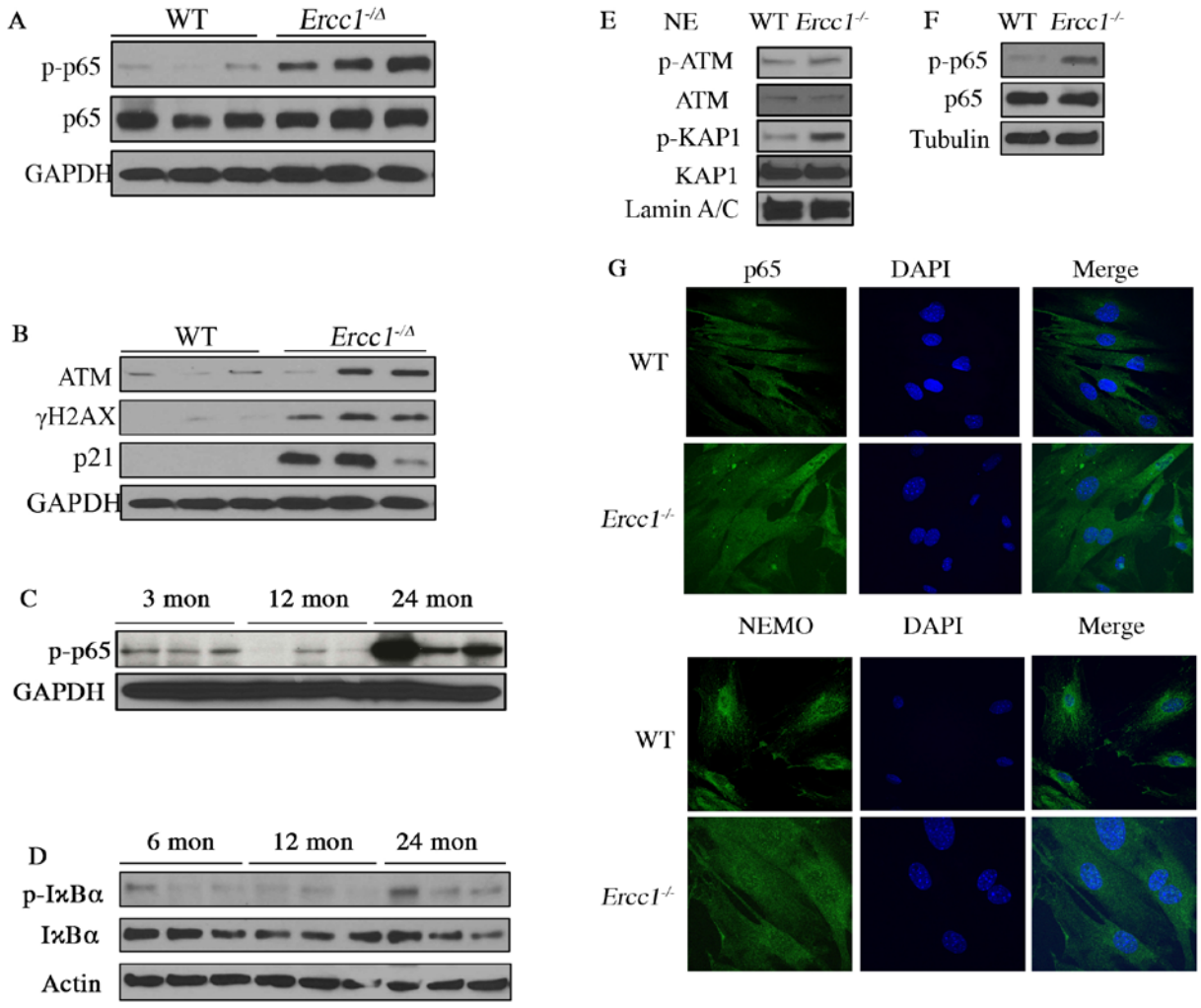

Figure 6: DDR and NF-κB are activated simultaneously in senescent MEFs, *Ercc1*$^{-/\Delta}$ and old WT mice. (A) Western blots of p-p65 (Ser536) and p65 were performed with liver lysate from 16-week-old WT (n=3) and *Ercc1*$^{-/\Delta}$ (n=3) mice. GAPDH was used as an internal loading control. (B) Immunoblot analysis was performed against DDR proteins, including ATM, γH2AX and p21, with liver lysate from 16-week-old WT and *Ercc1*$^{-/\Delta}$ mice. (C) Levels of p-p65 were measured with liver tissues from 3, 12, 24 months old WT mice. n=3 mice per group. (D) The levels of p-IκBα (Ser 32/36) and IκBα were measured by western blot with liver tissues from 6, 12, 24 months old WT mice. (E) Primary MEFs were cultured in 20% oxygen to induce oxidative stress-induced senescence. Immunoblotting for DDR activation was performed with

nuclear extract from passage 5 senescent MEFs. (F) Whole cell lysates of passage 5 MEFs were immunoblotted for p-p65 and total p65. (G) Passage 4 MEFs were sub-cultured for 24 hrs and cytoplasmic and nuclear localized p65 (green) and NEMO (green) were detected by immunofluorescent staining. Nuclei were counterstained with DAPI (blue). Representative images were taken at the magnification of 40x.

2.3.2 Pharmacologic inhibition of ATM rescues oxidative stress-induced senescence by suppressing ATM- and NEMO-dependent NF-κB activation

To further elucidate the causative role of DDR signaling, specifically ATM kinase, in driving senescence, we employed a selective ATM kinase inhibitor, KU-55933 (179). To mimic physiological conditions, ambient oxygen tension (20%) was used to induce endogenous DNA damage in primary WT and *Ercc1*$^{-/-}$ MEFs. *Ercc1*$^{-/-}$ MEFs exhibited increased SA-βgal positive staining with serial passaging at 20% oxygen, and maximal cellular senescence was observed at passage 5 represented by enlarged and flat morphology as well as increased SA-βgal staining (Fig. 7A) (137). KU-55933 remarkably reduced SA-βgal staining in senescent *Ercc1*$^{-/-}$ MEFs to a level similar to WT MEFs (Fig. 7A&B). Additional senescent markers, tumor suppressors p21 and p16, were also decreased by the treatment of KU-55933, confirming reduced cellular senescence by the inhibition of ATM (Fig. 7C). As expected, ATM activation, as indicated by autophosphorylation at Ser1981, was downregulated by KU-55933 (Fig. 7D). Moreover, p-KAP1 and γH2AX were found at lower levels after the treatment (Fig. 7E). Poly [ADP-ribose] polymerase 1 (PARP1) has been shown to participate in DNA repair and chromatin remodeling by consuming NAD^+, the depletion of which has been linked to mitochondrial dysfunction observed in neurodegeneration and aging. Interestingly, ATM inhibition for 72 hr was able to

decrease the level of PARP1, suggesting that the suppression of primary DDR signaling may have a broader effect (Fig. 7D). Notably, the treatment with ATM inhibitor also decreased p65 activity, as represented by reduced level of p-p65 and less nuclear-translocated p65 and NEMO, detected by western blot (Fig. 7F&G). Taken together, DNA damage plays an essential role in driving senescence and the inhibition of DDR signaling not only reverses cellular senescence, but also inhibits NF-κB activation in an ATM- and NEMO-dependent manner.

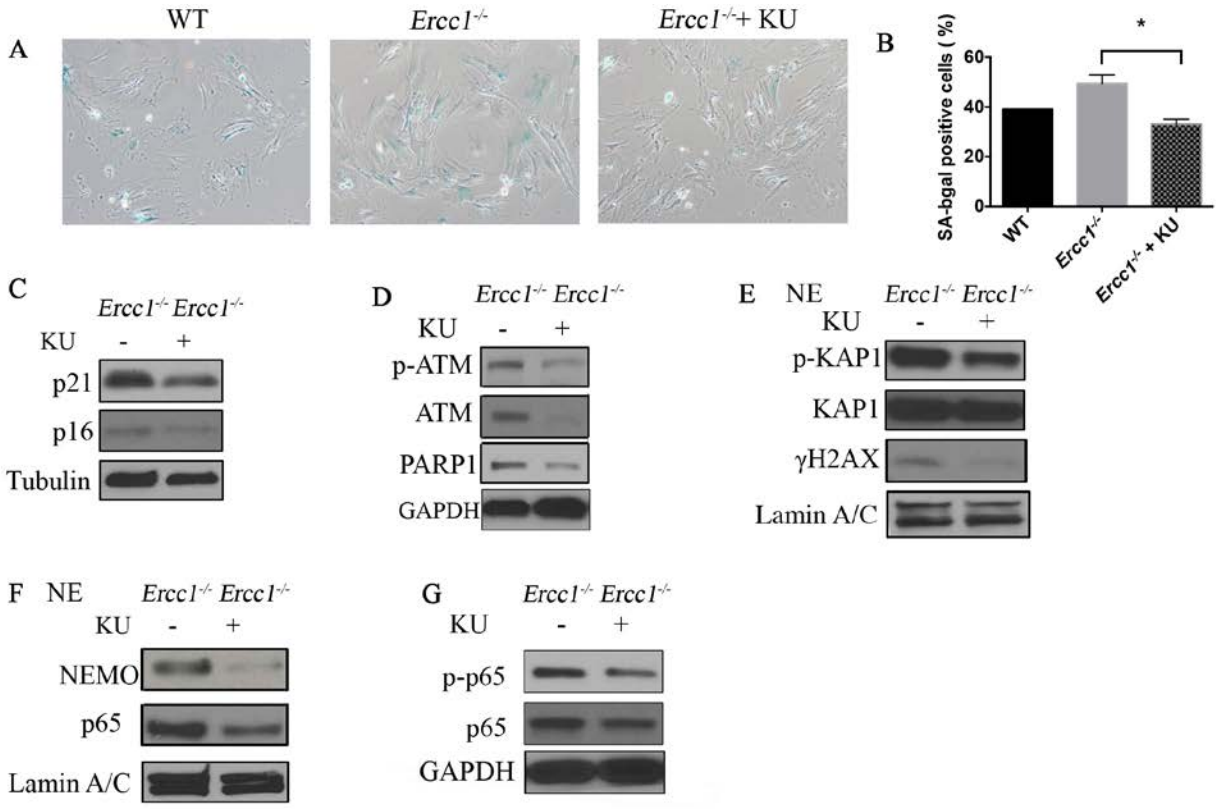

Figure 7: Pharmacologic inhibition of ATM rescues oxidative stress-induced senescence by suppressing ATM- and NEMO-dependent NF-κB activation. (A) Passage 5 primary WT and *Ercc1*$^{-/-}$ MEFs were cultured in 20% oxygen in the presence of ATM inhibitor (10 μM of KU-55933) or vehicle for 72 hr. Senescent cells were detected by SA-βgal staining shown in blue. Representative images were obtained at the magnification of 10x. (B) Quantitation showed the

average percentage of SA-βgal positive cells from 3 independent experiments. (C) Passage 5 primary *Ercc1*$^{-/-}$ MEFs were treated with 10 μM of KU-55933 for 72 hours. Whole cell lysate and nuclear extract were prepared for western blot analysis. Immunoblot for senescent markers p16 and p21 (C) and DNA damage sensors p-ATM, ATM and PARP1 (D) were performed with whole cell lysate. (E) Nuclear extract were blotted for ATM substrates, p-KAP1, KAP-1 and γH2AX. LaminA/C was used as a loading control. (F) The levels of nuclear translocated NEMO and p65 were determined by western blot using nuclear extract. (G) The levels of p-p65 and total p65 were detected by immunoblot with the whole cell lysate.

2.3.3 Deletion of one allel of *Atm* decreases oxidative stress-induced cellular senescence

To rule out potential off-target effects of KU-55933, *Ercc1*$^{-/-}$ MEFs missing one allele of *Atm* (*Atm*$^{+/-}$*;Ercc1*$^{-/-}$) were generated. Proliferation assays comparing the growth of WT, *Ercc1*$^{-/-}$, and *Atm*$^{+/-}$*;Ercc1*$^{-/-}$ MEFs revealed an arrested population doubling in *Ercc1*$^{-/-}$ MEFs from passage 4 to passage 5, which was partialy restored in *Atm*$^{+/-}$*;Ercc1*$^{-/-}$ MEFs (Fig. 8A). SA-βgal staining also showed reduced senescent cells in *Atm*$^{+/-}$*;Ercc1*$^{-/-}$ MEFs at each indicated passage compared to *Ercc1*$^{-/-}$ MEFs (Fig. 8B&C). In addition, immunoblot analysis showed decreased expression of p16^{Ink4a} in *Atm*$^{+/-}$*;Ercc1*$^{-/-}$ MEFs (Fig. 8D). Taken together, our results suggest that both pharmacologic and genetic reduction of ATM could successfully reverse oxidative stress-induced cellular senescence.

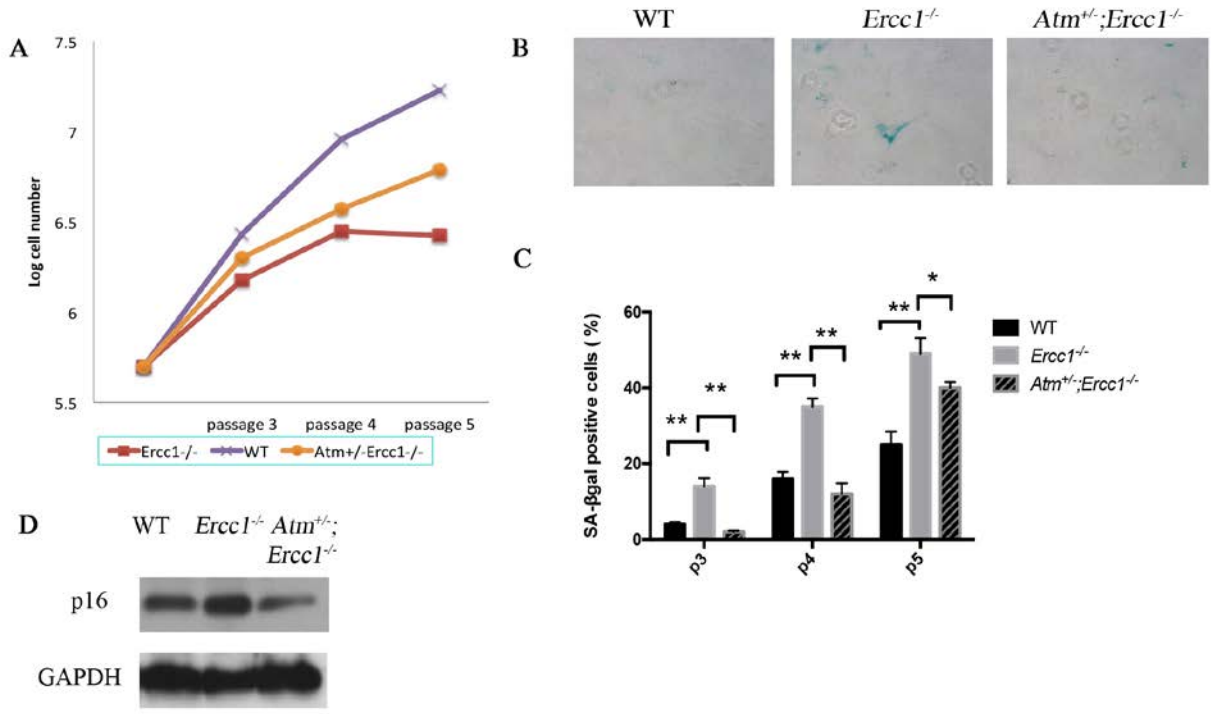

Figure 8: Oxidative stress-induced cellular senescence is reduced in *Atm*$^{+/-}$;*Ercc1*$^{-/-}$ MEFs.

(A) Cellular proliferation was determined in passage 3, 4 and 5 WT (purple), *Ercc1*$^{-/-}$ (red) and *Atm*$^{+/-}$;*Ercc1*$^{-/-}$ MEFs cultivated in 20% oxygen. (B) Primary MEFs were cultured in 20% oxygen at indicated passages for 72 hr and SA-βgal staining was conducted to quantify blue positive cells. Representative images were taken at the magnification of 10x. (C) The quantification of the average percentage of SA-βgal positive cells was plotted at each passage. (D) Passage 5 WT, *Ercc1*$^{-/-}$ and *Atm*$^{+/-}$;*Ercc1*$^{-/-}$ MEFs was cultured in 20% oxygen for 72 hr and lysed for immunoblot analysis. The level of p16 was determined relative to GAPDH.

2.3.4 *Atm* haploinsufficiency reduces DDR signaling and NF-κB activation in *Ercc1*$^{-/\Delta}$ mice

To determine if DDR signaling indeed mediates NF-κB activation in aging, *Ercc1*$^{-/\Delta}$ mice heterozygous for *Atm* were generated, showing dampened DDR activation. Livers from 16-week-old WT, *Ercc1*$^{-/\Delta}$, and *Atm*$^{+/-}$*;Ercc1*$^{-/\Delta}$ mice were analyzed by western blot. We found markedly downregulated DDR signaling in *Atm*$^{+/-}$*; Ercc1*$^{-/\Delta}$ mice compared to *Ercc1*$^{-/\Delta}$ mice, as indicated by lower levels of total ATM, p-KAP1 and γH2AX (Fig. 9A). Reduced p21 was found in *Atm*$^{+/-}$*; Ercc1*$^{-/\Delta}$ livers suggesting decreased cellular senescence (Fig. 9A). Intriguingly, phospho-p65 was also reduced to WT level in *Atm*$^{+/-}$*;Ercc1*$^{-/\Delta}$ mice, suggesting NF-κB activation in DNA damage-induced premature aging is mainly caused by ATM activation (Fig. 9B). Similarly, we found lower level of total IκBα in both WT and *Atm*$^{+/-}$*; Ercc1*$^{-/\Delta}$ mice compared to *Ercc1*$^{-/\Delta}$ mice, again suggesting that activated ATM in *Ercc1*$^{-/\Delta}$ mice may lead to increased NF-κB transcriptional activity leading to increased synthesis of IκBα (Fig. 9B). This is consistent with previous finding that *p65*$^{+/-}$ MEFs express less total IκBα and IκBβ proteins compared to WT MEFs, and *p65*$^{-/-}$ MEFs contain only 35% of IκBα and almost no IκBβ (180, 181). To determine if *Atm*$^{+/-}$*; Ercc1*$^{-/\Delta}$ mice mirror molecular changes in *p65*$^{+/-}$*;Ercc1*$^{-/\Delta}$ mice, western blot analysis was performed to determine NF-κB activation and DDR signaling in *Ercc1*$^{-/\Delta}$ and *p65*$^{+/-}$*; Ercc1*$^{-/\Delta}$ mice. We found reduced p-p65 and total IκBα in *p65*$^{+/-}$*;Ercc1*$^{-/\Delta}$ livers, suggesting reduced NF-κB activation in *p65*$^{+/-}$*;Ercc1*$^{-/\Delta}$ liver (Fig. 9C). However, γH2AX level was found to be unaffected, confirming that DDR signaling is the upstream of NF-κB. Taken together, the results suggest that DDR signaling plays an essential role in NF-κB activation in DNA damage-induced premature aging. Moreover, the deletion of one ATM allele is sufficient to downregulate

DDR signaling and further decrease NF-κB activity in tissues accumulating DNA damage over time.

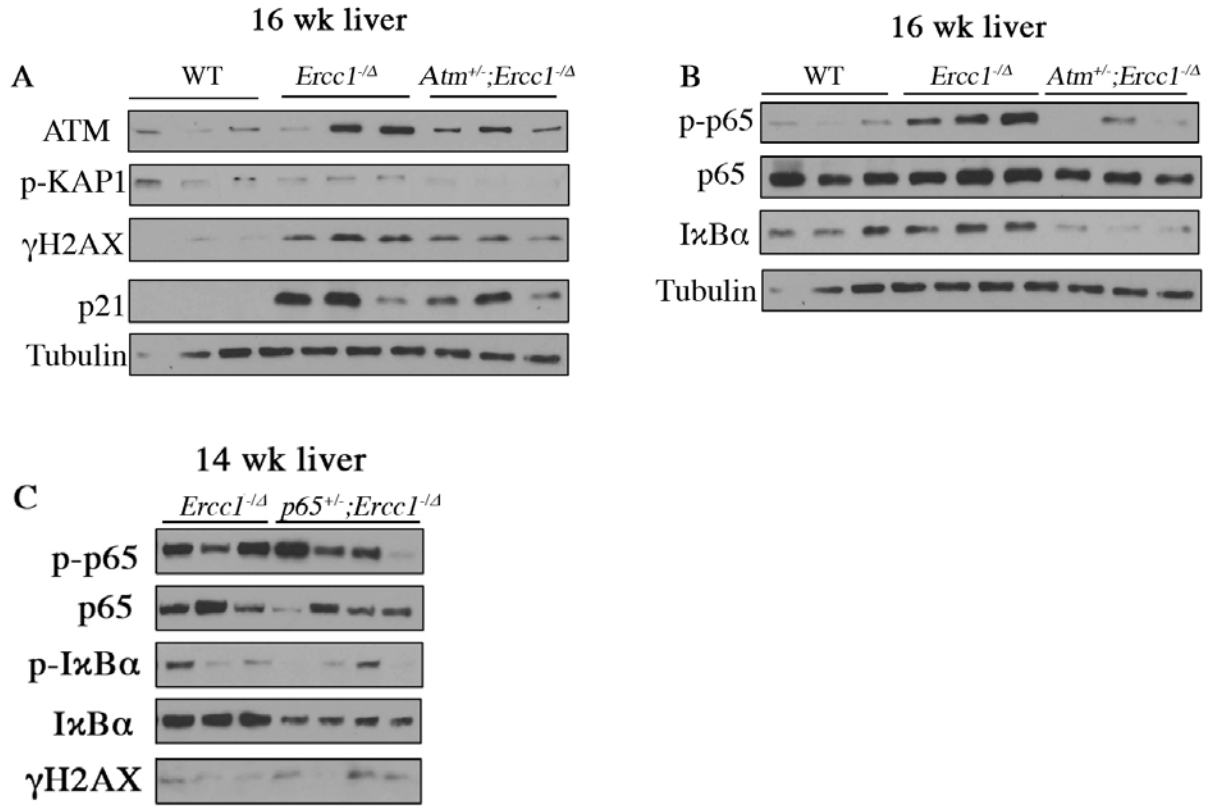

Figure 9: NF-κB activation and DDR signaling are downregulated in *Ercc1*$^{-/\Delta}$ mice heterozygous for *Atm*. (A) 16-week-old livers from WT (n=3), *Ercc1*$^{-/\Delta}$ (n=3) and *Atm*$^{+/-}$*;Ercc1*$^{-/\Delta}$ (n=3) were collected for western blot analysis and the levels of DDR proteins were blotted, including ATM, γH2AX, and p21. (B) The levels of p-p65, p65 and total IκBα were determined by immunoblot. Tubulin was used as a loading control. (C) 14-week-old livers from *Ercc1*$^{-/\Delta}$ (n=3) and *p65*$^{+/-}$*;Ercc1*$^{-/\Delta}$ (n=4) were analyzed for the levels of NF-κB activation and DDR signaling by western blot.

2.3.5 Genetic reduction of *Atm* extends healthspan and alleviates progeroid symptoms by reducing cellular senescence

We previously reported that genetic reduction of the RelA/p65 subunit of NF-κB could delay the onset of aging symptoms in *Ercc1*$^{-/\Delta}$ mice, where chronic accumulation of DNA damage is the major driving force of aging symptoms. We hypothesized that *Atm* heterozygosity could phenocopy *p65* haploinsufficiency and alleviate aging symptoms. Aging-related symptoms, including dystonia, kyphosis, tremor, ataxia, gait disorder, hindlimb paralysis and forelimb grip strength, were assessed weekly to closely monitor the onset, severity and progression of aging symptoms in *Ercc1*$^{-/\Delta}$ mice. Total symptom score was used to evaluate the general health condition of mice. *Ercc1*$^{-/\Delta}$ mice showed a gradual progression of aging symptoms exacerbating greatly at 12 weeks old, whereas *Atm*$^{+/-}$*; Ercc1*$^{-/\Delta}$ mice had less severe symptoms at younger ages, as well as slower progression of aging symptoms (Fig. 10A). A major neurological symptom that progresses rapidly in *Ercc1*$^{-/\Delta}$ mice is dystonia (hindlimb clasping), which also occurs in neurodegenerative diseases such as Parkinson's disease (PD) (182). The severity and exacerbation of dystonia were slowed in *Atm* haploinsufficent mice, indicating attenuated neurodegeneration (Fig. 10B). We also found reduced SA-βgal staining in adipose tissue, indicating less senescent adipocytes in *Atm*$^{+/-}$*; Ercc1*$^{-/\Delta}$ mice, consistent with qRT-PCR analysis showing reduced transcription of p16^{Ink4a} and p21 (Fig. 10C&D).

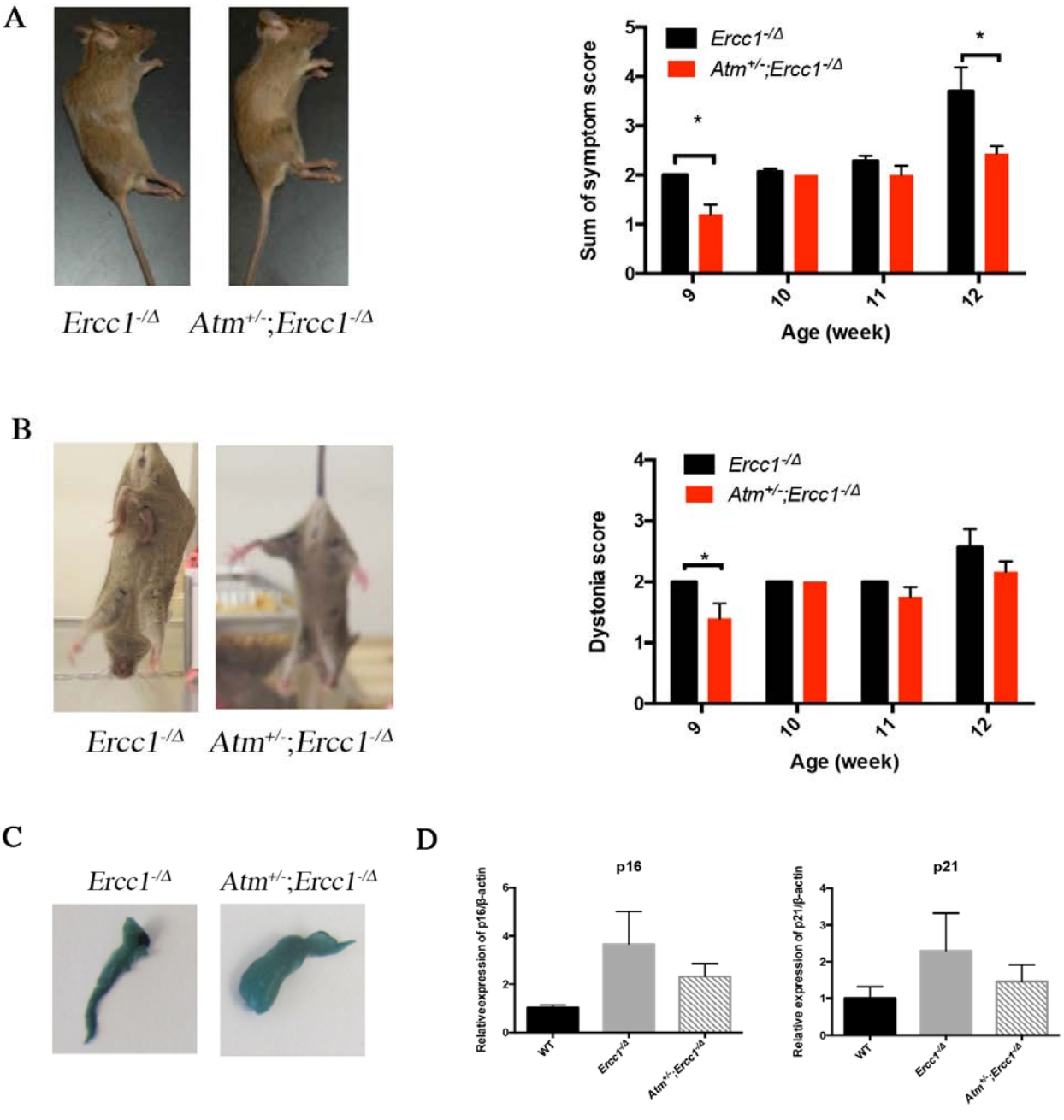

Figure 10: *Atm*$^{+/-}$*;Ercc1*$^{-/\Delta}$ mice exhibit attenuated aging phenotype and reduced cellular senescence. (A) Aging symptoms were assessed weekly on *Ercc1*$^{-/\Delta}$ and *Atm*$^{+/-}$*;Ercc1*$^{-/\Delta}$ mice. The total score of aging symptoms was calculated and plotted at indicated ages. Representative pictures show the general health condition, body size and kyphosis of a pair of littermate at 15

weeks of age. n=8-10 mice per group. (B) Dystonia was assessed and the score was plotted in bar graph. (C) SA-βgal staining of parametrial fat from 12-week-old *Ercc1*$^{-/\Delta}$ and *Atm*$^{+/-}$;*Ercc1*$^{-/\Delta}$ mice. (D) Adipose tissue from 12-week-old WT, *Ercc1*$^{-/\Delta}$ and *Atm*$^{+/-}$;*Ercc1*$^{-/\Delta}$ mice was analyzed for p16^{INK4a} and p21 expression by qRT-PCR. n=3-4 mice each group.

Consitent with these data, IL-6 and TNFα, the major SASP factors and NF-κB target genes, were downregulated in *Atm*$^{+/-}$;*Ercc1*$^{-/\Delta}$ liver compared to *Ercc1*$^{-/\Delta}$ mice, in particular a significant reduction in IL-6 (Fig. 11A). p21 expression was also significantly reduced in *Atm*$^{+/-}$;*Ercc1*$^{-/\Delta}$ liver, while no significant reduction was observed in p16 transcription, suggesting decreased p53/p21 and unaffected p16/Rb activity in *Atm*$^{+/-}$; *Ercc1*$^{-/\Delta}$ mice (Fig. 11A). Declined kidney function has been demonstrated in aged humans and mice, reflected by decreased glomerular filtration rate (GFR), accompanied by the increase in p16^{INK4a}, p21 and SASP proteins. Our previous study found elevated NF-κB-eGFP expression in renal cortex, which led us to study molecular changes in kidney by qRT-PCR (137). However, we only found trends toward reduced IL-6 and p21 in *Atm*$^{+/-}$; *Ercc1*$^{-/\Delta}$ kidney, likely due to the rapid loss of senescent population in renal cortex, which was supported by our observation of decreased cortical thickness in *Ercc1*$^{-/\Delta}$ kidney (Fig. 11B). Consistent with the western blot analysis, *p65*$^{+/-}$;*Ercc1*$^{-/\Delta}$ livers displayed significantly reduced IL-6 and TNF-α expression, but with p21 and p16 remaining unaltered (Fig. 11C). Taken together, genetic reduction of ATM kinase led to an delayed aging symptoms as well as reduced cellular senescence *in vivo*. Moreover, our data suggest that NF-κB may be a direct downstream effector of ATM.

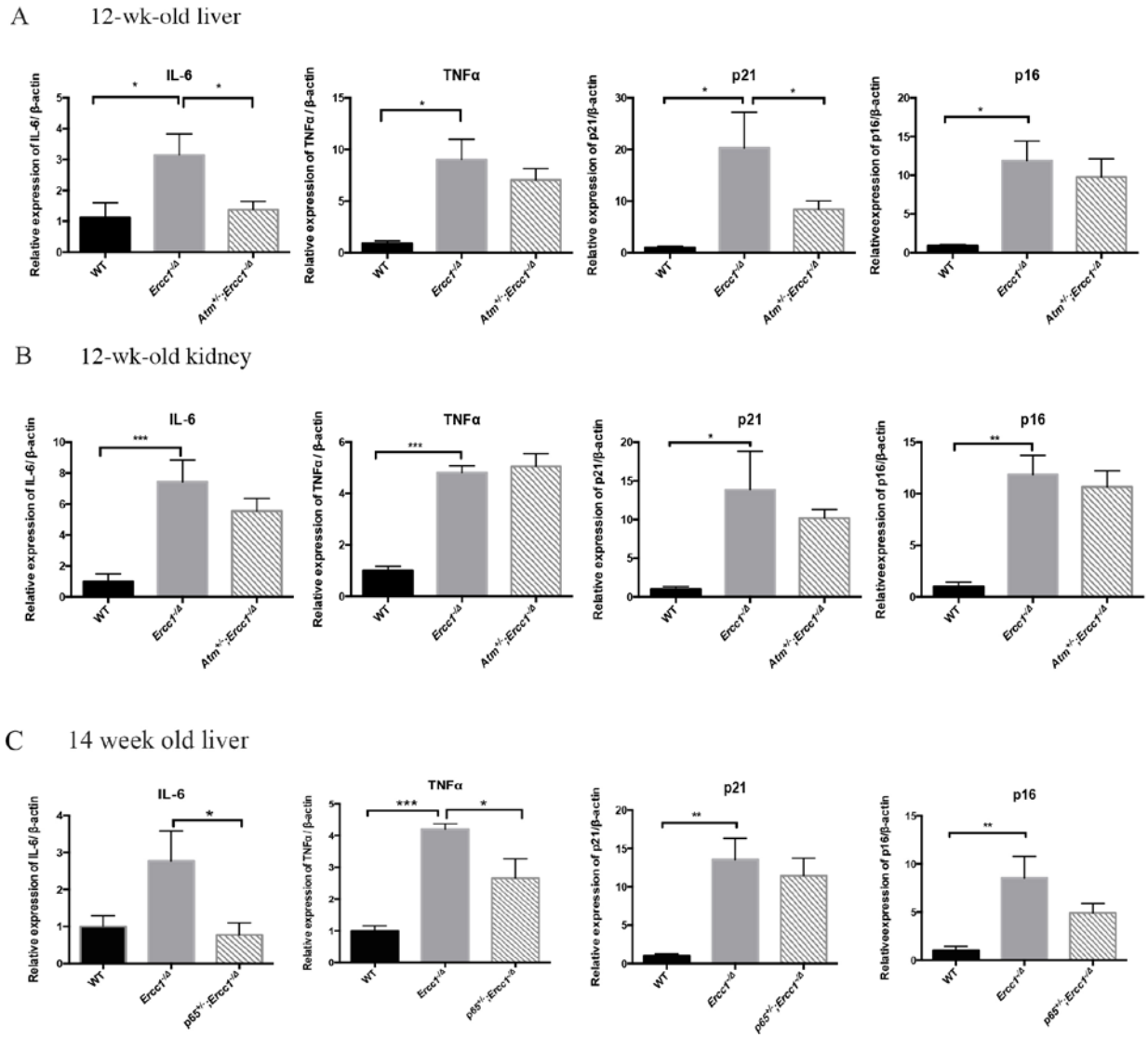

Figure 11: Cellular senescence is reduced in *Atm*$^{+/-}$;*Ercc1*$^{-/\Delta}$ mice. Livers (A) and kidneys (B) from 12-week-old WT, *Ercc1*$^{-/\Delta}$ and *Atm*$^{+/-}$;*Ercc1*$^{-/\Delta}$ mice were analyzed for the expression of p16, p21, IL-6 and TNF-α by qRT-PCR analysis. n=4-6 per group. (C) Livers from 14-week-old WT, *Ercc1*$^{-/\Delta}$ and *p65*$^{+/-}$;*Ercc1*$^{-/\Delta}$ mice were analyzed for p16, p21, IL-6 and TNFα expression by qRT-PCR. n=4-5 per group.

2.3.6 *Atm* haploinsufficiency improves aging-related pathology in tissues

Aging-associated kidney function decline has been noted for decades (183). Aged kidney is characterized by distinct pathological changes, including loss of cortical mass, as well as increased hyalinization, glomerular sclerosis, tubular atrophy and interstitial fibrosis (183). Histological analysis by H&E staining indicated attenuated glomerular sclerosis and tubular atrophy in $Atm^{+/-};Ercc1^{-/\Delta}$ mice, compared to $Ercc1^{-/\Delta}$ mice alone (Fig. 12A). In addition, decline of stem cell function has long been associated with aging (164, 184). We previously reported that muscle-derived stem/progenitor cells (MDSPCs) isolated from $Ercc1^{-/\Delta}$ mice failed to proliferate or differentiate properly. Increased number of myocytes with central nuclei was found in $Atm^{+/-};Ercc1^{-/\Delta}$ mice, suggesting an increased capacity of muscle regeneration *in vivo* (Fig. 12B) (160). Osteoporosis and intervertebral disc degeneration are major degenerative changes that deteriorate progressively with aging. Glycosaminoglycan (GAG), a major proteoglycan in nucleus pulposus (NP) of the disc, is critical in protecting spines from mechanical compressive force and decreases significantly with aging (185). The loss of GAGs also leads to lower back pain and shortened spinal height. Surprisingly, although the disc is an avascular structure, $Atm^{+/-};Ercc1^{-/\Delta}$ mice showed higher levels of GAGs in lumbar spines, consitant with Safranin O staining where proteoglycan was stained red, in comparison to $Ercc1^{-/\Delta}$ mice (Fig. 12C) (186-188). Micro Computed Tomography (CT) analysis of lumber spines demonstrated an alleviated osteoporosis in $Atm^{+/-};Ercc1^{-/\Delta}$ mice compared to $Ercc1^{-/\Delta}$ mice (Fig. 12D). Additionally, oral glucose tolerance test (OGTT) showed that $Atm^{+/-};Ercc1^{-/\Delta}$ mice clear glucose given by oral gavage more rapidly than $Ercc1^{-/\Delta}$ mice (Fig. 12E). Taken together, our results suggest that herterozygosity of *Atm* improves aging pathology and aging-related diseases.

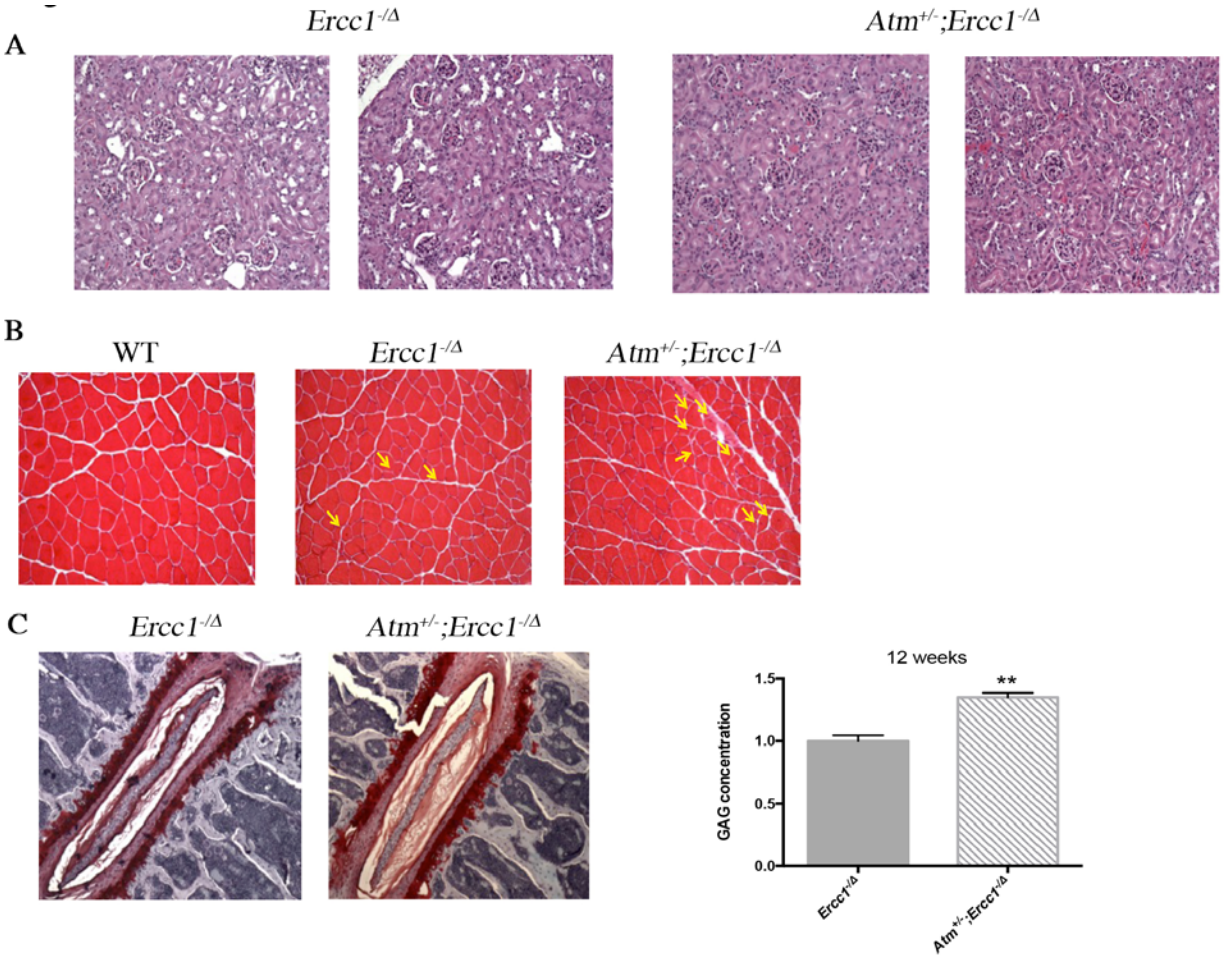
A
Ercc1-/Δ
Atm+/-;Ercc1-/Δ
B
WT
Ercc1-/Δ
Atm+/-;Ercc1-/Δ
C
Ercc1-/Δ
Atm+/-;Ercc1-/Δ
12 weeks
GAG concentration
1.5
1.0
0.5
0.0
**
Ercc1-/Δ
Atm+/-;Ercc1-/Δ
D
WT
Ercc1-/Δ
Atm+/-;Ercc1-/Δ
E
OGTT
Blood Glucose (mg/dl)
200
150
100
50
0
*
*
Ercc1-/Δ(n=5)
Atm+/-;Ercc1-/Δ (n=8)
0'
5'
15'
30'
60'
90'
Time

Figure 12: Genetic reduction of *Atm* improves aging pathology in progeroid *Ercc1*$^{-/\Delta}$ mice.

(A) H&E staining of kidney from 12-week-old *Ercc1*$^{-/\Delta}$ and *Atm*$^{+/-}$*;Ercc1*$^{-/\Delta}$ mice. Representative images of renal cortex were taken at the magnification of 20x. n=2-3 per group. (B) Muscle sections were stained with trichrome to assess the number of myocytes with central nuclei. n=3 each group. (C) Safranin O staining of thoracic discs from 12-week-old *Ercc1*$^{-/\Delta}$ and *Atm*$^{+/-}$*;Ercc1*$^{-/\Delta}$ mice. GAG levels from NP isolated from lumber discs were analyzed. n=3 each group. (D) Representative images of Micro CT analysis of lumber discs from 12-week-old WT, *Ercc1*$^{-/\Delta}$ and *Atm*$^{+/-}$*;Ercc1*$^{-/\Delta}$ mice. (E) OGTT analysis performed in 10-week-old *Ercc1*$^{-/\Delta}$ and *Atm*$^{+/}$*;Ercc1*$^{-/\Delta}$ mice. Blood glucose was measured at 0, 5, 15, 30, 60 and 90 min post dosing of glucose by oral gavage.

2.4 DISCUSSION

The accumulation of DNA lesions has long been considered a critical factor in cellular senescence and aging (96). Human progeroid diseases are closely related to inherited defects in maintaining genome integrity, such as xeroderma pimentosum, Cockayne syndrome, Fanconi anemia and Werner's syndrome (152, 189). Moreover, a recent study indicates that genetic and pharmacologic reduction of ATM could attenuate mutant Huntingtin toxicity *in vivo* and *in vitro*, where increased levels of γH2AX have been implicated (70). Although there is increasing evidence suggesting that ATM kinase is a central mediator of DSB-induced cellular senescence, most studies were done *in vitro* by using inhibitors or RNA interference (RNAi) of ATM (99). Thus, *in vivo* evidence supporting a causal role of ATM in senescence and aging is still lacking and poorly documented. In this study, we demonstrated that genetic reduction of *Atm* i*n vivo* was

able to extend healthspan, attenuate aging-related pathology as well as reduce cellular senescence in a mouse model of progeria, strongly supporting a causative role of ATM in aging.

In our study, *Atm* haploinsufficiency showed substantially reduced NF-κB activation to a similar extent to *p65* heterozygosity in *Ercc1*$^{-/\Delta}$ mice, indicating that ATM kinase is a major activator of NF-κB in the context of DNA-damage mediated senescence and aging. In addition, significant downregulation of SASP factors, especially IL-6 at mRNA level, was discovered in both *Atm*$^{+/-}$*;Ercc1*$^{-/\Delta}$ and *p65*$^{+/-}$*;Ercc1*$^{-/\Delta}$ mice. These findings support previous studies reporting that ATM activation and perisistent DDR signaling are required for the SASP phenotype, secreting inflammatory cytokines (62, 99). Notably, *p65* heterozygosity exhibited a stronger inhibition on IL-6 and TNF-α expression compared to *Atm* heterozygosity, suggesting the existence of an ATM-independent parallel pathway. A previous study suggested that extensive DSBs could lead to an ATM- and NEMO-dependent primary activation of NF-κB which induces the production of TNF-α (190). TNF-α in turn, via RIP1, triggers a second wave of NF-κB activation, as well as JNK3/AP-1 pathway (190). Thus we speculate that *Atm* haploinsufficiency only dampens the primary activation of NF-κB, while p65 heterozygosity targets both primary and secondary NF-κB activation, conferring a stronger inhibition of the SASP phenotype.

Persistent DNA damage-mediated DDR signaling, in particular ATM activation, has been demonstrated to be essential for the SASP phenotype *in vitro*. However, mediators bridging ATM with SASP factors are still poorly identified (99). Miyamoto *et al.* previously revealed a novel NF-κB pathway in response to genotoxic stress, which requires the involvement of a nuclear translocated ATM-NEMO complex (4). In line with this, Osorio *et al.* reported increased ATM phosphorylation and nuclear-localized NEMO in *Zmpste24*$^{-/-}$ mice, where accumulated prelamin A led to a perturbation of NF-κB signaling, suggesting the involvement of an ATM-

and NEMO-dependent NF-κB pathway (138). However, recently a novel mechanism was raised by Kang et al. revealing that GATA4 might be one of the central mediators connecting DDR signaling to NF-κB, and further leading to the senescent SASP phenotype (191). In our study, we observed increased nuclear localization of NEMO in *Ercc1*$^{-/-}$ MEFs, which could be ablated by ATM inhibitor. This finding supports an activation of ATM- and NEMO-dependent NF-κB pathway in response to chronic DNA damage. However, simultaneous involvement of GATA4 cannot be excluded without further testing of TRAF3IP2 and GATA4.

Chronic low-grade inflammation locally and systemically has been linked to aging and multiple aging-related diseases, highlighting a pathological role of NF-κB activation, which transcriptionally regulates most inflammatory mediators (175). In addition, SASP factors secreted by senescent cells lead to an elevation of circulating pro-inflammatory cytokines, which further promotes many manifestations of aging-related pathology, such as sarcopenia, muscle wasting and insulin resistance (175, 192). Elevated levels of IL-6 and TNF-α have been observed in numerous aging-related diseases (175, 193). Anti-inflammatory treatments, such as nonsteroidal anti-inflammtory drug (NSAID), resveratrol, aspirin and metformin, have been suggested to improve frailty (194-197). Moreover, caloric restriction (CR), which is the most robust non-genetic anti-aging intervention across species, and physical exercise, have been shown to suppress chronic systemic inflammation (175, 198, 199). In line with these studies, we found significantly attenuated kidney pathology, improved stem cell function and alleviated disc degeneration, supporting a pathological role of NF-κB in aging-related diseases.

Although *Atm*$^{+/-}$*;Ercc1*$^{-/\Delta}$ mice phenocopy *p65*$^{+/-}$*;Ercc1*$^{-/\Delta}$ mice in many aspects of aging molecularly and phenotypically, interestingly we found significant reduction of p21 expression only in *Atm*$^{+/-}$*;Ercc1*$^{-/\Delta}$ mice. This is consistent with current evidence that ATM/ATR-mediated

DDR signaling is responsible for the activation of p53/p21 pathway, leading to a CDK2-dependent cell cycle arrest in G1 (200). However, whether ATM/ATR directly activates the p16/Rb pathway remains unknown. Our results showed no significant downregulation of p16 expression in *Atm*$^{+/-}$;*Ercc1*$^{-/\Delta}$ mice, while p21 expression was dramatically reduced by 50%. This evidence is in agreement with previous studies that ATM activation regulates p53/p21 in aging. In addition, our finding suggests no direct regulation of p16/Rb by ATM or DDR signaling. SASP factors have been linked to the regulation of senescence and aging through unknown mechanisms. Conditional medium from senescent cells was demonstrated to induce secondary senescence in cell culture (165). An observation that senescent hepatocytes clustered together in mouse livers also confirmed a paracrine effect mediated by SASP factors (165, 166). It has been previously reported that conditional medium from senescent cells induced a full senescence response, including the activation of p16 and p21 and elevated levels of DNA damage (165, 166). However, our data showed no reduction in γH2AX level or p16 and p21 expression in *p65*$^{+/-}$;*Ercc1*$^{-/\Delta}$ mice. Thus it is plausible that NF-κB-mediated SASP factors do not directly upregulate p53/p21 and p16/Rb pathways in senescence and aging.

Increasing evidence indicates that ATM, in addition to its nuclear functions regulating DNA repair machinery, also plays important roles in the cytoplasm (75). Previous studies indicated a cytoplasmic function of ATM that negatively regulated the mammalian target of rapamycin complex1 (mTORC1) via tuberous sclerosis complex 2 (TSC2), thus promoting autophagy and suppressing cell growth in response to ROS (53, 75, 79). In addition, a small fraction of ATM has been identified in mitochondria, linking ATM to aberrant mitophagy (53, 78, 80). Thereby it would be of great importance to characterize the impact of ATM reduction on mTORC1 signaling in response to ROS, given that oxidative stress is a major culprit of aging.

More importantly caloric restriction (CR) and rapamycin treatment inhibiting mTORC1 have been demonstrated to robustly prolong lifespan (201).

Our results suggest that ATM acts as the main stimulus of NF-κB activation in DNA damaged-induced senescence and aging. Genetic reduction of *Atm* could extend healthspan, reduce cellular senescence as well as alleviate aging-related pathology, suggesting a causal role of ATM activation/DDR in aging. Our study also supports an activation of genotoxic stress-mediated NF-κB pathway in *Ercc1*$^{-/\Delta}$ mice which is ATM- and NEMO-dependent. Taken together, our results suggest that ATM/NF-κB may be potential therapeutic targets for improving frailty and aging-related diseases.

3.0 DEVELOPMENT OF NOVEL NEMO-BINDING DOMAIN MIMETICS FOR INHIBITING IKK/NF-κB ACTIVATION

3.1 INTRODUCTION

Nuclear factor κB (NF-κB) is a transciption factor important for regulating immune responses, cell proliferation, apoptosis, embryonic development, senescence and cancer (3). In mammalian cells, NF-κB family is comprised of five subunits, RelA/p65, RelB, C-Rel, p50 (p105/NF-κB1) and p52 (p100/NF-κB2), all containing a Rel-homology domain (RHD) required for homo- or hetero-dimerizaiton (3). NF-κB dimers are sequestered in the cytoplasm by an inhibitory protein IκBα, which masks the conserved nuclear localization sequence (NLS) on RelA/p65 to prevent nuclear translocation (3). Upon stimulation, IκBα undergoes phosphorylation, polyubiquitination and proteasome-mediated degradation, and eventually releases the NF-κB dimers to the nucleus (3). Nuclear-translocated NF-κB dimers up- or down-regulates target gene expression by binding to the κB enhancer or promoter elements (3). Inducers of NF-κB activity include pro-inflammatory cytokines, including tumor necrosis factor α (TNF-α), interleukin-1 (IL-1), lipopolysaccharide (LPS), T-cell receptor (TCR) ligands and genotoxic and oxidative stress (3).

NF-κB activation is regulated by the IκB kinase (IKK) complex, comprised of two identified catalytic subunits, IKKα and IKKβ, and a regulatory subunit NEMO/IKKγ (10, 20, 38). The domains in IKKα and IKKβ, required for the assembly of IKK complexes by facilitating

association with the α-helical region in N-terminus of NEMO, reside in the C-termini (11). An 11 amino acid peptide derived from the NEMO binding domain (NBD) of IKKβ, amino acids 735-745, is able to disrupt the association of IKKβ and NEMO and reduced NF-kB activation when fused to a protein transduction domain (PTD) for intracellular delivery (11).

Duchenne muscular dystrophy (DMD) is an X-linked recessive inherited disease caused by the deficiency of dystrophin (202). Respiratory and cardiac failures are the primary causes of death in DMD patients in their 20's due to progressive muscle wasting (203). Dystrophic muscle is characterized by necrosis, inflammatory infiltration, muscle degeneration and fibrosis (203). A role of NF-κB dysregulation in the pathogenesis of muscle dystrophy is previously established via p65 haploinsufficiency and conditional deletion of IKKβ, both of which improved the muscular pathology and muscle function (48, 204). It is becoming clear that the persistent secondary inflammation and extensive necrosis mediated by NF-κB cause the consecutive degeneration and regeneration cycles in satellite cells, which eventually lead to an exhaustion of their regenerating capacity and the irreversible muscle dystrophy (203). Thus, alleviation of NF-κB-mediated chronic inflammation prevents the exhaustion of satellite cells and substantially improves the outcome of this genetic disease.

LPS stimulates the canonical NF-κB pathway through toll-like receptor 4 (TLR4) via the adaptor protein myeloid differentiation primary response gene 88 (MyD88), regulating the production of various inflammatory cytokines and chemokines (205). The systemic endotoxemia induced by acute LPS administration can lead to multiple organ failure, in particular acute lung injury (ALI) (206). ALI is mainly characterized by lung edema and impaired pulmonary function, which are mediated by neutrophil infiltration and a pro-inflammatory response. The elevation of pro-inflammatory mediators, adhesion molecules, inducible nitric oxide synthase

(iNOS) and cyclooxygenase-2 (COX-2) occurs rapidly as early as 1hr, and maintains for 4 to 6 hour post LPS administration (207, 208). Thus, this model was employed in our study to determine the inhibitory effects of NBD mimetics in an acute inflammatory model.

The NBD peptide has strong therapeutic effects in various inflammatory disease models in mice and other species. Chronic, systemic administration of NBD peptide attenuates macrophage-mediated muscle necrosis and degeneration in *mdx* mice, a murine model of Duchenne muscular dystrophy (DMD) (48, 209), as well as in the golden retriever muscular dystrophy (GRMD) canine model of DMD (52). Similarly, the NBD peptide ameliorates active chronic colitis in IL-10-deficient mice without affecting NF-κB basal activity when administered systemically (47). Intra-articular injection of NBD peptide also attenuates synovial inflammation and the severity of arthritis in a rat model of adjuvant arthritis (210). It also ameliorates inflammation-induced osteoclastogenesis and arthritis by downregulating NF-κB target genes, TNF-α and IL-1β (211). Moreover, systemic delivery of the NBD peptide reduces the severity of Parkinson's disease by suppressing nigral microglial activation and reducing dopaminergic neuronal loss as well as alleviates nephropathy and atherosclerosis in Type 1 diabetic mice (46, 49, 212). In addition, the peptide prevents an LPS-induced pulmonary inflammation in sheep and improves pulmonary function in a piglet model of acute respiratory distress syndrome by topical administration (213, 214). Also, clinical testing of the NBD peptide for local treatment of canine diffuse large B-cell lymphoma revealed a reduction in the proliferation of malignant B cells (51).

Despite these strong and varied therapeutic effects of PTD-NBD peptides in animal models, the expense of peptide synthesis, the short half-life of the peptide and its lack of oral bioavailability limit its clinical use. Thus the goal of this study was to develop small molecules that mimic the NBD peptide, targeting the NEMO binding domain of IKKβ to disrupt its binding

to NEMO. An *in silico* screen for structural similarity was conducted using a pharmacophore model based on the crystal structure of IKK complexes to identify novel NBD mimetics (42). Following multiple round of optimization, several compounds were demonstrated to significantly inhibit LPS- and TNFα-induced NF-κB activation by disrupting the association between IKKβ and NEMO. In addition, these compounds exhibited potent therapeutic effects in murine models of LPS-induced endotoxemia and Duchenne muscular dystrophy, suggesting their potential as therapeutic drugs for clinical management of diseases driven by IKK/NF-κB activation.

3.2 METHODS

3.2.1 Cells and mice

HEK293 cells were grown in Dulbecco's Modification of Eagles Medium (with 4.5g/L glucose and L-glutamine), supplemented with 10% fetal bovine serum, penicillin and streptomycin. Raw264.7 cells were cultured in RPMI-1640 media containing 10% heat-inactivated fetal bovine serum, penicillin and streptomycin. C57BL/10ScSn-*Dmd*^{mdx}/J and female C57BL/6 mice were purchased form the Jackson Laboratory. Mice were housed in the animal facilities of Scripps Florida under constant temperature and humidity. Animal protocols used in this study were approved by Scripps Florida Institutional Animal Care and Use Committees. Three week-old sex-matched mdx mice were dosed with SR12343 (30 mg/kg), SR1246 (30 mg/kg), 8K-NBD peptide (10 mg/kg) or vehicle by intraperitoneal (i.p.) injection 3 times per week for 4 weeks. Mice were sacrificed at 7 weeks of age by carbon dioxide inhalation and tibialis anterior was collected for histological analysis.

3.2.2 8K-NBD peptide and small molecules

8K-NBD (KKKKKKKKGGTALDWSWLQTE) peptide was synthesized at the peptide core facility of University of Pittsburgh. For i.p. injections, peptide was dissolved in 10% DMSO in PBS. The SR small molecules were designed and synthesized by Dr. Kamenecka lab at Scripps Florida. They were formulated in 10:10:80 of DMSO:Tween 80:Water for *in vivo* administration. ZINC small molecules were purchased from. All stock solutions for *in vitro* experiments were prepared in DMSO at 40 μM.

3.2.3 LPS-induced acute lung inflammation

LPS (strain O111:B4) was prepared in PBS at a sub-lethal dose of 10 mg/kg. 8-10 weeks old female WT mice (20-30 g) were dosed i.p. with vehicle, NBD peptide (10 mg/kg) or small molecules (10 mg/kg) for 30 min and followed by i.p. injection of saline (1 ml/kg) or LPS (10 mg/kg). Mice were euthanized 2-4 hr post-treatment and lung was collected for further analysis.

3.2.4 Functional grip strength analysis

Seven week-old treated or untreated mdx mice were measured for forelimb grip strength using a digital grip strength meter paired with a metal grid (Bioseb). Mice were allowed to grip the metal grid tightly and readings were obtained by gently pulling the tail backward until release. Five sequential measurements were performed and the average force was calculated.

3.2.5 Firefly luciferase assay

HEK293 cells stably transfected with luciferase reporter plasmid driven by NF-κB were seeded in 96-well plate in triplicate and pretreated with DMSO or varying small molecules at indicated concentration for 30 min, followed by the stimulation of 10 ng/ml of TNFα for 3 hr. Cell were washed with PBS once and harvested in passive lysis buffer. Luciferase assay (Promega) was performed using a luminometer according to the manufacturer's instructions.

3.2.6 Dual-luciferase reporter assay

Blank HEK293 cells grown in 10 cm plates were co-transfected with co-reporter of Renilla plasmid driven by SV40 and luciferase plasmid driven by NF-κB at the ratio of 1:3 with Lipofectamine 2000 (Invitrogen). Transiently transfected HEK293 were grown and treated as described above and subjected to a dual-luciferase reporter assay according to the manufacturer's instruction. Firefly luciferase activity was normalized to Renilla luciferase to get the relative luciferase activity.

3.2.7 MTT assay

HEK293 cells were grown in a 96-well plate at 3×10^4 cells/well in triplicate and treated with DMSO or varying small molecules at indicated concentration for 24 hr. Cell survival was determined by adding 20 ul of 5 mg/ml MTT (thiazolyl blue tetrazolium bromide) to each well followed by incubation for 3hr in an 37^oC incubator. Media was removed and purple formazan

was dissolved in 100 ul of DMSO. Absorbance was measured at 590 nm on a microplate reader (Perkin Elmer). Cell viability was calculated by normalizing values to untreated control.

3.2.8 Western blot

HEK293 cells grown in a 6-well plate at 1 x 10^6 cells/well were left untreated or treated with 100 μM of ZINC12909780 or ZINC3369392 for 30 min, followed by 10 ng/ml of TNFα for 0, 5 and 10 min. Cells were then harvested for western blot. Cell lysate was prepared in RIPA buffer (20 mM Tris-HCl (pH 7.5), 150 mM NaCl, 1 mM Na^2EDTA, 1 mM EGTA, 1% NP-40, 1% sodium deoxycholate, 2.5 mM sodium pyrophosphate, 1 mM beta-glycerophosphate, 1 mM Na_3VO_4, 1 μg/ml leupeptin, 1X protease inhibitor cocktails (sigma) and 1X Halt phosphatase inhibitor cocktail (Thermo)). 30 ug of protein was resolved by MINI-PROTEAN TGX 4-15% SDS-PAGE. Blots were blocked in 5% non-fat milk. Primary antibodies were incubated at 4^{o}C overnight and secondary antibodies were incubated at room temperature for 1 hour. Anti-p-IκBα (1:1000 CST) and anti-IκBα (1:2000 CST) were used to assess NF-κB activation. Anti-GAPDH (1:5000 CST) was used as a loading control.

3.2.9 Immunoprecipitation of endogenous IKKβ and NEMO

HEK293 or Raw264.7 cells were seeded at 1 x 10^6 cells/well in 6-well plates and treated with vehicle, small molecule or NBD peptide for indicated time. Cells were lysed in NP-40 lysis buffer supplemented with 1X protease inhibitor cocktails (sigma). Protein was immunoprecipitated by incubating 150 μg of lysate with 1 μg of anti-NEMO antibody (Santa Cruz) on a rotating shaker at 4^{o}C for 4 hrs, followed by incubation with 20 ul of Protein A

agarose beads (ThermoFisher) for 1hr. Beads were washed in NP40 buffer 3 times and PBS once. Protein was then denatured in SDS-sample buffer and resolved by MINI-PROTEAN TGX 4-15% SDS-PAGE. Anti-IKKβ (1:1000 CST) was used to assess binding of IKKβ to NEMO and anti-NEMO (1:1000 CST) or IgG were used to as a loading control.

3.2.10 Electrophoretic mobility shift assay (EMSA)

Cytoplasmic and nuclear fractions were extracted using the NE-PER nuclear and cytoplasmic extraction reagents (ThermoFisher) according to the manufacturer's instructions. The gel shift assay was performed by following the previously described method (215). In brief, 5 μg of nuclear extract was incubated with gel shift binding buffer and an a-^{32}P-deoxycytodine triphosphate–radiolabeled NF-κB probe for 20 min at room temperature (MP Biomedicals). The oligonucleotide sequences are as follows: NF-κB template, 5′-CAGGGCTGGGGATTCCCCATCTCCACAGTTTCACTTC-3′; NF-κB annealing, 5′-GAAGTGAAACTGTGG-3′. The reaction product was separated on a 6% non-denaturing polyacrylamide gel.

3.2.11 Quantitative reverse transcription-polymerase chain reaction

Snap frozen tissues were preserved in RNAlater RNA stabilization solution (ThermoFisher) before processed. Total RNA was extracted from cells or tissues using TRIZOL reagent (Life Technologies) and 1500 ng of messenger RNA (mRNA) was subjected to synthesize complementary DNA (cDNA) using SuperScript VILO cDNA synthesis kit. qRT-PCR was performed in a StepOnePlus Real-Time PCR system using Platinum SYBR Green qPCR

SuperMix-UDG (ThermoFisher). Target gene expression was calculated using the comparative C_T method ($\Delta\Delta C_T$) and normalized to an internal control gene Actb (β-actin). Primers used are as follows: *Ptgs2* (COX-2) forward: ACTCATAGGAGAGACTATCAAG; *Ptgs2* (COX-2) reverse: GAGTGTGTTGAATTCAGAGG; *Nfkbia* (IκBα) forward: CAGAATTCACAGAGGATGAG; *Nfkbia* (IκBα) reverse: CATTCTTTTTGCCACTTTCC; *Il1b* (IL-1β) forward: GGATGATGATGATAACCTGC; *Il1b* (IL-1β) reverse: CATGGAGAATATCACTTGTTGG; *Nos2* (iNOS) forward: TGAAATCCCTCCTGATCTTG; *Nos2* (iNOS) reverse: CCATGTACCAACCATTGAAG; *Tnf* (TNF) forward: CTATGTCTCAGCCTCTTCTC; *Tnf* (TNF) reverse: CATTTGGGAACTTCTCATCC; *Il6* (IL-6) forward: AAGAAATGATGGATGCTACC; *Il6* (IL-6) reverse: GAGTTTCTGTATCTCTCTGAAG. *Actb* (β-actin) forward: GATGTATGAAGGCTTTGGTC; *Actb* (β-actin) reverse: TGTGCACTTTTATTGGTCTC;

3.2.12 Enzyme-linked immunosorbent assay (ELISA)

Raw264.7 cells were grown in a 96-well plate and pretreated with vehicle, IKKi VII (2 uM) and small molecules (at indicated concentration) for 1hr, followed by the stimulation with 1 ug/ml of LPS. Supernatant was collected 24 hr later for ELISA analysis. IL-6 concentration was measured using a mouse IL-6 ELISA kit (BD) according to the manufacturer's instructions.

3.2.13 Hematoxylin and eosin (H&E) staining

Tissues fixed in 10% neutral buffered formalin (NBF) overnight were imbedded in paraffin. Tissue was sectioned at 5 μm using a microtome. H&E staining was conducted following a standard protocol (REF).

3.2.14 Pharmacokinetics study

The pharmacokinetic profile of the NBD Mimetics was determined in male C57BL/6J mice (n=3). The drugs were formulated in 10:10:80 of DMSO:Tween 80:water and were dosed by intraperitoneal injection at a final dose of 10 mg/kg. Blood, brain, muscle, spleen, and liver were collected 2 hr post-treatment and were analyzed by mass spectrometry by following the protocol described in ref. 215 (216).

3.2.15 Pharmacophore Model Generation

X-ray structure of the complex NEMO/IKKβ retrieved from the Protein Data Bank [PDB ID: 3BRV], was used to generate a structure-based pharmacophore model (42). The three-dimensional (3D) pharmacophore model was created with LigandScout (217, 218) and was based on interactions that define the protein-protein interaction, such as hydrophobic interactions, hydrogen bonding, and electrostatic interactions. Features identified by the LigandScout software are those that take into consideration chemical functionality but not strict structural topology or definite functional groups. As a result, completely new potential pharmacons can be identified through database screening. Moreover, to increase the selectivity,

the LigandScout model includes spatial information regarding areas inaccessible to any potential ligand, thus reflecting possible steric restrictions. In particular, excluded volume spheres placed in positions that are sterically not allowed are automatically added to the generated pharmacophore model. In this way, the structure-derived pharmacophore model contains the pharmacophore elements of the candidate ligands in response to the protein's active site environment.

3.2.16 Similarity Search

The morphological similarity is a similarity technique dependent only on surface shape and charge characteristics of ligands (219). Morphological similarity is defined as a Gaussian function of the differences in the molecular surface distances of two molecules at weighted observation points on a uniform grid. The computed surface distances include both distances to the nearest atomic surface and distances to donor and acceptor surfaces. This function is dependent on the relative alignment of the molecules, and consequently their alignment and conformation must be optimized. The conformational optimization problem is solved by fragmentation, conformational search, alignment, and scoring, followed by incremental reconstruction from high-scoring aligned fragments. The alignment problem is addressed by exploiting the fact that two unaligned molecules or molecular fragments that have some degree of similarity will have some corresponding set of observers that are seeing the same things. Optimization of the similarity of two unaligned molecules or molecular fragments is enabled by finding similar sets of observers of each molecule that form triangles of the same size (219).

3.2.17 In silico ADME and toxicity screening

Computational modeling tools were used to estimate the bioavailability, aqueous solubility, blood brain barrier potential, human intestinal absorption, the cytochrome P450 (i.e. CYP2D6) enzyme inhibition potential, mutagenicity, and hERG inhibition of the hits obtained from the database screening. The bioavailability, aqueous solubility, and human intestinal absorption were estimated using the Advanced Chemistry Development, Inc. (ACD/Labs)/ADME Boxes software while mutagenicity, hERG and CYP2D6 inhibition were estimated with ACD/Tox screening (ACD Labs, Toronto, Canada) (220).

3.2.18 Statistical analysis

All values were presented as mean+/-S.E.M. Microsoft Excel and Graphpad Prism 6 were used for statistical analysis. Two-tailed Student's *t*-test was performed to determine differences between two groups. When comparing difference in more than two groups, one-way ANOVA (Dunnett test) was conducted. A value of $p < 0.05$ was considered as statistically significant, shown as $*p < 0.05$, $**p < 0.01$, and $***p < 0.001$.

3.3 RESULTS

3.3.1 Generation of a structure-based pharmocophore model using a computational approach based on the conserved interactions between IKKα/β and NEMO

Recognition of small molecules by proteins is largely mediated by molecular surface complementarities (221, 222). Our working hypothesis was that the protein-protein interaction site of NEMO/IKKβ protein complex is a potentially good target for in-silico drug development. To test this hypothesis, we generated a structure-based pharmacophore model. The X-ray structure of the NEMO/IKKβ complex retrieved from the Protein Data Bank [PDB ID: 3BRV] (42), was used to generate a structure-based pharmacophore (Fig. 13A) to investigate the chemical features important in the protein-protein interaction. This was performed using the pharmacophore generation module of LigandScout (217, 218).

Each interacting atom from each residue was “translated” into a pharmacophoric feature, resulting in the structure-based pharmacophore (Fig. 13B). The structure-based pharmacophore model consists of eight features (F1,…, F8) and 13 exclusion volumes (V1, …, V13) representing important atoms from the protein’s environment.

This model was used to screen a subset of the drug-like ZINC 10.0 database set (approximately 3.5 million compounds) (219). We were able to identify 161 hits that matched at least 6 features out of eight (F1, …, F8) of the pharmacophore model. Twenty hits had an RMSD < 1, and were further prioritized using Absorption, Distribution, Metabolism, Excretion, and Toxicity (ADME/Tox) predicted properties. Three compounds have successfully passed these filters and were purchased for biological testing (Fig. 13C).

A

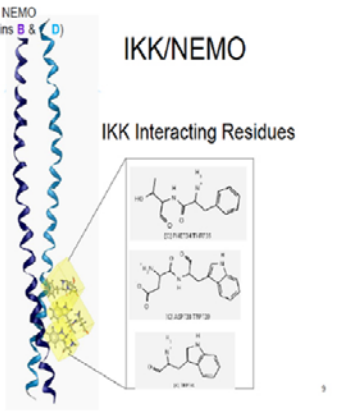

Phe734

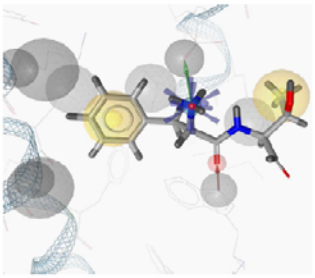

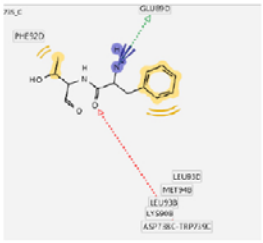

Trp739

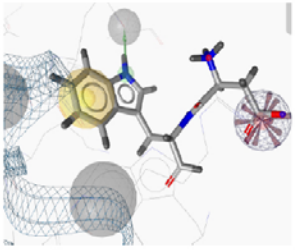

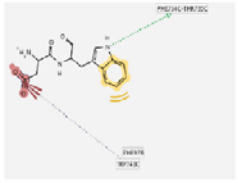

Trp741

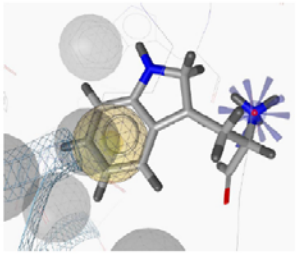

B

F1	Cat&(DonS|DonP)
F2	HydS|HydP
F3	AccS|AccP
F4	HydS|HydP
F5	DonS|DonP
F6	Ani
F7	HydS|HydP
F8	Cat
V1	Excl
V2	Excl
V3	Excl
V4	Excl
V5	Excl
V6	Excl
V7	Excl
V8	Excl
V9	Excl
V10	Excl
V11	Excl
V12	Excl
V13	Excl

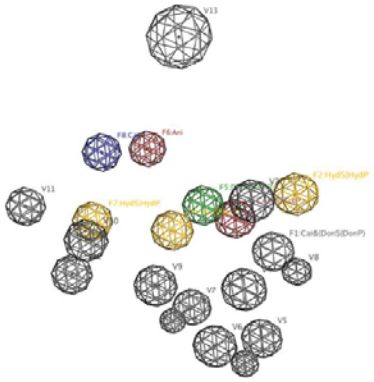

C

ZINC05682947

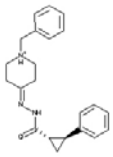

ZINC09327678

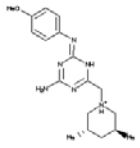

ZINC12909780

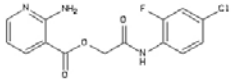

Figure 13: The development of a structure-based pharmacophore model for in *silico* screen of NBD mimetics. (A) Interacting residues extracted from the X-ray structure of the NEMO/IKKβ complex [PDB ID: 3BRV] used in the generation of the structure-based pharmacophore model (42). (B) A three-dimensional representation of the structure-based pharmacophore model. Three hydrophobic groups (F2, F4 and F7 - yellow spheres), one hydrogen-bond acceptor features (F3 - red sphere), one hydrogen-bond donor (F5 - green sphere), one positive ionizable area (F8 – blue sphere), one negative ionizable (F6 – red sphere) and 13 excluded volumes (gray spheres) are shown. (C) Chemical structures of three compounds that entered biological testing (219).

3.3.2 Identification of small molecule inhibitors of NF-κB activation.

To test if the small molecules identified by the *in silico* screen inhibit NF-κB activation, a HEK293 cell line stably expressing a luciferase reporter driven by a synthetic, NF-κB-dependent promoter was utilized. To induce NF-κB activation, cells were treated with 10 ng/ml of TNF-α and harvested three hours post-treatment for analysis of luciferase activity. Treatment with ZINC12909780 slightly downregulated NF-κB activation at a concentration of 100 μM whereas the luciferase activity remained unchanged in cells treated with ZINC05682974 or ZINC09327678 (Fig. 14A). To determine if ZINC12909780 inhibited NF-κB in a dose dependent manner, concentrations were tested at 0, 6.25, 25, 50 and 100 μM. We found that only high concentrations (50 and 100 μM) of the compound were able to inhibit TNF-α-induced NF-κB activation significantly, which is consistent with previous studies that NBD peptide tends to work at higher concentrations compared to kinase inhibitors in cell culture (Fig. 14B).

To identify NBD mimetics with higher biological activity than ZINC12909780 or the NBD peptide, we next screened the ZINC 10.0 database (approximately 3.5 million compounds) *in silico* for structurally similar compounds (223). Fifteen analogs with a similarity score > 90% were identified, and thirteen that passed all the ADME/Tox filters were acquired for testing (Table 1). Four of the compounds, ZINC9642366 (Zinc1), ZINC3369392 (Zinc5), ZINC3269261 (Zinc8) and ZINC3264658 (Zinc9), lowered NF-κB activity robustly while other analogs had minimal effects (Fig. 14C). To rule out the possibility that the reduction observed in luciferase assays was actually caused by drug toxicity, an MTT assay was performed to assess cell viability. Treatment with ZINC8 resulted in 40% of cell death at 24 hours, suggesting that at least part of the reduction in luciferase activity could be attributed to cytotoxicity (Fig. 14D). Since ZINC5 displayed potent NF-κB inhibitory efficacy in cell culture showing little toxicity (less than 10%), it was tested for dose-response inhibition of NF-□B. ZINC5 showed a greater extent of inhibitory effect compared to ZINC12909780 at 50 and 100 μM, with no cell toxicity observed, suggesting a higher efficacy of ZINC5 (Fig. 14E & F).

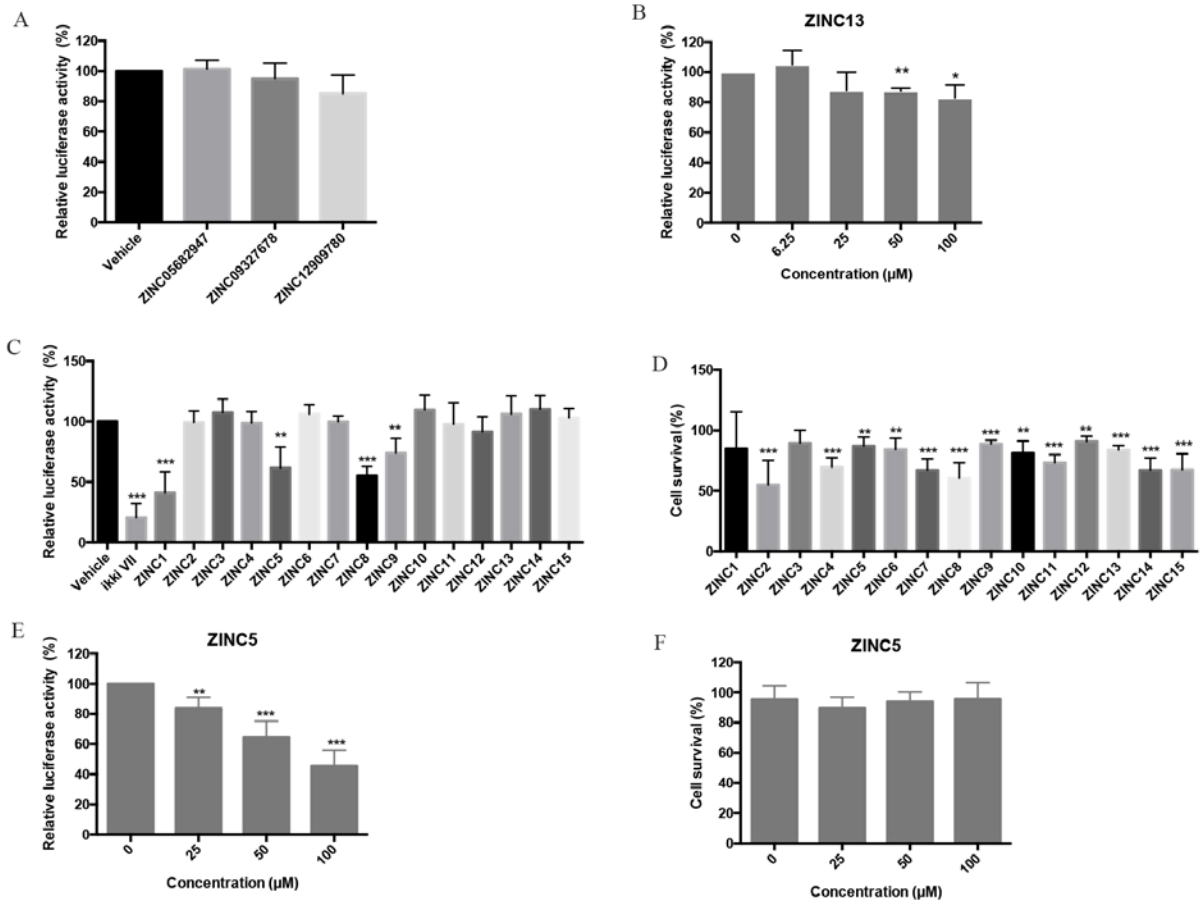

Figure 14: Identification of small molecules that suppress TNF-α-induced NF-κB activation. (A) HEK 293 cells stably expressing NF-κB luciferase reporter were pretreated with indicated small molecules at 100 μM for 30 min, followed by stimulation with TNF-α (10 ng/ml) for 3 hours. Luciferase activity was normalized to untreated stimulated control cells. Data show the mean values of two independent experiments +/- SD. (B) A dose-dependent response of ZINC12909780 was tested by NF-κB luciferase assay in HEK293 cells. Three independent experiments were performed and data shown represent mean +/- SD. (C) NF-κB luciferase assay was performed at 100 μM to screen for small molecules with greater NF-κB inhibitory effect. Data show the pooled results of five independent experiments and are the mean +/- SD. (D) The same HEK293 cells were cultured in the presence of 100 μM of indicated derivatives for 24 hr

and cell survival was determined by MTT assay. Cell viability was calculated by normalizing to untreated cells. (E) Dose-dependent inhibitory effects and (D) drug toxicity were determined for ZINC5 at 0, 25, 50 and 100 μM. HEK293 were cultivated in the presence of ZINC5 at listed concentrations for 24 hr and drug toxicity was assessed by MTT assay. Data represent the mean +/- SD from 4-5 independent experiments.

Table 1: Small molecule derivatives selected from ZINC 10.0 database share structural similarity to ZINC12909780.

ZINC ID	Abbreviation	Popular name	Structure
09642366	ZINC1	(5-chloro-2-pyridyl)carbamoylmethyl	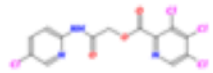
09645305	ZINC2	(3,5-dichloro-2-pyridyl)carbamoylmethyl	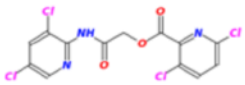
04767282	ZINC3	(5-chloro-2-pyridyl)carbamoylmethyl	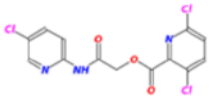
05752323	ZINC4	[3-chloro-5-(trifluoromethyl)-2-pyridyl]carbamoylmethyl	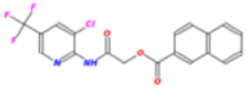
03369392	ZINC5	2-(2-fluorophenyl)acetic-acid-[2-[(5-chloro-2-pyridyl)amino]-2-keto-ethyl]-ester	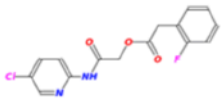
03270295	ZINC6	2-chloronicotin-[2-[(3,5-dichloro-2-pyridyl)amino]-2-keto-ethyl]-ester	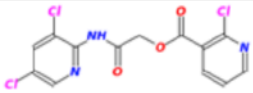
03269263	ZINC7	anthracene-9-carboxylic-acid-[2-[[3-chloro-5-(trifluoromethyl)-2-pyridyl]amino]-2-keto-ethyl]-ester	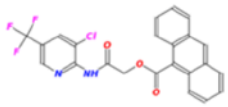
03269261	ZINC8	naphthalene-1-carboxylic-acid-[2-[[3-chloro-5-(trifluoromethyl)-2-pyridyl]amino]-2-keto-ethyl]-ester	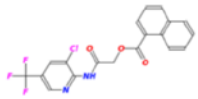
03264658	ZINC9	2-phenylacetic-acid-[2-[(3,5-dichloro-2-pyridyl)amino]-2-keto-ethyl]-ester	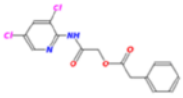
03260222	ZINC10	picolin-[2-[[3-chloro-5-(trifluoromethyl)-2-pyridyl]amino]-2-keto-ethyl]-ester	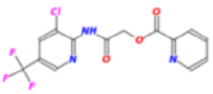
03257323	ZINC11	6-chloronicotin-[2-[(3,5-dichloro-2-pyridyl)amino]-2-keto-ethyl]-ester	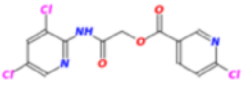
03434956	ZINC12	2,4-difluorobenzoic-acid-[2-[(5-chloro-2-pyridyl)amino]-2-keto-ethyl]-ester	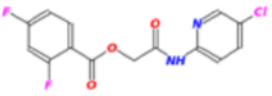

3.3.3 NBD mimetics inhibit NF-κB DNA binding activity.

To confirm that the NBD mimetics reduce IKK activity, the extent of phosphorylation of the IKK target, IκBα, in response to 10 ng/ml of TNF-α was determined by Western blot at 0, 5 and 10 min after TNF-α stimulation. ZINC5 reduced the level of p-IκBα dramatically following stimulation, while ZINC12909780 led to a mild reduction (Fig. 15A). To determine if the mimetics also reduce NF-κB DNA binding activity, electrophoretic mobility shift assay (EMSA) was conducted both *in vitro* and *in vivo*. ZINC5 and ZINC12909780 significantly decreased TNFα-induced NF-κB DNA binding activity at 200 μM in C2C12 cells, a mouse myoblast cell line (Fig. 15B). Similarly, a single ip injection of these two small molecules at 10 mg/kg inhibited NF-κB DNA binding activity in quadriceps in *mdx* mice (Fig. 15C). However, chronic treatment of *mdx* mice with these compounds showed no therapeutic benefit (data not shown).

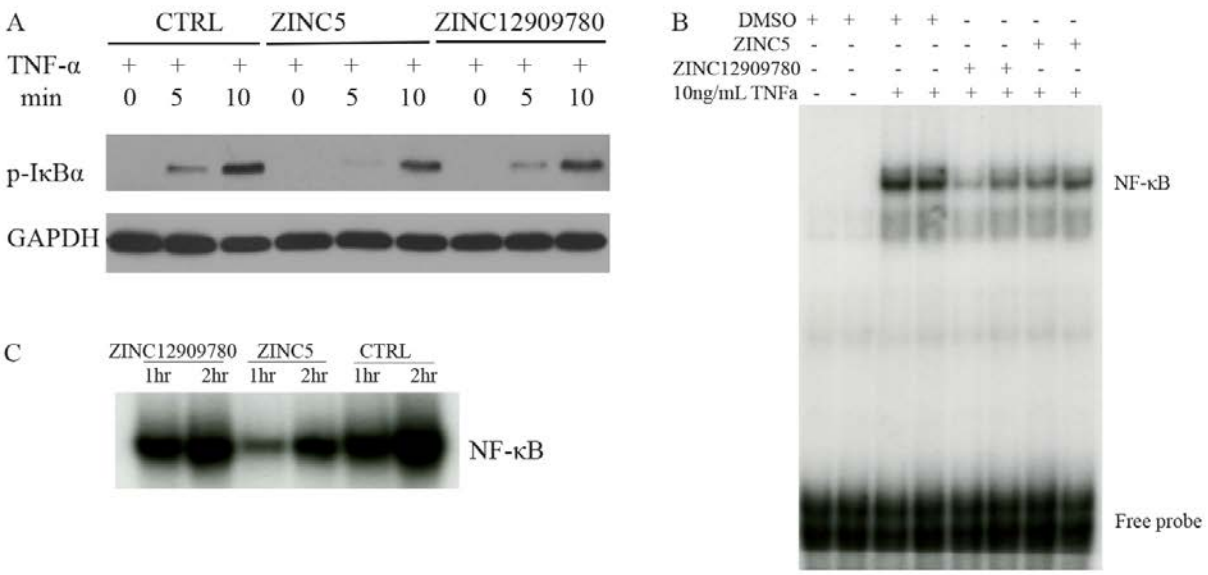

Figure 15: Two identified small molecules reduce NF-κB DNA binding activity *in vivo* and *in vitro*. (A) Levels of p-IκBα with or without treatment in response to TNF-α were determined by western blot analysis. HEK293 cells were pretreated with DMSO, ZINC12909780 and ZINC5 at 100 μM for 30 mins followed by the stimulation of 10 ng/ml of TNF-α for 0, 5 and 10 min. Cell lysates were prepared for immunoblot against p-IκBα. GAPDH was used as a loading control. (B) EMSA analysis detecting NF-κB DNA binding activity was performed in C2C12 myoblasts. Cells were pretreated with 200 μM of DMSO, ZINC12909780 and ZINC5 in serum-free media for 1 hr. TNF-α was then added directly to the media to a final concentration of 10 ng/ml and incubated for 15 min. Nuclear extract was obtained for EMSA analysis. (C) EMSA analysis assessing NF-κB DNA binding activity was performed in quadriceps from *mdx* mice post-treatment. Single dose of ZINC12909780 and ZINC5 at 10 mg/kg was given by i.p. to *mdx* mice. Quadriceps was harvested at 1 hr and 2 hrs post-injection for EMSA analysis.

3.3.4 Optimization of the NBD mimetics

ZINC5 and ZINC12909780 both contain ester bonds, leading to their rapid degradation in the presence of serum (data not shown). Thus seven rounds of structural modification and optimization were performed to improve bioactivity and stability and more than one hundred small molecules were tested (data not shown). Four lead NBD mimetics were identified that showed enhanced inhibitory effects, compared to the original ZINC compounds, including three non-esters, SR12343, SR12460 and SR12454, and one ester SR11481 (Fig. 17A & B). To minimize the influence of drug toxicity on the screening assay, a renilla luciferase reporter driven by the SV40 promoter was cotransfected with the NF-κB luciferase reporter into HEK293 cells as a co-reporter for normalization. Three non-esters showed markedly enhanced inhibition of TNF-α-mediated NF-κB activation: SR12460 with an IC_{50} of 11.34 μM, SR12454 of 20.24 μM and SR12343 of 37.02 μM (Table 2 & Fig. 17B & Fig. 16A). The ester SR11481 only worked at a higher concentration, with an IC_{50} of 45.03 μM, possibly due to the instability of the ester bond (Fig. 17B). To determine whether these more potent, novel NBD mimetics disrupt NEMO and IKKβ binding, co-immunoprecipitation was performed using Raw 264.7 macrophages (Fig. 17C) and HEK293 cells (data not shown). After treatment with the mimetics or NBD peptide, NEMO was immunoprecipitated by an anti-NEMO antibody and IKKβ was immunoblotted to determine the binding of IKKβ to NEMO. The control 8K-NBD peptide was able to disrupt the protein-protein interaction in macrophages at 400 μM (Fig. 17C). All four of the mimetics dissociated IKKβ-NEMO interaction at 100 μM, with SR12343, having the strongest activity (Fig. 17C).

To determine whether the inhibitory effect of the mimetics is TNF-α-dependent, LPS-mediated NF-κB activation via TLR4 was examined to determine a broader inhibitory effect of

the novel NBD mimetics. NF-κB was stimulated in Raw 264.7 by 1 ug/ml of LPS for 2hr and genes transcriptionally regulated by NF-κB were determined by qRT-PCR analysis. Both an IKK active site inhibitor IKKi VII (2 μM) and the 8K-NBD peptide (400 μM) were included as positive controls and the expression of COX2, IL-6, IL-1β, TNF-α, IκBα and iNOS were assessed. SR12460 and SR12454, which are closely structure-related, were able to significantly downregulate the transcription of all NF-κB target genes tested, indicating a comprehensive inhibition of LPS-induced NF-κB activation (Fig. 17D). SR12343 displayed a similar profile to 8K-NBD peptide, showing significant inhibition on COX2, IL-6 and iNOS expression at a much lower concentration (50 μM) compared to NBD peptide (400 μM). SR11481 failed to suppress all NF-κB target genes, likely due to its poor stability. Interestingly, IKKi VII, while able to inhibit most NF-κB target gene expression, failed to downregulate iNOS expression, which was significantly inhibited by the NBD peptide and all non-ester NBD mimetics. This suggests that IKK inhibitors targeting the ATP-binding pocket, likely downregulates the expression of a distinct subset of genes.

To confirm the qRT-PCR result, LPS-mediated IL-6 production was analyzed in Raw 264.7 cells by ELISA. SR12460 and SR12454 were able to decrease mIL-6 production in a dose-dependent manner, decreasing by half at 25 μM and even to a greater extent at 50 μM (Fig. 17E). Similarly, SR12343 suppressed mIL-6 production in a dose-dependent manner. However, SR12343 exhibited a less potent inhibitory effect and required a higher working concentration, which is consistent with the IC_{50} in HEK293 cells. Although SR11481 failed to downregulate IL-6 significantly at the mRNA level, there was reduction in the accumulation of IL-6 protein at 24 hr. Moreover, SR11481 appears to work more efficiently at a lower concentration around 25 μM. Taken together, four lead compounds were identified through seven rounds of optimization and

modification. They exhibited suppression on both TNF-α- and LPS-induced NF-κB activation by blocking NEMO and IKKβ association at a significantly lower concentration than NBD peptide.

Table 2: The IC_{50} of NBD Mimetics.

NBD Mimetics	IC_{50} (μM)
SR12460	11.34
SR12454	20.24
SR12343	37.02
SR11481	45.03

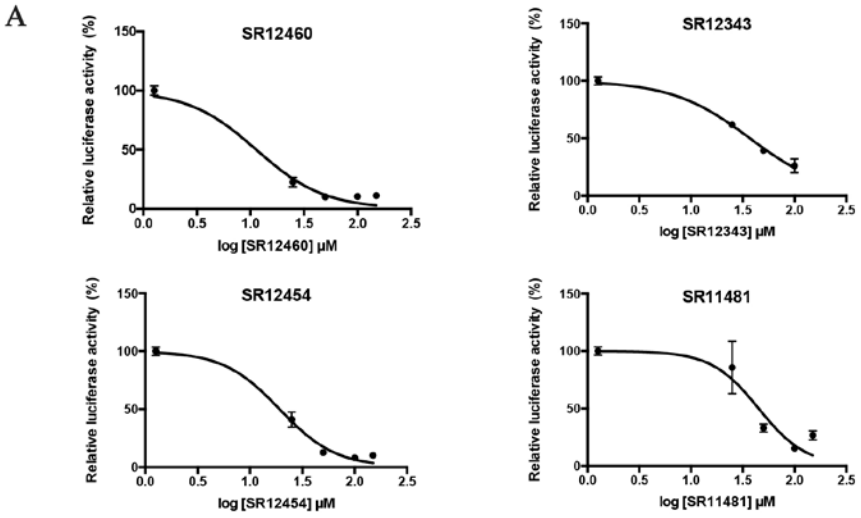

Figure 16: Dose-dependent curve of lead NBD mimetics. (A) Dose-dependent curve of NBD mimetics ranging from 0 to 150 μM was determined by NF-κB luciferase assays in HEK293 cells.

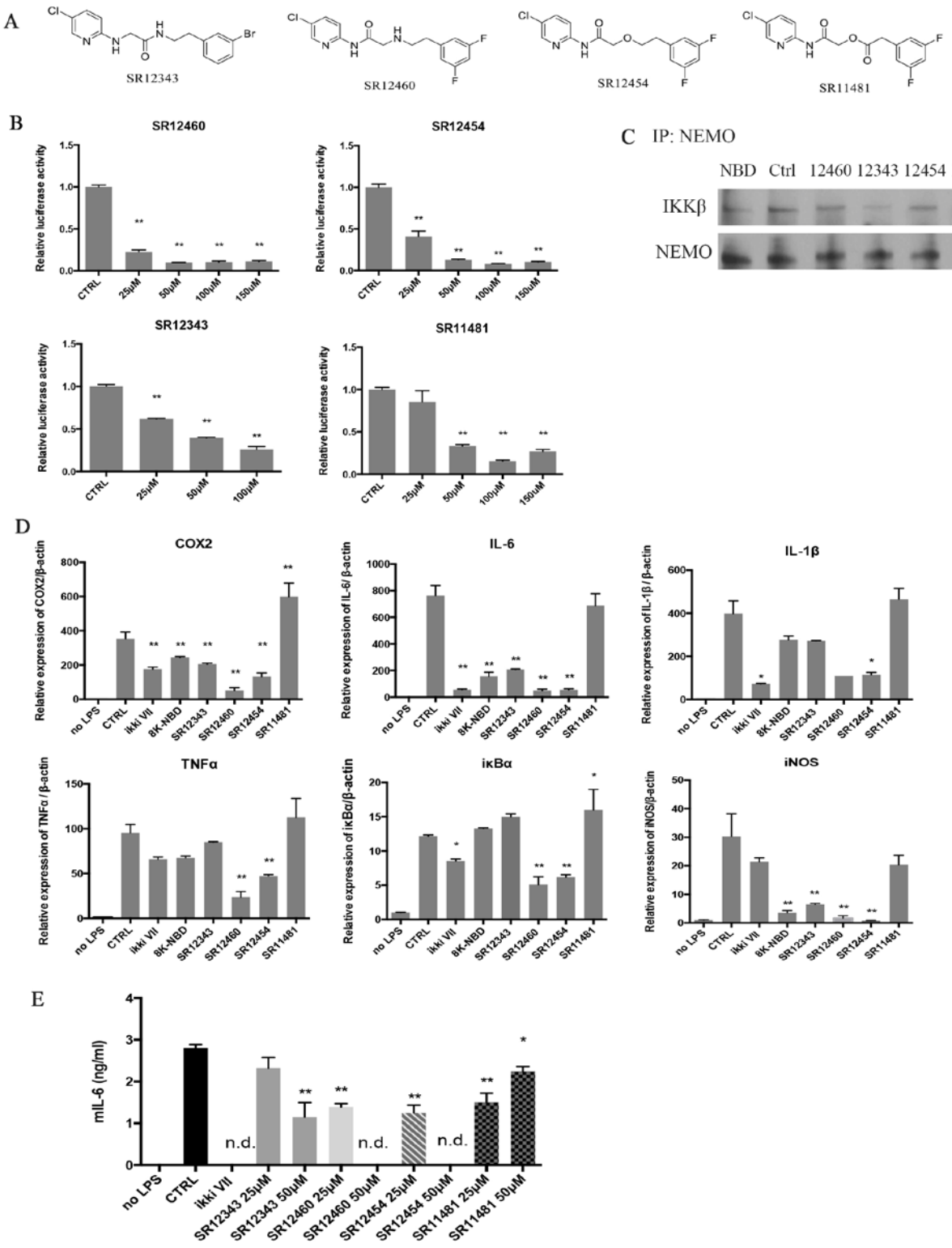
A
SR12343
SR12460
SR12454
SR11481
B
SR12460
SR12454
SR12343
SR11481
Relative luciferase activity
CTRL
25μM
50μM
100μM
150μM
C
IP: NEMO
NBD
Ctrl
12460
12343
12454
11481
IKKβ
NEMO
D
COX2
IL-6
IL-1β
TNFα
iκBα
iNOS
Relative expression of COX2/β-actin
Relative expression of IL-6/ β-actin
Relative expression of IL-1β / β-actin
Relative expression of TNFα / β-actin
Relative expression of iκBα/β-actin
Relative expression of iNOS/β-actin
no LPS
CTRL
ikki VII
8K-NBD
SR12343
SR12460
SR12454
SR11481
E
mIL-6 (ng/ml)
n.d.
no LPS
CTRL
ikki VII
SR12343 25μM
SR12343 50μM
SR12460 25μM
SR12460 50μM
SR12454 25μM
SR12454 50μM
SR11481 25μM
SR11481 50μM

Figure 17: Modified lead NBD mimetics inhibit TNF-α- and LPS-induced NF-κB activation by disrupting the association between NEMO and IKKβ. (A) Structures of top NBD mimetics after seven rounds of optimization and screen. (B) Measurement of NF-κB activation in response to TNF-α by a luciferase assay. HEK293 cells cotransfected with NF-κB luciferase reporter and SV40-Renilla plasmids were pretreated with DMSO or listed small molecules at 0, 25, 50, 100 and 150 μM for 30 min, followed by the induction of TNF-α for 3hr. Dual-luciferase reporter assay was then performed to detect NF-κB luciferase and Renilla luciferase activity sequentially. The relative luciferase activity was calculated by normalizing NF-κB luciferase to Renilla luciferase activity. Data shown are representative of 2-3 independent experiments. (C) Co-immunoprecipitation (Co-IP) analysis detecting protein-protein interaction between IKKβ and NEMO. Raw 264.7 cells were pretreated with indicated drugs, DMSO, 8K-NBD peptide (400 μM), and 100 μM of SR12460, SR12343, SR12454 and SR11481 for 30 min. Cells were then harvested for CO-IP. NEMO was immunoprecipitated from the cell lysate by using an anti-NEMO antibody and the binding product was then subjected to immunoblot probing for IKKβ. NEMO was probed as a loading control. (D) NBD mimetics downregulated the expression of NF-κB target genes in reponse to LPS. Raw 264.7 cells were pretreated with indicated drugs for 30 min and then stimulated with 1 ug/ml of LPS for 2 hrs. Cells were then harvested for RNA extraction and qRT-PCR analysis. Relative expression of target genes was normalized to β-actin. Drug concentrations used are as follows: IKKi VII (2 μM), 8K-NBD peptide (200 μM), SR 12343 (50 μM), SR12460 (50 μM), SR12454 (50 μM) and SR11481 (50 μM). Data are representative of 2 independent experiments. (E) Mouse IL-6 production induced by LPS was downregulated by NBD mimetics. Raw 264.7 cells pretreated with DMSO or drugs at indicated

concentrations were exposed to 1 ug/ml of LPS for 24 hr and supernatant was collected for ELISA analysis of mouse IL-6.

3.3.5 Novel NBD Mimetics suppress LPS-induced acute pulmonary inflammation *in vivo*

To determine the stability of the NBD mimetics *in vivo*, the pharmacokinetics of the compounds was determined in serum following ip injection. SR12460 showed significant stability 2 hr after injection. SR12343 and SR12454 showed moderate stability, whereas SR11481 was extremely unstable with undetectable levels at 2 hr (Fig. 18A). Since SR12454 and SR12460 share very similar chemical structures and SR11481 is extremely unstable *in vivo*, SR12460 and SR12343 were selected for further *in vivo* analysis.

SR12343 and SR12460 initially were tested in an acute model of LPS-induced systemic endotoxemia to determine their NF-κB inhibitory effects *in vivo*. C57BL/6J mice were pretreated with vehicle control, 8K-NBD peptide or NBD mimetics at 10 mg/kg for 30 min, followed by LPS induction at 10 mg/kg (Fig. 18B). Lung and liver were harvested 2-4 hr post-treatment for qRT-PCR analysis of NF-κB target genes. SR12343 was able to downregulate NF-κB transcriptional activity significantly in lung, as demonstrated by the inhibition of iNOS, iκBα, COX2 and IL-6, while leaving TNF-α unchanged (Fig. 18C). Its NF-κB inhibitory effect in liver was less effective compared to lung, inhibiting only COX2 expression significantly (Fig. 18C). Intriguingly, although SR12460 is more stable than SR12343, its inhibition of NF-κB/IKK in liver and lung were less potent compared to SR12343 (Fig. 18C). Taken together, the results demonstrate that SR12343 and SR12460 are effective at attenuating LPS-induced acute lung inflammation by suppressing NF-κB target gene expression.

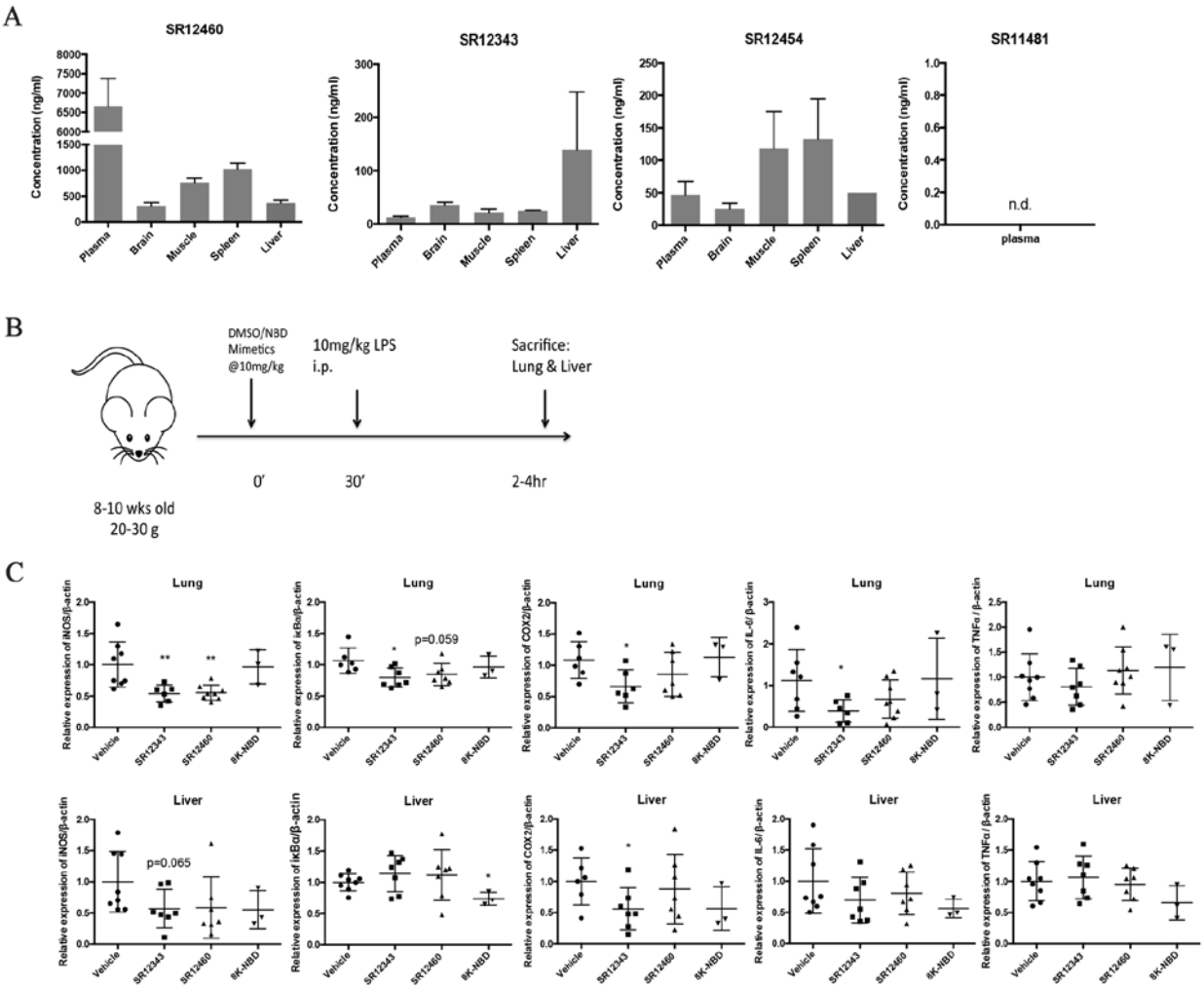

Figure 18: Newly identified NBD mimetics suppress LPS-induced acute inflammation *in vivo*. (A) The bioavailability property of SR12460, SR12343, SR12454 and SR11481. Concentrations of NBD mimetics were determined in plasma, brain, muscle, spleen and liver 2 hrs post a single i.p. injection of 10 mg/kg of drugs. n=3 per group. n.d. means non-detectable. (B) Shown are the model of LPS-induced acute inflammation and the treatment regimen. (C) NBD Mimetics suppressed LPS-induced acute inflammation in lung and liver by downregulating NF-κB target gene expression. Acute inflammation was induced by intraperitoneal injection of 10 mg/kg LPS. Vehicle, SR12343, SR12460 and 8K-NBD peptide were dosed at 10mg/kg 30

min prior to the LPS treatment. Lung and liver were collected 2-4 hr post-LPS injection and analyzed by qRT-PCR. n=3-8 each group.

3.3.6 Novel NBD Mimetics improve muscle pathology in *mdx* mice

Since SR12343 and SR12460 both reduced LPS-induced NF-κB activation *in vivo*, they were further tested in *mdx* mice, a mouse model of Duchenne muscular dystrophy. *Mdx* mice develop normally at birth, and then undergo a massive myonecrosis starting at three weeks. Treatment of *mdx* mice with IKK/NF-kB inhibitors effectively reduces inflammation, block necrosis and increase muscle regeneration. *Mdx* mice were chronically treated with vehicle, SR12343, SR12460 or 8K-NBD starting from day 21, 3 times/week for 4 weeks (Fig. 19A). No significant weight loss was observed in chronically treated *mdx* mice (Fig. 20A). To determine if SR12343 and SR12460 improve muscle pathology, tibialis anterior (TA) muscle was stained with hematoxylin and eosin (H&E) to assess inflammatory infiltration, necrosis, central nucleation and fibrosis. Vehicle treated TA muscles exhibited extensive infiltration and necrosis as reflected by clusters of inflammatory cells, disorganized myofibers and nonuniform staining, with limited muscle regeneration. Consistent with previous studies, 8K-NBD peptide reduced inflammatory cell infiltration and necrosis and also promoted muscle regeneration as shown by centralized nuclei (224, 225). Interestingly, SR12343 treatment led to the most significant pathological improvement, as represented by limited infiltration and enhanced muscle reconstruction (Fig. 19B&C). Similarly, SR12460 treatment partly improved muscle pathology, although not as significant as SR12343. As compared to the control group, qRT-PCR analysis revealed significant improvement of myofiber regeneration in SR12343 treated TA muscle, by increasing expression of eMyHC as well as Pax 7, a marker of skeletal muscle satellite cells (Fig. 19D).

SR12460 and 8K-NBD also increased eMyHC expression, but to a lower extent compared to SR12343. Fiber size in centrally nucleated myofibers and total myofibers were also smaller in mice treated with SR12343 and 8K-NBD, indicating active reconstruction of myofiber during the regenerative phase (Fig. 19E).

To determine muscle strength post-treatment, grip strength test on forelimbs was performed 2 weeks and 4 weeks post-treatment. Compared to vehicle group, SR12343 significantly improved forelimb strength after 2 weeks of treatment, indicating rapid muscle repair and inflammatory flameout. All treatment groups, compared to control, significantly strengthened forelimb muscles 4 weeks post-treatment (Fig. 19F). Taken together, the two lead compounds, SR12460 and, in particular, SR12343, markedly improved muscle function and muscular pathology in *mdx* mice.

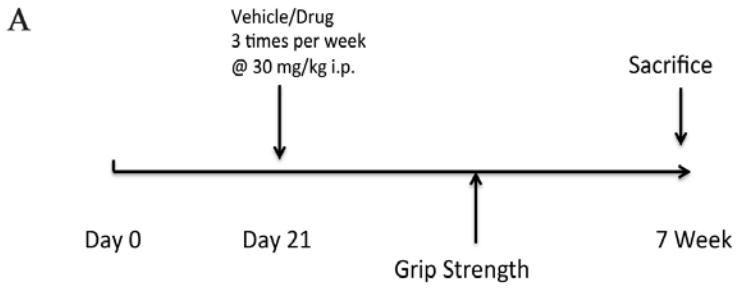
A
Vehicle/Drug
3 times per week
@ 30 mg/kg i.p.
Sacrifice
Day 0
Day 21
Grip Strength
7 Week

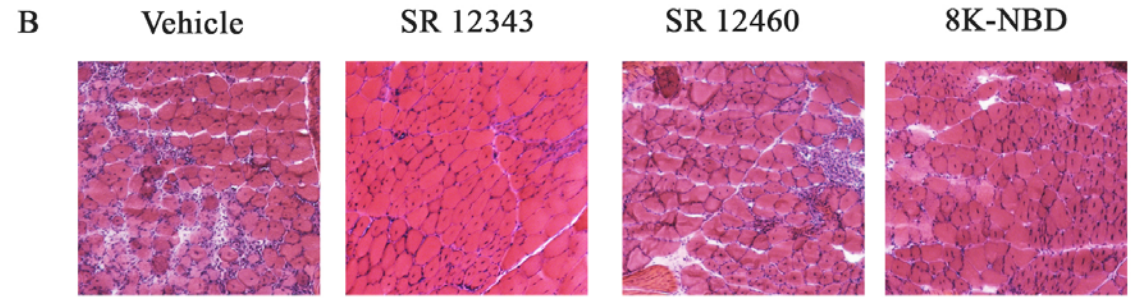
B
Vehicle
SR 12343
SR 12460
8K-NBD

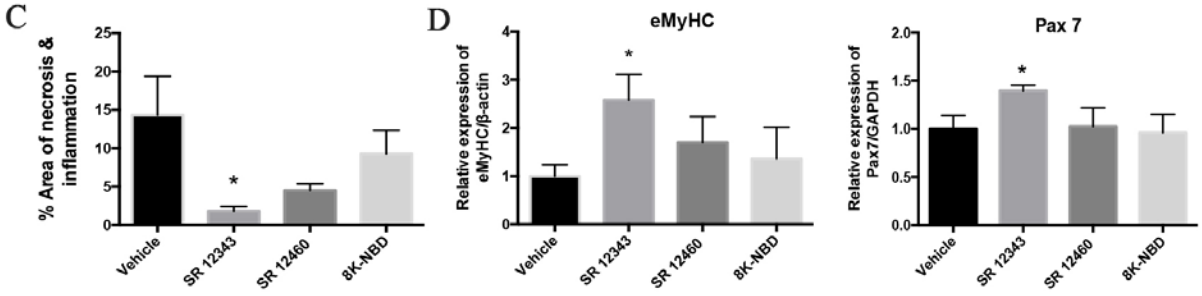
C
% Area of necrosis & inflammation
Vehicle
SR 12343
SR 12460
8K-NBD
D
eMyHC
Relative expression of eMyHC/β-actin
Pax 7
Relative expression of Pax7/GAPDH

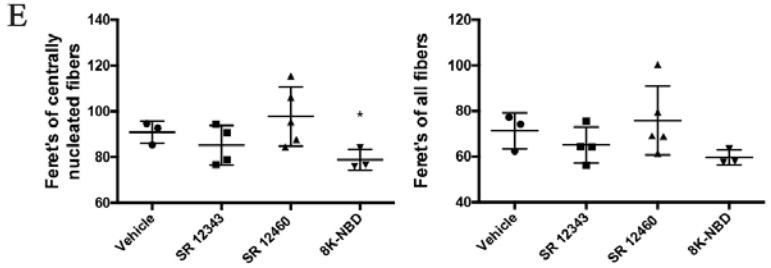
E
Feret's of centrally nucleated fibers
Feret's of all fibers
Vehicle
SR 12343
SR 12460
8K-NBD

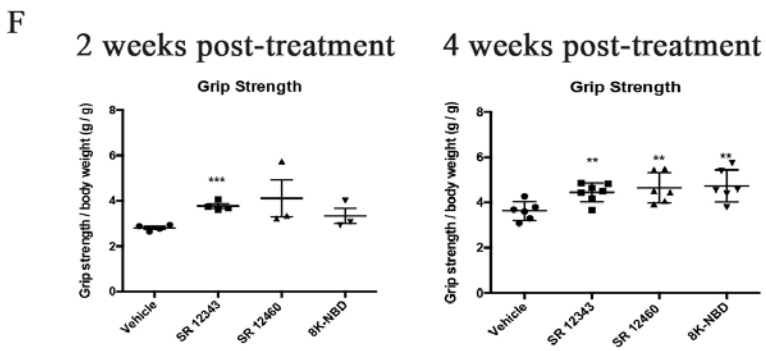
F
2 weeks post-treatment
4 weeks post-treatment
Grip Strength
Grip strength / body weight (g / g)
Vehicle
SR 12343
SR 12460
8K-NBD

Figure 19: NBD mimetics improve muscular pathology and grip strength in *mdx* mice. (A) Shown is the treatment regimen of NBD mimetics in *mdx* mice. (B) H&E staining of tibialis anterior muscle from 7-week-old age-matched *mdx* mice, treated or untreated. Images were taken at the magnification of 10x. Representative images were shown for each treatment group. (C) Quantitation of the percentage of area exhibiting necrosis or infiltration. (D) qRT-PCR analysis of eMyHC and Pax 7 in tibialis anterior muscle. (E) Quantitation of minimum Feret's diameter in centrally nucleated and total myofibers. Myocytes were outlined with laminin staining and were quantified by using Image J. (F) Forelimb force was determined by grip strength test. 5-wk-old (2 weeks post treatment) and 7-wk-old (4 weeks post treatment) *mdx* mice, treated with vehicle, NBD peptide or NBD Mimetics, were tested for forelimb grip strength. Five sequential tests were performed and the force was normalized to body weight. Data were shown as mean +/- SEM. Dosages used are as follows: SR 12343 (30 mg/kg), SR 12460(30 mg/kg) and 8K-NBD peptide (10 mg/kg). n=6-7 each group.

A

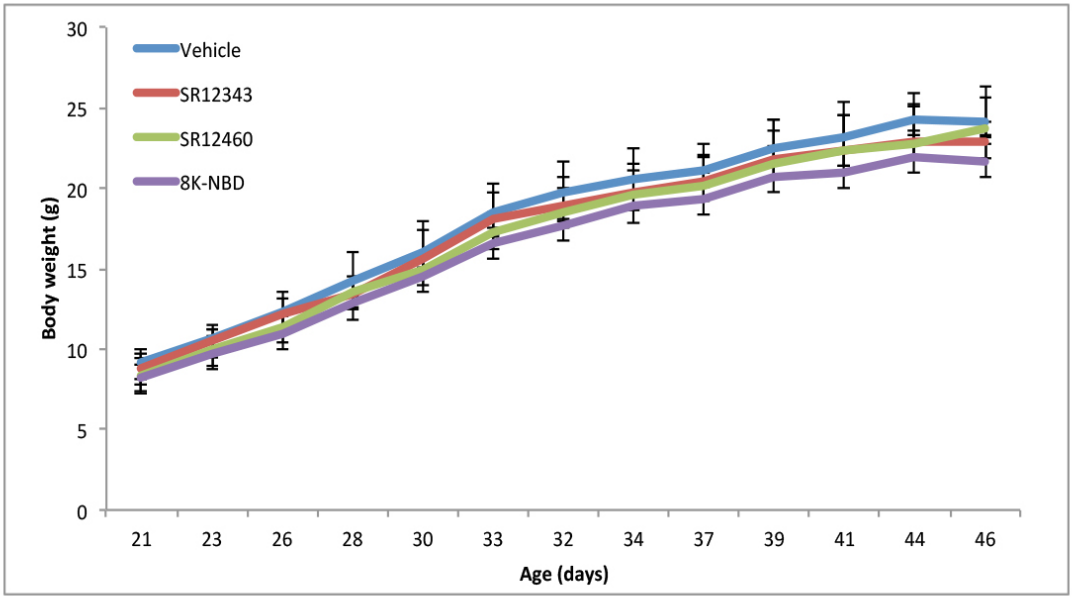

Figure 20: NBD mimetics display no effects on body weight in treated *mdx* mice. (A) Body weight was monitored in chronically treated *mdx* mice and no significant differences were found.

3.4 DISCUSSION

Since a peptide derived from the NEMO binding domain in IKKβ has been demonstrated to be highly therapeutic in numerous mouse models of inflammatory and degenerative diseases, the development of NBD mimetics would have significant clinical utility. Here we identified and optimized novel NBD mimetics that selectively inhibited IKK/NF-κB activity. The two lead compounds, SR12343 and SR12460, inhibited both TNF-α- and LPS-induced NF-κB activation more effectively and at a lower concentration than the NBD peptide in both HEK293 and Raw 264.7 cells. The NBD mimetics also were demonstrated to disrupt the IKK complexes by co-immunoprecipitation, which is distinct from the existing ATP-competitive inhibitors targeting

IKKβ or IKKα. Although SR12343 is less stable *in vivo* compared to SR12460, it showed stonger inhibitory and therapeutic effects in the LPS-induced ALI model and *mdx* mice, where the pathology is mainly mediated by immune cells.

To identify the NBD mimetics, a computational screening based on the pharmacophore model was used (42). A crystal structure study previously identified amino acid residues W741, W739 and F734 as the essential hydrophobic motifs interacting with NEMO (42). Also, a mutated 11-mer NBD peptide (735-745), with substitutions of alanine for W741 and W739, lost NEMO binding ability (43). Moreover, a longer IKKβ-derived peptide (701-746) containing all residues and domains, were tested and shown to exhibit the strongest affinity to NEMO with IC_{50} around 10 nm, while the traditional NBD peptide (11-mer) was less potent, with IC_{50} around 100 μm (42, 226). Thus, to identify NBD mimetics, the third residue F734 (in the linker domain) that was left out of the 11-mer NBD peptide, was included in our pharmacophore model and *in silico* screening. The NBD mimetics were able to inhibit NF-kB activity in a dose-dependent manner with an EC_{50} around 10-40 μM, which is still lower than the extent of inhibition with the 45-mer NBD peptide (42, 226). These results are consistent with the current evidence that the IKK helix region significantly contributes to the high binding affinity between IKKβ and NEMO (227).

We demonstrated that the novel NBD mimetics were able to block preformed NEMO/IKKβ complexes, consistent with previous reports that NBD peptide blocks the association in preformed IKK complexes (43, 226). However, there is evidence suggesting that NBD peptide preferably forces IKKβ, but not IKKα, to leave the IKK complex (226). It also has been reported that NBD peptide disrupts the association between IKKα and NEMO and block IL-1 induced IKKβ-independent NF-κB activation via IKKα at a much lower affinity (43, 44). This could explain why NBD peptide exhibited greater therapeutic efficacy in various *in vivo*

models than IKK kinase inhitors, most of which preferentially target IKKβ. Clearly, further analysis of the interaction of not only the mimetics with IKK, but also the NBD peptide is needed.

The NBD peptide was reported not to affect basal activity of NF-κB (11, 226). We too have not observed a signficant reduction in basal NF-κB transcription. This is important since complete abolishment of NF-κB activity in mice lacking IKKβ has been demonstrated to lead to extensive apoptosis, tissue injury and embryonic lethality, due to TNFα-induced apoptosis (13, 228). We observed no apparent signs of liver or kidney toxicity, nor infection tendency from the chronic treatment study, consistent with previous findings that no signs of toxicity has been reported with chronic dosing of NBD peptide (211).

It is of interest that the NBD mimetics inhibited a unique subset of target genes compared to IKK kinase inhibitors, particularly iNOS which is involved in the production of nitric oxide. The role of iNOS, as a central mediator of neutrophil recruitment, has been well established in the pathophysiology of LPS-induced ALI and sepsis (229, 230). iNOS-knockout mice and mice treated with NOS inhibitors have been reported to exhibit an attenuated inflammatory response and tissue injury in multiple models of lung inflammation (231-234). Thus, NBD mimetics may exhibit stronger therapeutic effects in inflammatory diseases driven by iNOS production.

The analysis of the NBD mimetics in *mdx* mice provides compelling evidence that the small molecule NBD mimetics inhibited pro-inflammatory responses and improved muscle degeneration, showing an even greater improvement in pathology than NBD peptide. IKK is responsible for persistently amplified NF-κB signaling cascade and the exhaustion of regeneration capacity of injured myofibers, contributing to the pathology and phenotype of

muscle dystrophy in DMD (48). Thus, novel NBD mimetics could be used clinically to treat DMD.

We previously have demonstrated that chronic treatment of the *Ercc1*$^{-/\Delta}$ mouse model of accelerated aging with the NBD peptide delayed onset of numerous age-related symptoms, improved pathology and reduced cellular senescence. Similar to the NBD peptide, chronic treatment of *Ercc1*$^{-/\Delta}$ mice with SR12343 resulted in an extension of healthspan. In addition, in a moue model of skin photoaging, topical treatment with SR12343 improved molecular markers of skin aging as well as the overall appearance of the skin. Thus these novel NBD mimetics could be used not only for treatment of inflammatory and degenerative diseases, but also aging.

Collectively, our data demonstrate that the novel small molecule NBD mimetics are potent and highly selective IKK inhibitors by disrupting the association of IKK complexes. They exhibited significant inhibitory effects on NF-κB activation in the model of LPS-induced ALI and murine model of DMD (*mdx* mice), suggesting the potential of NBD mimetics becoming a distinct class of anti-inflammatory drugs. Taken together, NBD mimetics may provide therapeutic values for the chronic management of inflammatory diseases and cancers in the future.

4.0 A NOVEL NBD MIMETIC EXTENDS HEALTHSPAN AND IMPROVES METABOLIC ABNORMALITIES IN *Ercc1*$^{-/\Delta}$ MICE

4.1 INTRODUCTION

Aging, referring to a state of gradual deterioration of physical activity and organ function, has been associated with various aging-related diseases, including diabetes, atherosclerosis, intervertebral disc degeneration, osteoporosis, neurodegeneration and cancer (201). The concept of cellular senescence was first described as irreversible growth arrest, termed replicative senescence (85). Extensive studies have shown that DNA damage, telomere shortening, oncogene activation and oxidative stress all contribute to cellular senescence (87, 96). Recently, Baker *et al.* demonstrated that the clearance of p16^{Ink4a}-positive senescent cells reduced tissue senescence and moreover extended healthspan in the *BubR1*$^{H/H}$ mouse model of accelerated aging (122).

Cellular senescence is a mechanism that cells employ in response to endogenous and exogenous stresses. Two major effector pathways p53/p21 and p16/Rb have been demonstrated to increase with aging (87). DNA damage induced by telomere shortening, genotoxic stress and oxidative stress induces a signaling cascade to maintain the genome integrity, called the DNA damage response (DDR) (87, 96). DDR signaling has been demonstrated to mediate cell growth arrest by suppressing Cdk2 via p53/p21 (87). Similarly, the p16/Rb pathway inhibits Cdk4/Cdk6

to block cell cycle progression, which is a common pathway employed by oncogene-induced senescence (OIS) that is DDR-independent (87, 235). Senescent cells exhibit a senescence-associated secretory phenotype (SASP), producing cytokines, chemokines, growth factors and extracellular proteases, which negatively impact neighboring cells (129, 132). In particular, pro-inflammatory cytokines, interleukin-6 (IL-6), interleukin-1α (IL-1α) and tumor necrosis factor-α (TNF-α), were shown to enhance primary senescence and induce secondary senescence in cell-autonomous and cell-nonautonomous pathways *in vitro* (129, 165, 166).

A causal role of NF-κB activation in natural and accelerated aging was recently established. Genetic ($p65^{+/-}$) and pharmacologic (NBD peptide) inhibition of NF-κB delayed the onset of aging symptoms and extended healthspan in $Ercc1^{-/\Delta}$ progeroid mice (137). Hypothalamus- and brain-specific knockout of IKKβ attenuated aging-related neurodegeneration and extended lifespan, suggesting a causal role of IKKβ/NF-κB in aging, as well as the involvement of hypothalamus in systemic aging (139). The transcriptional activity of RelA/p65 can be negatively regulated by p50 homodimers (3). Thus, in contrast, $Nfkb1^{-/-}$ ($p50^{-/-}$) mice, where RelA/p65 is chronically activated, exhibited reduced lifespan, impaired tissue regeneration and neurodegeneration (141, 143, 173, 174).

NBD peptide contains eleven amino acids derived from the NEMO-binding domain (NBD) of the C-terminus of IKKβ/α and is a highly selective IKK complex inhibitor, by disrupting the association between IKKβ/α and NEMO (11). The therapeutic effects of NBD peptide have been well established in various murine disease models driven by NF-κB activation, including chronic colitis, Duchenne muscular dystrophy (DMD), Parkinson's disease, Type 1 diabetes, osteoclastogenesis and diffuse large B-cell lymphoma (46, 47, 49, 51, 212, 224, 225). A small molecule inhibitor, SR12343, which was developed based on NBD peptide, has been

shown to work similarly to the peptide (Chapter 3) by showing positive therapeutic effects in a murine model of DMD.

In this study, we used the *Ercc1*$^{-/\Delta}$ mouse model of accelerated aging, which spontaneously develops osteoporosis, sarcopenia, disc degeneration, glomerulonephropathy and neurodegeneration, to study DNA damage-induced cellular senescence and aging. Here we further examined the role of NF-κB in senescence and aging using the small molecule inhibitor SR12343. Chronic administration of SR12343 extended healthspan in *Ercc1*$^{-/\Delta}$ mice as well as reduced the level of cellular senescence in tissues. Moreover, SR12343 was shown to attenuate aging-related lipodystrophy and impaired glucose tolerance partly by reducing senescence in the adipose tissue. Thus, our results suggest SR12343 could be a promising clinical approach to attenuate frailty and aging-related diseases.

4.2 MATERIALS AND METHODS

4.2.1 Cells and mice

Primary mouse embryonic fibroblasts (MEFs) were isolated on embryonic day 12.5-13.5. In brief, mouse embryos were isolated from yolk sac followed by the complete removal of viscera, lung and heart if presented. Embryos were then minced into fine chunks, fed with MEFs medium, cultivated under 3% oxygen to reduce stresses. Cells were split at 1:3 when reaching confluence. MEFs were grown at a 1:1 ratio of Dulbecco's Modification of Eagles Medium (supplemented with 4.5g/L glucose and L-glutamine) and Ham's F10 medium, supplemented with 10% fetal bovine serum, penicillin, streptomycin and non-essential amino acid. To induce

oxidative stress-mediated DNA damage, *Ercc1*$^{-/-}$ MEFs were switched to 20% oxygen for cultivation starting at passage 3.

Ercc1$^{+/-}$ and *Ercc1*$^{+/\Delta}$ mice from C57BL/6J and FVB/n backgrounds were crossed to generate *Ercc1*$^{-/\Delta}$ mice to prevent potential strain-specific pathology. For low dose study, 6-week-old sex-matched *Ercc1*$^{-/\Delta}$ mice were dosed with 10 mg/kg of SR12343 or vehicle by intraperitoneal injection three times per week up untill 15 weeks of age. For high dose study, 8-week-old sex-matched *Ercc1*$^{-/\Delta}$ mice were dosed with 30 mg/kg of SR12343 or vehicle by intraperitoneal injection 3 times per week untill 15 weeks of age. SR12343 was formulated in 10:10:80 of DMSO:Tween 80:water for *in vivo* administration. Animal protocols used in this study were approved by Scripps Florida Institutional Animal Care and Use Committees.

4.2.2 Health Evaluation

Health assessment was conducted twice per week to evaluate age-related symptoms, including body weight, tremor, forelimb grip strength, kyphosis, hindlimb paralysis, gait disorder, dystonia and ataxia. Kyphosis, body condition and coat condition were used to reflect general health conditions. Ataxia, dystonia, gait disorder and tremor were used as indicators of aging-related neurodegeneration. Muscle wasting was studies by monitoring hindlimb paralysis and forelimb grip strength. All aging symptoms were scored based on a scale of 0, 0.5 and 1, with the exception of dystonia that has a scale from 0 to 5. The sum of aging scores of each group was used to determine the overall aging conditions, with zero means no symptom presented.

4.2.3 Nuclear magnetic resonance (NMR)

Bruker's minispec LF50 body composition analyzer was used to measure lean tissue, fat and fluid in mice according to the manufacturer's instructions. Mice were placed into a restrainer and body composition was measured by the analyzer. Readings of lean tissue, fat and fluid were normalized to body weight to get the percentage of each body composition.

4.2.4 Oral glucose tolerance test (OGTT)

11-week-old mice were fasted overnight prior to OGTT test. Baseline fasting blood glucose was obtained before glucose administration at 0 min. A bolus of glucose (2g/kg) was administrated to each mouse by oral gavage and blood glucose was measured at 5, 15, 30, 60 min with tail-tip blood.

4.2.5 Senescence-associated β-galactosidase staining *in vivo* and *in vitro*

Fresh fat was fixed in 2% formaldehyde and 0.2% glutaraldehyde in PBS for 10 minutes at room temperature. After the removal of fixative, adipose tissue was stained with SA-βgal staining (pH 6.0) solution (40 mM citric acid in sodium phosphate buffer, 5 mM $K_4[Fe(CN)_6]$ $_3H2O$, 5 mM $K_3[Fe(CN)_6]$, 150 mM sodium chloride, 2 mM magnesium chloride and 1 mg/ml X-gal dissolved in N,N-dimethylformamide) for 16-20 hours in a 37^oC incubator without CO_2 injection. Images were taken at 5 hr into the staining. Fresh liver tissue was fixed in 10% neutral buffered formalin (NBF) for 3-4 hours and then transfered to 30% sucrose overnight. Tissue was then imbeded in optimal cutting temperature compound (OCT) and stored at -80^oC. 5μM cyrosetions were

performed and slides were stained in SA-βgal staining solution (pH 5.8) at 37^{o}C for 16-24 hours. To quantify, 10 random images were captured using a bright-field microscopy at 10x magnification and the number of SA-βgal^{+} cells per field was counted. The quantification was shown as mean+/- SE.

4.2.6 Fluorescence-based C_{12}FDG staining

Ercc1$^{-/-}$ MEFs grown in 20% oxygen were seeded into 96-well plates, allowed to attach overnight and treated with vehicle or SR12343 at indicated concentration for 48 hr. Prior to staining, cells were incubated with 100 nM of bafilomycin A1 for 1 hr to induce lysosomal alkalinization. C_{12}FDG was then added to the media to reach a final concentration of 10 μM and incubated for 2 hr. Images were captured and analyzed by IN Cell Analyzer 6000 (GE healthcare). Percentage of positive cells was calculated by dividing senescent cells (C_{12}FDG) by total cell number (DAPI).

4.2.7 Quantitative reverse transcription-polymerase chain reaction

Snap frozen tissues were preserved in RNAlater RNA stabilization solution (ThermoFisher). Total RNA was extracted using TRIZOL reagent (Life Technologies) and 1.5 ug of RNA was transcribed into complementary DNA (cDNA) using SuperScript VILO cDNA synthesis kit. qRT-PCR was performed in a StepOnePlus Real-Time PCR system using Platinum SYBR Green qPCR SuperMix-UDG (ThermoFisher). Target gene expression was calculated using the comparative C_T method ($\Delta\Delta C_T$) and normalized to an internal control gene Actb (β-actin). Primers used are as follows: *Cdkn1a* (p21) forward: GTCAGGCTGGTCTGCCTCCG; *Cdkn1a*

(p21) reverse: CGGTCCCGTGGACAGTGAGCAG; *Cdkn2a* (p16) forward: CCCAACGCCCCGAACT; *Cdkn2a* (p16) reverse: GCAGAAGAGCTGCTACGTGAA; *Tnf* (TNF) forward: CTATGTCTCAGCCTCTTCTC; *Tnf* (TNF) reverse: CATTTGGGAACTTCTCATCC; *Il6* (IL-6) forward: AAGAAATGATGGATGCTACC; *Il6* (IL-6) reverse: GAGTTTCTGTATCTCTCTGAAG; *Actb* (β-actin) forward: GATGTATGAAGGCTTTGGTC; *Actb* (β-actin) reverse: TGTGCACTTTTATTGGTCTC;

4.2.8 Statistical analysis

All values were presented as mean+/-S.E.M. Microsoft Excel and Graphpad Prism 6 were used for statistical analysis. Two-tailed Student's *t*-test was performed to determine differences between two groups. To determine differences in more than two groups, one-way ANOVA (Dunnett test) was used. A value of $p < 0.05$ was considered as statistically significant, shown as $*p < 0.05$, $**p < 0.01$, and $***p < 0.001$.

4.3 RESULTS

4.3.1 SR12343 extends the healthspan of *Ercc1*$^{-/\Delta}$ mice

Naturally aged wild type (WT) mice develop aging-associated symptoms over time, including graying hair, alopecia, kyphosis, cachexia, lipodystrophy, muscle wasting and gait disorder (141). The premature aging symptoms observed in *Ercc1*$^{-/\Delta}$ mice recapitulate most natural aging features with the exception of developing more severe neurodegeneration (152). We previously

reported that p65/RelA heterozygosity or treatment with IKK/NF-κB inhibitor (8K-NBD peptide) delayed the onset of aging-related symptoms and improved aging pathology in multiple tissues in *Ercc1*$^{-/\Delta}$ mice (137). As mentioned in Chapter 3, we developed a novel NBD mimetic (SR12343) that selectively suppresses IKK/NF-κB signaling by disrupting the association between IKKβ and NEMO. To determine its anti-aging effects, *Ercc1*$^{-/\Delta}$ mice were dosed with vehicle or SR12343 three times per week for 8 weeks, starting from 6-8 weeks of age. Health assessments were performed twice per week to evaluate aging symptoms (Fig. 21A). Tremor, kyphosis, dystonia, ataxia, gait disorder, hindlimb paralysis and forelimb grip strength were scored separately. The composite score of all aging symptoms reflects the overall health condition of *Ercc1*$^{-/\Delta}$ mice. Mice treated with SR12343 showed reduced frailty and delayed progression of aging symptoms (Fig. 21B). A gender-matched comparison also showed delayed onset, reduced severity and slowed progression of aging symptoms (Fig. 21C). Among neurodegenerative symptoms, dystonia occurs as early as 8 weeks and worsens gradually with time. We found significantly attenuated dystonia in mice treated with SR12343 (Fig. 21D). Taken together, the data demonstrated that SR12343, by inhibiting IKK/NF-κB activity, extended healthspan and delayed the onset of aging symptoms in progeroid mice.

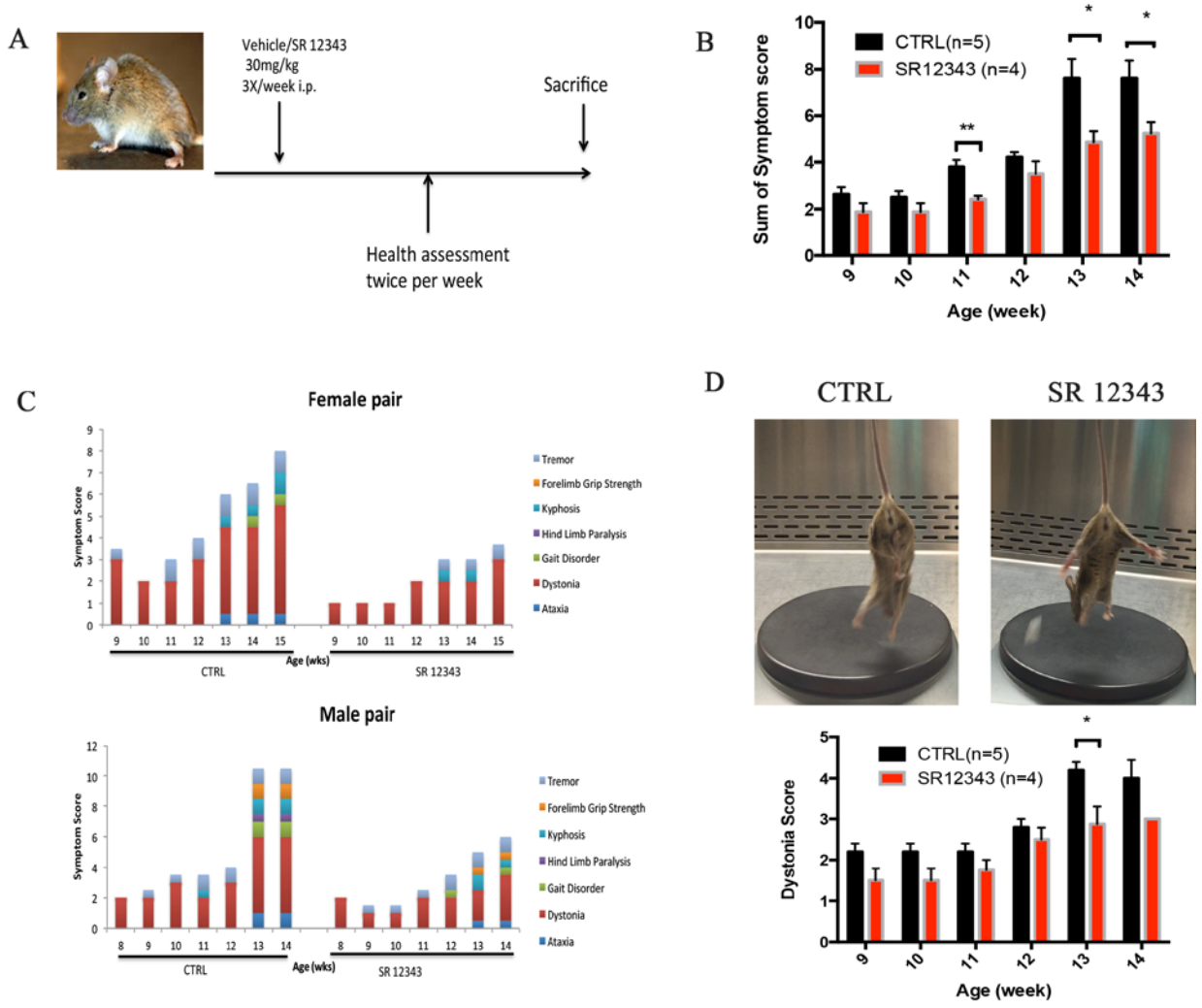

Figure 21: Chronic treatment with IKK inhibitor (SR12343) extends healthspan in *Ercc1*$^{-/\Delta}$ mice. (A) *Ercc1*$^{-/\Delta}$ mice were treated i.p. with SR12343 or vehicle 3 times per week, starting from 6-8 weeks of age. Mice were sacrificed around 15 weeeks of age and tissues were collected for analysis. n=4-5 mice each group. (B) The sum of symptom score of *Ercc1*$^{-/\Delta}$ mice was presented, reflecting general health condition, neurodegeneration and muscle wasting. (C) Pair-based plotting of aging symptoms. Higher stacking score indicates early onset and/or rapid progression of aging symptoms. (D) Dystonia was measured twice per week and scored based on

the severity and the time required for the pathological contraction. Representative images were shown in the upper panels. n=4-5 each group.

4.3.2 Chronic treatment with SR12343 decreases cellular senescence in *Ercc1*$^{-/\Delta}$ progeroid mice

8K-NBD peptide was previously demonstrated to extend healthspan in *Ercc1*$^{-/\Delta}$ progeroid mice, likely by reducing levels of cellular senescence, as demonstrated by reduced SA-βgal staining in liver (137). To determine if SR12343 reduces senescence, we first tested the drug in primary *Ercc1*$^{-/-}$ mouse embryonic fibroblasts (MEFs), which exhibited accelerated cellular senescence under atmospheric oxygen levels (20%). Using C_{12}FDG (a fluorescence-based staining specific for β-galactosidase), senescent cells were shown to be reduced from 50% to 35% by SR12343 (100 mM) without inducing significant cell death, suggesting non-senolytic effects of SR12343 (Fig. 22A). To assess the effect of SR12343 on cellular senescence *in vivo*, staining of senescence-associated β-galactosidase (SA-βgal), a biomarker of cellular senescence, was performed in liver, with senescent cells developing a blue color. A significant reduction of the number of SA-βgal^{+} hepatocytes was found in SR12343 treated animals (Fig. 22B). qRT-PCR analysis of aging biomarkers in liver revealed a reduction of IL-6 and TNFα expression, although this was not statistically significant yet (Fig. 22C). No significant changes in p16 and p21 expression were found; however a trend toward a reduction of p16 expression was found in female mice (Fig. 22C). Taken together, chronic suppresion of IKK/NF-κB led to reduced cellular senescence in liver.

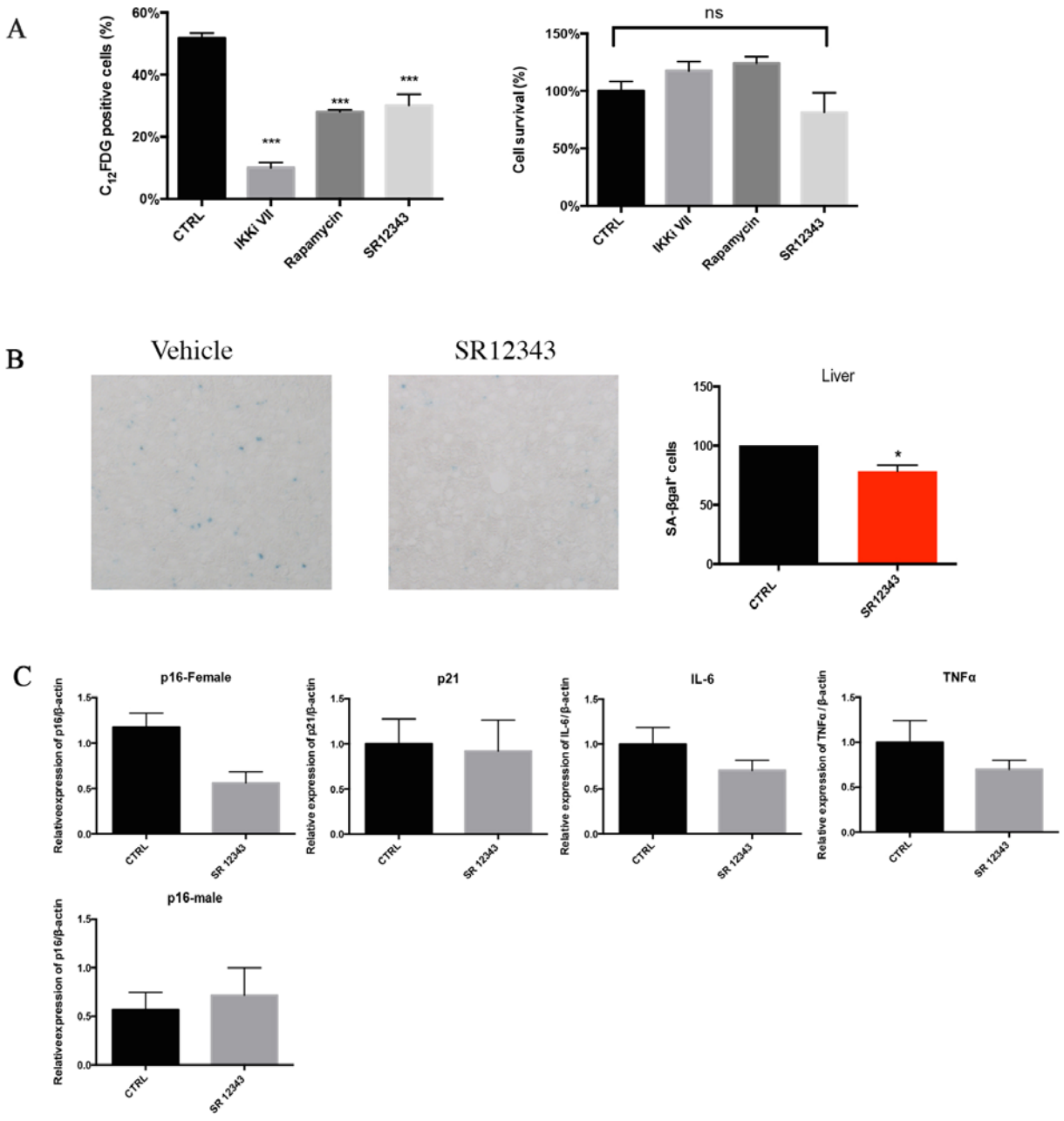

Figure 22: Chronic treatment of SR12343 reduces cellular senescence in liver in *Ercc1*$^{-/\Delta}$ mice. (A) C_{12}FDG staining was performed to assess cellular senescence in primary *Ercc1*$^{-/-}$ MEFs cultured in 20% oxygen. Cells were seeded overnight to allow attachment and treated with vehicle (CTRL), IKKi VII (600 nm), rapamycin (200 nm) or SR12343 (100 μM) for 48 hour prior to reading. Senolytic effects were determined by DAPI counterstain. The absolute number

of live cells (DAPI) was counted by In Cell analyzer 6000 and was normalized to untreated controls to obtain the % of cell survival. (B) Treated or untreated livers from 15-week-old sex-match *Ercc1*$^{-/\Delta}$ mice were stained for SA-βgal. Ten random fields (at 10x magnification) were captured and data were presented as the average of the absolute number of SA-βgal^{+} cells. Representative images were taken at 20x magnification. n=3 mice each group. (C) qRT-PCR analysis of livers was performed to evaluate the expression of senescent markers and SASP factors. p16, p21, IL-6 and TNF-α were analyzed with 15-week-old sex-matched livers. ns means not significant. n=4-5 per group; n=2 per female group; n=2-3 each male group.

4.3.3 Chronic inhibition of the IKK complex by SR12343 delays lipodystrophy and improves metabolic abnormalities in *Ercc1*$^{-/\Delta}$ mice

Lipodystrophy refers to the absent and altered distribution of adipose tissue, which may occur with metabolic abnormalities. Multiple progeria mouse models, such as *Zmpste24*$^{-/-}$, *Ercc1*$^{-/-}$, and aP2-*Ercc1*$^{F/-}$, have been shown to exhibit reduced fat depots similar to naturally aged WT mice (177, 236). We employed nuclear magnetic resonance (NMR) to determine the body composition, including fat, lean tissue and fluid, in *Ercc1*$^{-/\Delta}$ mice (237). We found a gradual decline of fat depot with aging starting from 8 weeks, which paralleled the onset of aging symptoms. In particular, severe loss of fat was observed around 14 weeks of age, at which point *Ercc1*$^{-/\Delta}$ mice contained close to 0% body fat (Fig. 23A). However, a delayed loss of fat was found in SR12343 treated mice, suggesting that suppression of NF-κB could attenuate the progression of lipodystrophy. An association of impaired glucose tolerance with reduced body-fat mass has been established and has been linked to reduced production of leptin (238-240). To determine if metabolic abnormality could be improved by suppressing IKK/NF-κB, an oral

glucose tolerance test (OGTT) was conducted on mice fasted overnight. Accelerated clearance and lower peak serum glucose were found in mice treated with SR12343 (Fig. 23B). To determine whether the levels of cellular senescence were altered in adipose tissue, SA-βgal staining was performed with parametrial fat, which showed reduced staining in treated mice, indicating less senescence in fat (Fig. 23C). Taken together, inhibition of IKK/NF-κB by SR12343 improved lipodystrophy and associated glucose intolerance, likely due to the lowered cellular senescence in adipose tissue.

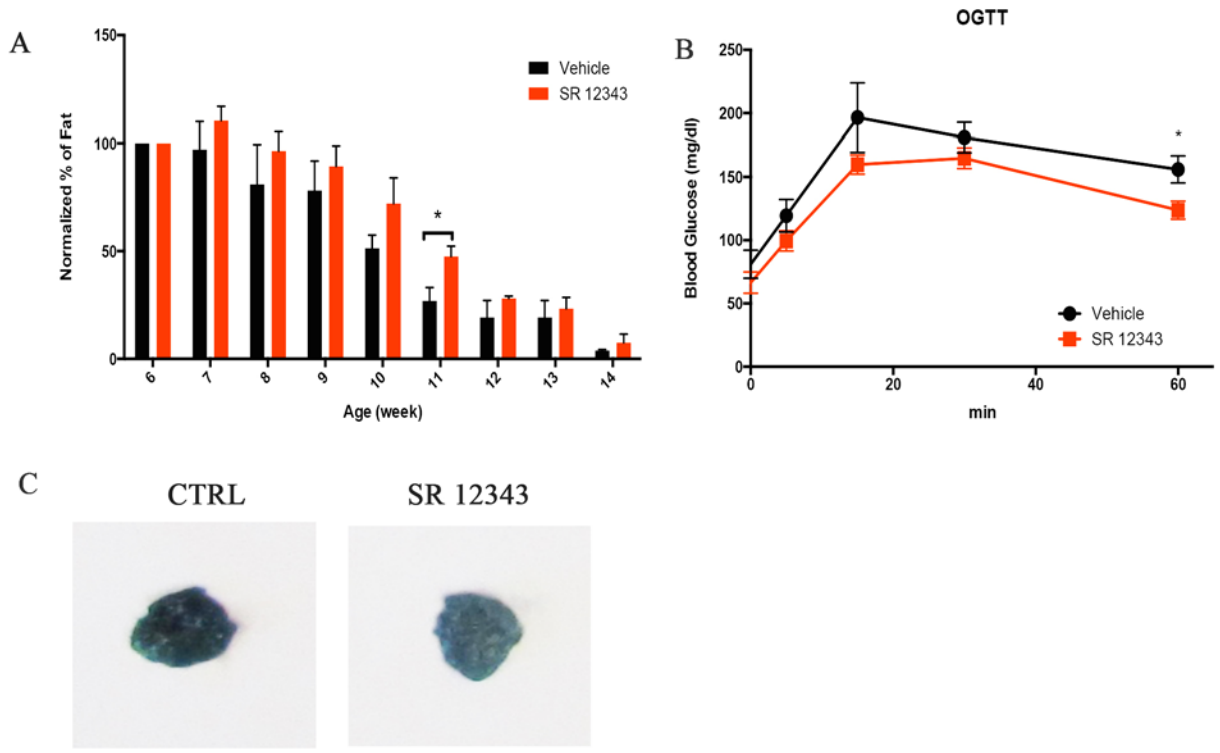

Figure 23: SR12343 attenuates lipodystrophy and glucose intolerance in *Ercc1*$^{-/\Delta}$ mice. (A) NMR was performed weekly on SR12343 treated or untreated mice from 6 to 14 weeks of age. Percentage of fat in males is shown and was normalized to the level at 6 weeks of age. n=3-4 each group. (B) *Ercc1*$^{-/\Delta}$ mice fasted overnight were dosed with a bolus of glucose (2g/kg) by oral gavage and blood glucose was measured at 0, 5, 15, 30 and 60 min. The fasting blood glucose was measured prior to the dosing of glucose. n=4-5 each group. (C) Fresh parametrial fat collected from 15-week-old *Ercc1*$^{-/\Delta}$ mice was stained for SA-βgal. Representative images taken 5 hr into the staining are shown. Two-tailed Student's *t*-test was used to determine the *p* value.

4.4 DISCUSSION

In this study, we demonstrated that pharmacologic inhibition of IKK/NF-κB by a novel NBD mimetics (SR12343) substantially prolonged healthspan by reducing senescence in multiple tissues. Intriguingly, a lipodystrophy-associated metabolic abnormality was also attenuated by IKK/NF-κB inhibition. Our study further supports a causal role of IKK/NF-κB in aging, consistent with the effects of knocking down Rel/p65 in *Sirt6*$^{-/-}$, *Ercc1*$^{-/\Delta}$ and *Zmpste24*$^{-/-}$ progeroid mice (136-138, 241). Although anti-inflammatory drugs, such as curcumin and metformin, have been shown to have therapeutic effects in diabetes and multiple aging-related diseases, these drugs have a broad range of targets (242). Thus, a selective IKK inhibitor (SR12343) was used in this study to dissect the role of IKK/NF-κB in regulating aging. Notably, we demonstrated that a single drug specifically targeting IKK could simultaneously improve healthspan and multiple aging-related diseases.

We found that the chronic treatment of progeroid mice with a specific IKK inhibitor (SR12343) could delay the onset, reduce the severity and slow the progression of aging symptoms, in line with previous evidence that NF-κB activation drives aging pathology (137). In addition, aging-related neurodegeneration has been an emerging problem since human lifespan has been remarkably prolonged. Multiple neurological symptoms, such as dystonia, gait disorder, hindlimb paralysis and ataxia, were improved by SR12343 in *Ercc1*$^{-/\Delta}$ mice. However, it remains unknown if this is due to systemic or local (in CNS) effects of NF-κB inhibition.

Chronic SR12343 treatment reduced cellular senescence in liver and adipose tissue, as demonstrated by the reduction in SA-βgal staining. This suggests the prolonged and improved healthspan is likely mediated by the reduction of cellular senescence and the attenuation of cell-nonautonomous pathway. Notably, the reduction of cellular senescence is not mediated by a

senolytic effect as reported by Kirkland et al (90). Thus SR12343 represents a different category of drugs which reverse or prevent the development of cellular senescence *in vitro* and *in vivo*. Notably, *Ercc1*$^{-/\Delta}$ mice treated with NBD peptide appear to exhibit a healthier phenotype compared to *p65*$^{+/-}$*:Ercc1*$^{-/\Delta}$ mice, suggesting the involvement of NF-κB-independent pathways in DNA damage-induced premature aging (137). There is evidence suggesting that IKK suppresses the translational activity of FOXO3a, which is associated with longevity by protecting against oxidative stress (243). Moreover, IKKβ has been shown to crosstalk with the mammalian target of rapamycin (mTOR) pathway, regulating the phosphorylation and activation of ribosomal protein S6 and eukaryotic initiation factor 4E binding protein 1 (4EBP1) (244). Thus, further exploration is needed to determine whether SR12343 simultaneously regulates NF-κB-independent pathways.

Using NMR, we were able to monitor aging-associated alteration of body composition in real-time. Here, we discovered a gradual but significant decline of fat depots in *Ercc1*$^{-/\Delta}$ mice, while body weight and percentage of lean mass remained unchanged (data not shown). Intriguingly, the loss of fat coincides with the onset of most aging symptoms, implicating that its occurrence is indeed aging-related. Moreover, pharmacologic inhibition of IKK by SR12343 was able to slow down the loss of fat depots in male group, supporting the hypothesis that chronic inflammation may impair adipogenesis and alter fat distribution, This is in agreement with previous studies reporting that lipodystrophy observed in aP2-*Ercc1*$^{F/-}$ and *Ercc1*$^{-/-}$ mice may be a consequence of a chronic pro-inflammatory response induced by persistent DNA damage (177).

Among interventions that prolong healthspan and/or lifespan are caloric restriction, growth hormone receptor deletion (GHRKO), insulin receptor substrate-1 and S6-kinase-1

knockout and rapamycin treatment, all of which display reduced fat mass, while obesity appears to accelerate aging leading to a reduced lifespan (245-247). Senescent adipose tissue has been previously associated with metabolic abnormalities, such as obesity and diabetes, where adipocytes in fact undergo senescence and express various senescent markers, including SA-βgal, γH2AX, p16, p21 and SASP components (247-249). However, most studies were performed to study the relationship between cellular senescence and positive energy balance. Here we wanted to understand the role of cellular senescence in negative energy balance, which is commonly associated with aging and premature aging induced by HIV treatment of combination antiretroviral therapy (cART) (250). We demonstrated cellular senescence in the adipose tissue of *Ercc1*$^{-/\Delta}$ mice, which is associated with the aging-related lipodystrophy, the opposite of obesity. Thus, it is plausible that there is a common mechanism connecting both positive and negative energy accumulation to aging in adipose tissue. Interestingly, our study indicates that SR12343, which suppresses IKK/NF-κB activity, could improve the broader aging-related metabolic profile in *Ercc1*$^{-/\Delta}$ mice.

Impaired glucose tolerance has been reported in aP2-*Ercc1*$^{F/-}$ mice, where insulin production was greatly increased, suggesting the presence of Type 2 diabetes (177). Our previous study also reported dyslipidemia in *Ercc1*$^{-/\Delta}$ mice by showing significantly elevated serum cholesterol but not triglyceride, which correlates with hepatic steatosis demonstrated by H&E staining (251). Specifically, a detrimental role of low-grade chronic inflammation in obesity and insulin resistance has been substantially documented (252, 253). Mice expressing constitutively active IKKβ in liver exhibited chronic inflammation and a Type 2 diabetes phenotype (254). In this study, we found impaired glucose metabolism in *Ercc1*$^{-/\Delta}$ mice in which glucose clearance was significantly delayed. SR12343 was shown to improve glucose clearance,

supporting the hypothesis that chronic inflammation in liver, adipose tissue and likely pancreas, contributes to glucose intolerance.

Taken together, we found that a novel NBD mimetic (SR12343) showed therapeutic effects in extending healthspan and attenuating metabolic abnormality in premature aging. This was demonstrated to be mediated by reduced cellular senescence in tissues and dampened systemic inflammation. Our results suggest that IKK/NF-κB is a key target for the management of healthy aging and SR12343 could be a promising approach to improve aging and aging-related diseases.

5.0 DISCUSSION AND FUTURE DIRECTIONS

5.1 GENERAL DISCUSSION

NF-κB is a family of pleiotropic transcription factors involved in multiple biological events. This pathway is activated by distinct cellular stress, such as inflammation, oxidative stress and genotoxic stress (3). Mounting evidence highlights that NF-κB activation is strongly associated with aging in both humans and rodents (136). We and others previously reported that reduction of p65/RelA genetically or pharmacologically could extend healthspan as well as improve aging-associated pathology in *Zmpste24*$^{-/-}$ and *Ercc1*$^{-/\Delta}$ progeria mouse models (137, 138). An essential role of elevated DNA damage response (DDR) has also been highlighted in numerous aging studies (62, 235). Moreover, Miyamoto and colleagues established a molecular linkage between ATM and NF-κB in response to DNA damage (4). Thus we hypothesize that accumulative DNA damage and subsequent activation of DDR are the driving forces of aging and result in NF-κB activation in *Ercc1*$^{-/\Delta}$ mice, a DNA repair-deficient murine model.

In the first part of this thesis, I confirmed an elevated NF-κB activity in *Ercc1*$^{-/\Delta}$ and WT mice, which is consistent with our previous finding using NF-κB^{eGFP} reporter mice (137). An increased DDR signaling was also found in aged tissues, which occurs concomitantly with NF-κB activation. *In vitro* assays suggest that the elevated NF-κB activity is at least in part induced by DNA damage, via nuclear-localized ATM and NEMO. Intriguingly, I observed reduced

cellular senescence in passage 5 senescent *Ercc1*$^{-/-}$ MEFs either treated with ATM inhibitor or with one *Atm* allele deleted. Moreover, reduced nuclear-localized NEMO was found after the treatment of ATM inhibitor. My results suggest a causative role of DDR activation in cellular senescence, which also mediates an ATM- and NEMO-dependent NF-κB activation.

To better elucidate the role of DDR signaling in premature aging, *Atm*$^{+/-}$*;Ercc1*$^{-/\Delta}$ mice were generated. *Atm* haploinsufficiency resulted in downregulated DDR signaling, as shown by reduced expression of ATM, γH2AX and p21. This observation correlates well with dramatically reduced phospho-p65 and total IκBα, indicating that elevated NF-κB levels in *Ercc1*$^{-/\Delta}$ mice are at least in part attributable to the activation of DDR signaling. A similar response was also detected in *p65*$^{+/-}$*;Ercc1*$^{-/\Delta}$ mice, however γH2AX was unchanged, confirming our hypothesis that DDR proteins lie upstream of NF-κB dimers.

Finally, I demonstrated that ATM heterozygosity was able to extend healthspan in *Ercc1*$^{-/\Delta}$ mice showing ameliorated neurodegeneration. As Baker et al. demonstrated that removal of p16 positive cells prolonged healthspan in *BubR1*$^{H/H}$ mice, I propose that the alleviated aging phenotype may be mediated by reduced cellular senescence (122). Indeed, a reduction of cellular senescence was demonstrated in multiple tissues in *Atm*$^{+/-}$*;Ercc1*$^{-/\Delta}$ mice, as determined by reduced p21 and IL-6 expression. These results strongly support the hypothesis that aberrant DDR activation plays a causative role in both cellular senescence and aging, partly by inducing NF-κB activation. This hypothesis was further supported by evidence showing better kidney function and disc health, along with better function of muscle-derived stem/progenitor cells.

Although elevated DDR signaling has been associated with aging by numerous studies, the data presented in this thesis pinpointed DDR activation as a causative factor of aging. However, conflicting roles of ATM reduction in aging have been reported. It is important to note

that ataxia-telangiectasia (A-T) patients exhibit segmental premature aging symptoms, in particular cerebellar degeneration, which is contradictory to the finding in this study (53). Primary *Atm*$^{-/-}$ MEFs have been shown to exhibit accelerated cellular senescence compared to WT MEFs (255). These accelerated senescence and aging phenotypes have been linked to the cytoplasmic functions of ATM kinase, particularly in response to oxidative stress (256-260). Thereby, it would be critical to investigate the state of redox balance, such as levels of ROS and oxidative DNA damage, *in vitro* and *in vivo* where ATM is reduced genetically or pharmacologically. Moreover, ATM has been demonstrated to negatively regulate mTORC1 activity via LKB1 and AMPK (79). As caloric restriction and rapamycin treatment, both of which are negatively modulators of mTOR, have been reported to significantly elongate longevity, future studies could be performed to investigate mTOR activity in ATM haploinsufficiency. Furthermore, ATM protein has been implicated in mitophagy, i.e. the destruction of abnormal mitochondria, the dysregulation of which has been related to neurodegeneration and aging (261). Thus, further exploration of the cytoplasmic functions of ATM kinase would be important before translating this study for clinical intervention.

The second part of this thesis focused on the development of small molecule inhibitors mimicking NBD peptide to selectively inhibit IKK/NF-κB activation. A bioinformatic approach identified two small molecules (SR12343 & SR12460) that were able to inhibit canonical NF-κB activation, without inducing significant cellular toxicity. As NBD peptide has been reported to disrupt preformed IKK complexes, in particular the association between NEMO and IKKα/β, I propose that these NBD mimetics inhibit NF-κB activation through similar mechanisms (41, 43). I demonstrated that SR12343 and SR12460 disrupted the binding of IKKβ and NEMO to a similar extent to NBD peptide, especially SR12343, which exhibited even greater disruption.

More importantly, in a mouse model of LPS-induced acute lung injury, SR12343 and SR12460 demonstrated inhibitory effects on NF-κB target genes. A predominant role of IKK/NF-κB activation has also been established in promoting macrophage activation and muscle degeneration in *mdx* mice, and NBD peptide has demonstrated profound therapeutic effects in murine and canine models of Duchenne muscular dystrophy (48, 52). I demonstrated reduced muscular necrosis, attenuated pro-inflammatory infiltration and increased muscle regeneration in *mdx* mice treated with SR12343 and SR12460, which were associated with increased grip strength. Thus, my results support previous finding that IKK/NF-κB dysregulation is a major contributor to the pathology in Duchenne muscle dystrophy. Moreover, SR12343 and SR12460 demonstrated similar efficacy to NBD peptide *in vivo*.

In the third part of my thesis, SR12343 was tested in *Ercc1*$^{-/\Delta}$ mice to define the interplay between NF-κB and aging-associated pathology. We previous reported that p65/RelA haploinsufficiency or treatment with NBD peptide extended healthspan in *Ercc1*$^{-/\Delta}$ mice, likely via the reduction of mitochondrial-derived oxidative stress (137). The results presented here suggest that SR12343 significantly improved and extended the healthspan of *Ercc1*$^{-/\Delta}$ mice, showing equivalent, if not greater efficacy as NBD peptide. Both *in vitro* and *in vivo* data suggest that the rescuing effects may be mediated by reducing cellular senescence, which implies that NF-κB may function to promote the maintenance of senescence, and/or initiation cell-cycle arrest in neighboring cells. Current studies support the model that NF-κB may propagate a secondary senescence via transcriptional upregulation of its targets genes, such as IL-6, TNF-α and IL-1α *in vitro* (165). Finally, my data suggest that NF-κB inhibition may reshape the metabolic profile in progeroid mice by preventing the loss of fat depot and attenuating glucose intolerance. This observation is consistent with previous reports that metabolic abnormality is

partly attributed to systemic chronic low-grade inflammation (175). I speculate that cellular senescence in adipocytes and β cells may contribute to the phenotype by functioning improperly, showing impaired secretion of leptin and insulin (238-240). My results demonstrated that NF-κB inhibition reduced cellular senescence in adipose tissue, providing indirect evidence supporting this hypothesis. Although no overt signs of side effects have been observed in treated mice, for future studies it would be important to determine liver and kidney toxicity carefully. To elucidate the role of NF-κB in aging-related metabolic abnormality, further studies could be done to characterize the senescence and functional profile of β cells, adipocytes and preadipocytes using SR12343.

Overall, this thesis demonstrated a causative role of aberrant DDR activation in premature aging and indicated a subsequent activation of ATM/NEMO-dependent NF-κB pathway. I developed NBD mimetics, which are small molecule inhibitors of IKK/NF-κB functioning similar to NBD peptide, and demonstrated that they have similar inhibitory and therapeutic efficacy to NBD peptide *in vivo*. Finally, using the NBD mimetic, I showed a deleterious role of NF-κB in regulating tissue senescence and systemic metabolism. To further confirm that ATM and NEMO mediate the NF-κB activation, NEMO-DK (K277A and K309A) mice where genotoxin-induced NF-κB activation is specifically blocked, will be utilized to determine the role of cell-autonomous pathway in cellular senescence, and aging (262). Furthermore, as SASP has been long speculated to mediate secondary senescence *in vivo*, mouse models with deleted TNFR or MyD88 will be studied to determine the role of SASP factors, such as TNF-α, IL-1α, IL-1β and IL-6, in cellular senescence and aging.

5.2 DNA DAMAGE-INDUCED AGING MODEL

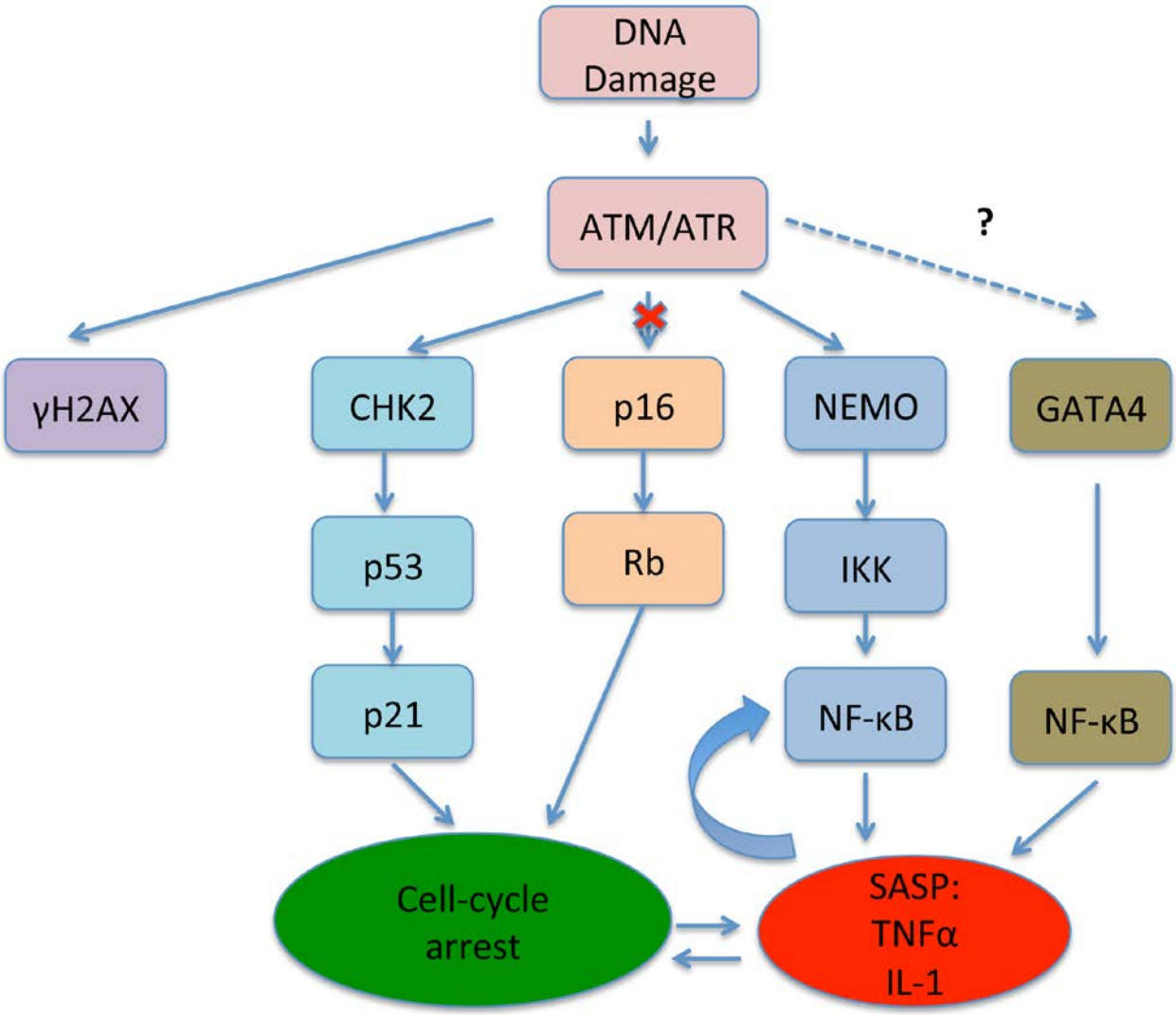

Figure 24: Aging model. Telomere shortening, oxidative stress and genotoxic stress induce cellular senescence by triggering a persistent DNA damage response. Upon DNA damage, ATM/ATR is activated and rapidly recruits, phosphorylates and activates an important DDR protein, γH2AX. In parallel, activated ATM leads to the activation of CHK2, which in turn stabilizes p53, leading to upregulated transcription of p21, a cell-cycle regulator. p21 then imposes an irreversible G1 cell-cycle arrest, leading to the establishment of cellular senescence. Our data suggest that ATM/ATR does not regulate the p16/Rb pathway directly, as ATM

haploinsufficiency showed no significant reduction in p16 expression. In addition, our data indirectly support an activation of ATM/NEMO-mediated NF-κB pathway, which leads to a SASP phenotype. However, it is still unknown if GATA4 is also involved as a mediator connecting ATM and NF-κB signaling in *Ercc1*$^{-/\Delta}$ mice. As SASP factors, such as TNF-α and IL-1, are not only target genes of NF-κB, but also activators of NF-κB. SASP is speculated to lead to a secondary NF-κB activation, which further enhances the SASP phenotype.

BIBLIOGRAPHY

1. Sen R & Baltimore D (Multiple nuclear factors interact with the immunoglobulin enhancer sequences. *Cell* 46(5):705-716.

2. Sen R & Baltimore D (1986) Multiple nuclear factors interact with the immunoglobulin enhancer sequences. *Cell* 46(5):705-716.

3. Perkins ND (2007) Integrating cell-signalling pathways with NF-kappaB and IKK function. *Nature reviews. Molecular cell biology* 8(1):49-62.

4. Wu ZH, Shi Y, Tibbetts RS, & Miyamoto S (2006) Molecular linkage between the kinase ATM and NF-kappaB signaling in response to genotoxic stimuli. *Science* 311(5764):1141-1146.

5. Sen R (2011) The origins of NF-[kappa]B. *Nat Immunol* 12(8):686-688.

6. Napetschnig J & Wu H (2013) Molecular Basis of NF-κB Signaling. *Annual review of biophysics* 42:443-468.

7. Lin L, DeMartino GN, & Greene WC (1998) Cotranslational Biogenesis of NF-κB p50 by the 26S Proteasome. *Cell* 92(6):819-828.

8. Perkins ND (0000) Post-translational modifications regulating the activity and function of the nuclear factor kappa B pathway. *Oncogene* 25(51):6717-6730.

9. Cohen S, Achbert-Weiner H, & Ciechanover A (2004) Dual Effects of IκB Kinase β-Mediated Phosphorylation on p105 Fate: SCFβ-TrCP-Dependent Degradation and SCFβ-TrCP-Independent Processing. *Molecular and cellular biology* 24(1):475-486.

10. Zandi E, Rothwarf DM, Delhase M, Hayakawa M, & Karin M (1997) The IκB Kinase Complex (IKK) Contains Two Kinase Subunits, IKKα and IKKβ, Necessary for IκB Phosphorylation and NF-κB Activation. *Cell* 91(2):243-252.

11. May MJ, *et al.* (2000) Selective inhibition of NF-kappaB activation by a peptide that blocks the interaction of NEMO with the IkappaB kinase complex. *Science* 289(5484):1550-1554.

12. DiDonato JA, Hayakawa M, Rothwarf DM, Zandi E, & Karin M (1997) A cytokine-responsive I[kappa]B kinase that activates the transcription factor NF-[kappa]B. *Nature* 388(6642):548-554.

13. Li Q, Antwerp DV, Mercurio F, Lee K-F, & Verma IM (1999) Severe Liver Degeneration in Mice Lacking the IκB Kinase 2 Gene. *Science* 284(5412):321-325.

14. Beg AA, Sha WC, Bronson RT, Ghosh S, & Baltimore D (1995) Embryonic lethality and liver degeneration in mice lacking the RelA component of NF-[kappa]B. *Nature* 376(6536):167-170.

15. Li ZW, *et al.* (1999) The IKKbeta subunit of IkappaB kinase (IKK) is essential for nuclear factor kappaB activation and prevention of apoptosis. *The Journal of experimental medicine* 189(11):1839-1845.

16. Tanaka M, *et al.* (1999) Embryonic Lethality, Liver Degeneration, and Impaired NF-κB Activation in IKK-β-Deficient Mice. *Immunity* 10(4):421-429.

17. Israël A (2010) The IKK Complex, a Central Regulator of NF-κB Activation. *Cold Spring Harbor perspectives in biology* 2(3).

18. Solt LA, Madge LA, Orange JS, & May MJ (2007) Interleukin-1-induced NF-κB Activation Is NEMO-dependent but Does Not Require IKKβ. *Journal of Biological Chemistry* 282(12):8724-8733.

19. Schmidt-Supprian M, *et al.* (NEMO/IKKγ-Deficient Mice Model Incontinentia Pigmenti. *Molecular cell* 5(6):981-992.

20. Rudolph D, *et al.* (2000) Severe liver degeneration and lack of NF-κB activation in NEMO/IKKγ-deficient mice. *Genes & development* 14(7):854-862.

21. Hu Y, *et al.* (1999) Abnormal Morphogenesis But Intact IKK Activation in Mice Lacking the IKKα Subunit of IκB Kinase. *Science* 284(5412):316-320.

22. Takeda K, *et al.* (1999) Limb and Skin Abnormalities in Mice Lacking IKKα. *Science* 284(5412):313-316.

23. Smahi A, *et al.* (2002) The NF-κB signalling pathway in human diseases: from incontinentia pigmenti to ectodermal dysplasias and immune-deficiency syndromes. *Human Molecular Genetics* 11(20):2371-2375.

24. Makris C, *et al.* (2000) Female Mice Heterozygous for IKKγ/NEMO Deficiencies Develop a Dermatopathy Similar to the Human X-Linked Disorder Incontinentia Pigmenti. *Molecular cell* 5(6):969-979.

25. Schmidt-Supprian M, *et al.* (2000) NEMO/IKKγ-Deficient Mice Model Incontinentia Pigmenti. *Molecular cell* 5(6):981-992.

26. Burns KA & Martinon F (2004) Inflammatory diseases: is ubiquitinated NEMO at the hub? *Current biology : CB* 14(24):R1040-1042.

27. Krappmann D & Scheidereit C (2005) A pervasive role of ubiquitin conjugation in activation and termination of IkappaB kinase pathways. *EMBO reports* 6(4):321-326.

28. Chen ZJ (2005) Ubiquitin signalling in the NF-kappaB pathway. *Nature cell biology* 7(8):758-765.

29. Hayden MS & Ghosh S (Shared Principles in NF-κB Signaling. *Cell* 132(3):344-362.

30. Ghosh S & Karin M (2002) Missing Pieces in the NF-κB Puzzle. *Cell* 109(2, Supplement 1):S81-S96.

31. Arenzana-Seisdedos F, *et al.* (1995) Inducible nuclear expression of newly synthesized I kappa B alpha negatively regulates DNA-binding and transcriptional activities of NF-kappa B. *Molecular and cellular biology* 15(5):2689-2696.

32. Liu S & Chen ZJ (2011) Expanding role of ubiquitination in NF-κB signaling. *Cell research* 21(1):6-21.

33. Gilmore TD (2006) Introduction to NF-κB: players, pathways, perspectives. *Oncogene* 25(51):6680-6684.

34. Bhoj VG & Chen ZJ (2009) Ubiquitylation in innate and adaptive immunity. *Nature* 458(7237):430-437.

35. Salek-Ardakani S & Croft M (2009) T cells need Nod too? *Nature immunology* 10(12):1231-1233.

36. Dejardin E (2006) The alternative NF-κB pathway from biochemistry to biology: Pitfalls and promises for future drug development. *Biochemical Pharmacology* 72(9):1161-1179.

37. Sun S-C (2011) Non-canonical NF-κB signaling pathway. *Cell Research* 21(1):71-85.

38. Yamaoka S, *et al.* (1998) Complementation cloning of NEMO, a component of the IκB kinase complex essential for NF-κB activation. *Cell* 93(7):1231-1240.

39. Rothwarf DM, Zandi E, Natoli G, & Karin M (1998) IKK-γ is an essential regulatory subunit of the IκB kinase complex. *Nature* 395(6699):297-300.

40. Zhang SQ, Kovalenko A, Cantarella G, & Wallach D (2000) Recruitment of the IKK signalosome to the p55 TNF receptor: RIP and A20 bind to NEMO (IKKγ) upon receptor stimulation. *Immunity* 12(3):301-311.

41. May MJ, *et al.* (2000) Selective Inhibition of NF-κB Activation by a Peptide That Blocks the Interaction of NEMO with the IκB Kinase Complex. *Science* 289(5484):1550-1554.

42. Rushe M, *et al.* (2008) Structure of a NEMO/IKK-Associating Domain Reveals Architecture of the Interaction Site. *Structure* 16(5):798-808.

43. May MJ, Marienfeld RB, & Ghosh S (2002) Characterization of the IκB-kinase NEMO Binding Domain. *Journal of Biological Chemistry* 277(48):45992-46000.

44. Solt LA, Madge LA, & May MJ (2009) NEMO-binding Domains of Both IKKα and IKKβ Regulate IκB Kinase Complex Assembly and Classical NF-κB Activation. *Journal of Biological Chemistry* 284(40):27596-27608.

45. Ziegelbauer K, *et al.* (2005) A selective novel low-molecular-weight inhibitor of IκB kinase-β (IKK-β) prevents pulmonary inflammation and shows broad anti-inflammatory activity. *British Journal of Pharmacology* 145(2):178-192.

46. Jimi E, *et al.* (2004) Selective inhibition of NF-[kappa]B blocks osteoclastogenesis and prevents inflammatory bone destruction in vivo. *Nature medicine* 10(6):617-624.

47. Davé SH, *et al.* (2007) Amelioration of Chronic Murine Colitis by Peptide-Mediated Transduction of the IκB Kinase Inhibitor NEMO Binding Domain Peptide. *The Journal of Immunology* 179(11):7852-7859.

48. Acharyya S, *et al.* (2007) Interplay of IKK/NF-kappaB signaling in macrophages and myofibers promotes muscle degeneration in Duchenne muscular dystrophy. *The Journal of clinical investigation* 117(4):889-901.

49. Ghosh A, *et al.* (2007) Selective inhibition of NF-κB activation prevents dopaminergic neuronal loss in a mouse model of Parkinson's disease. *Proceedings of the National Academy of Sciences* 104(47):18754-18759.

50. Rehman KK, *et al.* (2003) Protection of Islets by in SituPeptide-mediated Transduction of the IκB Kinase Inhibitor Nemo-binding Domain Peptide. *Journal of Biological Chemistry* 278(11):9862-9868.

51. Habineza Ndikuyeze G, *et al.* (2014) A phase I clinical trial of systemically delivered NEMO binding domain peptide in dogs with spontaneous activated B-cell like diffuse large B-cell lymphoma. *PloS one* 9(5):e95404.

52. Kornegay JN, *et al.* (2014) NBD delivery improves the disease phenotype of the golden retriever model of Duchenne muscular dystrophy. *Skeletal muscle* 4:18.

53. Shiloh Y & Ziv Y (2013) The ATM protein kinase: regulating the cellular response to genotoxic stress, and more. *Nature reviews. Molecular cell biology* 14(4):197-210.

54. Taylor AMR, *et al.* (1975) Ataxia telangiectasia: a human mutation with abnormal radiation sensitivity. *Nature* 258(5534):427-429.

55. Bakkenist CJ & Kastan MB (2003) DNA damage activates ATM through intermolecular autophosphorylation and dimer dissociation. *Nature* 421(6922):499-506.

56. Ditch S & Paull TT (2012) The ATM protein kinase and cellular redox signaling: beyond the DNA damage response. *Trends in biochemical sciences* 37(1):15-22.

57. Nam EA & Cortez D (2011) ATR signaling: more than meeting at the fork. *The Biochemical journal* 436(3):527-536.

58. Neal JA & Meek K (2011) Choosing the right path: does DNA-PK help make the decision? *Mutation research* 711(1-2):73-86.

59. Sharpless NE & Sherr CJ (2015) Forging a signature of in vivo senescence. *Nature reviews. Cancer* 15(7):397-408.

60. Lavin MF (2008) Ataxia-telangiectasia: from a rare disorder to a paradigm for cell signalling and cancer. *Nature reviews. Molecular cell biology* 9(10):759-769.

61. Polo SE & Jackson SP (2011) Dynamics of DNA damage response proteins at DNA breaks: a focus on protein modifications. *Genes & development* 25(5):409-433.

62. Rodier F, *et al.* (2011) DNA-SCARS: distinct nuclear structures that sustain damage-induced senescence growth arrest and inflammatory cytokine secretion. *Journal of cell science* 124(Pt 1):68-81.

63. Ciccia A & Elledge SJ (2010) The DNA damage response: making it safe to play with knives. *Molecular cell* 40(2):179-204.

64. Boder E & Sedgwick RP (1957) Ataxia-Telangiectasia. *Plastic and Reconstructive Surgery* 20(5).

65. Syllaba L & Henner K (1926) Contribution a l'independence de l'athetose double idiopathique et congenitale. *Rev Neurol* 1(541-562):147.

66. Zhang N, *et al.* (1997) Isolation of full-length ATM cDNA and correction of the ataxia-telangiectasia cellular phenotype. *Proceedings of the National Academy of Sciences of the United States of America* 94(15):8021-8026.

67. Gilad S, *et al.* (1996) Predominance of Null Mutations in Ataxia-Telangiectasia. *Human Molecular Genetics* 5(4):433-439.

68. Shiloh Y (1995) Ataxia-telangiectasia: closer to unraveling the mystery. *European journal of human genetics : EJHG* 3(2):116-138.

69. FitzGerald MG, *et al.* (1997) Heterozygous ATM mutations do not contribute to early onset of breast cancer. *Nature genetics* 15(3):307-310.

70. Lu XH, *et al.* (2014) Targeting ATM ameliorates mutant Huntingtin toxicity in cell and animal models of Huntington's disease. *Science translational medicine* 6(268):268ra178.

71. Barlow C, *et al.* (1996) Atm-deficient mice: a paradigm of ataxia telangiectasia. *Cell* 86(1):159-171.

72. Yamamoto K, *et al.* (2012) Kinase-dead ATM protein causes genomic instability and early embryonic lethality in mice. *The Journal of cell biology* 198(3):305-313.

73. Daniel JA, *et al.* (2012) Loss of ATM kinase activity leads to embryonic lethality in mice. *The Journal of cell biology* 198(3):295-304.

74. White JS, Choi S, & Bakkenist CJ (2010) Transient ATM Kinase Inhibition Disrupts DNA Damage–Induced Sister Chromatid Exchange. *Science Signaling* 3(124):ra44-ra44.

75. Alexander A & Walker CL (2010) Differential localization of ATM is correlated with activation of distinct downstream signaling pathways. *Cell cycle* 9(18):3685-3686.

76. Yang D-Q & Kastan MB (2000) Participation of ATM in insulin signalling through phosphorylation of eIF-4E-binding protein 1. *Nature cell biology* 2(12):893-898.

77. Bencokova Z, *et al.* (2009) ATM Activation and Signaling under Hypoxic Conditions. *Molecular and cellular biology* 29(2):526-537.

78. Guo Z, Kozlov S, Lavin MF, Person MD, & Paull TT (2010) ATM activation by oxidative stress. *Science* 330(6003):517-521.

79. Alexander A, *et al.* (2010) ATM signals to TSC2 in the cytoplasm to regulate mTORC1 in response to ROS. *Proceedings of the National Academy of Sciences* 107(9):4153-4158.

80. Valentin-Vega YA, *et al.* (2011) Mitochondrial dysfunction in ataxia-telangiectasia. *Blood* 119(6):1490-1500.

81. Oricchio E, Saladino C, Iacovelli S, Soddu S, & Cundari E (2005) ATM is Activated by Default in Mitosis, Localizes at Centrosomes and Monitors Mitotic Spindle Integrity. *Cell cycle* 5(1):88-92.

82. Watters D, *et al.* (1999) Localization of a portion of extranuclear ATM to peroxisomes. *The Journal of biological chemistry* 274(48):34277-34282.

83. Lim D-S, *et al.* (1998) ATM binds to β-adaptin in cytoplasmic vesicles. *Proceedings of the National Academy of Sciences* 95(17):10146-10151.

84. Aging NIo (Why Population Aging Matters: A Global Perspective.

85. Hayflick L & Moorhead PS (1961) The serial cultivation of human diploid cell strains. *Experimental cell research* 25:585-621.

86. Campisi J & di Fagagna FD (2007) Cellular senescence: when bad things happen to good cells. *Nat Rev Mol Cell Bio* 8(9):729-740.

87. van Deursen JM (2014) The role of senescent cells in ageing. *Nature* 509(7501):439-446.

88. Storer M, *et al.* (2013) Senescence is a developmental mechanism that contributes to embryonic growth and patterning. *Cell* 155(5):1119-1130.

89. Baker DJ, *et al.* (2011) Clearance of $p16^{Ink4a}$-positive senescent cells delays ageing-associated disorders. *Nature* 479(7372):232-236.

90. Zhu Y, *et al.* (2015) The Achilles' heel of senescent cells: from transcriptome to senolytic drugs. *Aging cell* 14(4):644-658.

91. Harley CB, Futcher AB, & Greider CW (1990) Telomeres shorten during ageing of human fibroblasts. *Nature* 345(6274):458-460.

92. Wright WE, Piatyszek MA, Rainey WE, Byrd W, & Shay JW (1996) Telomerase activity in human germline and embryonic tissues and cells. *Developmental genetics* 18(2):173-179.

93. Bodnar AG, *et al.* (1998) Extension of Life-Span by Introduction of Telomerase into Normal Human Cells. *Science* 279(5349):349-352.

94. Jaskelioff M, *et al.* (2011) Telomerase reactivation reverses tissue degeneration in aged telomerase-deficient mice. *Nature* 469(7328):102-106.

95. Takai H, Smogorzewska A, & de Lange T (2003) DNA damage foci at dysfunctional telomeres. *Current biology : CB* 13(17):1549-1556.

96. Collado M, Blasco MA, & Serrano M (2007) Cellular senescence in cancer and aging. *Cell* 130(2):223-233.

97. de Lange T (2005) Shelterin: the protein complex that shapes and safeguards human telomeres. *Genes & development* 19(18):2100-2110.

98. Fagagna FdAd, *et al.* (2003) A DNA damage checkpoint response in telomere-initiated senescence. *Nature* 426(6963):194-198.

99. Rodier F, *et al.* (2009) Persistent DNA damage signalling triggers senescence-associated inflammatory cytokine secretion. *Nature cell biology* 11(8):973-979.

100. Serrano M, Lin AW, McCurrach ME, Beach D, & Lowe SW (1997) Oncogenic ras Provokes Premature Cell Senescence Associated with Accumulation of p53 and p16INK4a. *Cell* 88(5):593-602.

101. Di Micco R, *et al.* (2006) Oncogene-induced senescence is a DNA damage response triggered by DNA hyper-replication. *Nature* 444(7119):638-642.

102. Kaplon J, *et al.* (2013) A key role for mitochondrial gatekeeper pyruvate dehydrogenase in oncogene-induced senescence. *Nature* 498(7452):109-112.

103. Denchi EL, Attwooll C, Pasini D, & Helin K (2005) Deregulated E2F Activity Induces Hyperplasia and Senescence-Like Features in the Mouse Pituitary Gland. *Molecular and cellular biology* 25(7):2660-2672.

104. Nardella C, Clohessy JG, Alimonti A, & Pandolfi PP (2011) Pro-senescence therapy for cancer treatment. *Nature reviews. Cancer* 11(7):503-511.

105. Shamma A, *et al.* (2009) Rb Regulates DNA Damage Response and Cellular Senescence through E2F-Dependent Suppression of N-Ras Isoprenylation. *Cancer cell* 15(4):255-269.

106. Harman D (1992) Free radical theory of aging. *Mutation Research/DNAging* 275(3):257-266.

107. Parrinello S, *et al.* (2003) Oxygen sensitivity severely limits the replicative lifespan of murine fibroblasts. *Nature cell biology* 5(8):741-747.

108. Moiseeva O, Bourdeau V, Roux A, Deschênes-Simard X, & Ferbeyre G (2009) Mitochondrial Dysfunction Contributes to Oncogene-Induced Senescence. *Molecular and cellular biology* 29(16):4495-4507.

109. Ziegler DV, Wiley CD, & Velarde MC (2015) Mitochondrial effectors of cellular senescence: beyond the free radical theory of aging. *Aging cell* 14(1):1-7.

110. Chen QM, *et al.* (1998) Molecular analysis of H2O2-induced senescent-like growth arrest in normal human fibroblasts: p53 and Rb control G1 arrest but not cell replication. *Biochemical Journal* 332(Pt 1):43-50.

111. Colavitti R & Finkel T (2005) Reactive Oxygen Species as Mediators of Cellular Senescence. *IUBMB Life* 57(4-5):277-281.

112. Dimri GP, *et al.* (1995) A biomarker that identifies senescent human cells in culture and in aging skin in vivo. *Proceedings of the National Academy of Sciences of the United States of America* 92(20):9363-9367.

113. Kurz DJ, Decary S, Hong Y, & Erusalimsky JD (2000) Senescence-associated (beta)-galactosidase reflects an increase in lysosomal mass during replicative ageing of human endothelial cells. *Journal of cell science* 113(20):3613-3622.

114. Debacq-Chainiaux F, Erusalimsky JD, Campisi J, & Toussaint O (2009) Protocols to detect senescence-associated beta-galactosidase (SA-betagal) activity, a biomarker of senescent cells in culture and in vivo. *Nature protocols* 4(12):1798-1806.

115. Dimri GP, *et al.* (1995) A biomarker that identifies senescent human cells in culture and in aging skin in vivo. *Proceedings of the National Academy of Sciences of the United States of America* 92(20):9363-9367.

116. Lee BY, *et al.* (2006) Senescence-associated β-galactosidase is lysosomal β-galactosidase. *Aging cell* 5(2):187-195.

117. Kamijo T, *et al.* (1998) Functional and physical interactions of the ARF tumor suppressor with p53 and Mdm2. *Proceedings of the National Academy of Sciences of the United States of America* 95(14):8292-8297.

118. Zhang Y, Xiong Y, & Yarbrough WG (1998) ARF Promotes MDM2 Degradation and Stabilizes p53: ARF-INK4a Locus Deletion Impairs Both the Rb and p53 Tumor Suppression Pathways. *Cell* 92(6):725-734.

119. Pomerantz J, *et al.* (1998) The Ink4a Tumor Suppressor Gene Product, p19Arf, Interacts with MDM2 and Neutralizes MDM2's Inhibition of p53. *Cell* 92(6):713-723.

120. Baker DJ, Jin F, & van Deursen JM (2008) The yin and yang of the Cdkn2a locus in senescence and aging. *Cell cycle* 7(18):2795-2802.

121. Baker DJ, *et al.* (2008) Opposing roles for p16Ink4a and p19Arf in senescence and ageing caused by BubR1 insufficiency. *Nature cell biology* 10(7):825-836.

122. Baker DJ, *et al.* (2011) Clearance of p16Ink4a-positive senescent cells delays ageing-associated disorders. *Nature* 479(7372):232-236.

123. Gartel AL & Radhakrishnan SK (2005) Lost in Transcription: p21 Repression, Mechanisms, and Consequences. *Cancer research* 65(10):3980-3985.

124. Di Leonardo A, Linke SP, Clarkin K, & Wahl GM (1994) DNA damage triggers a prolonged p53-dependent G1 arrest and long-term induction of Cip1 in normal human fibroblasts. *Genes & development* 8(21):2540-2551.

125. Stein GH, Drullinger LF, Soulard A, & Dulić V (1999) Differential Roles for Cyclin-Dependent Kinase Inhibitors p21 and p16 in the Mechanisms of Senescence and Differentiation in Human Fibroblasts. *Molecular and cellular biology* 19(3):2109-2117.

126. Choudhury AR, *et al.* (2007) Cdkn1a deletion improves stem cell function and lifespan of mice with dysfunctional telomeres without accelerating cancer formation. *Nature genetics* 39(1):99-105.

127. Abbas T & Dutta A (2009) p21 in cancer: intricate networks and multiple activities. *Nature reviews. Cancer* 9(6):400-414.

128. Carnero A (2013) Markers of cellular senescence. *Methods in molecular biology* 965:63-81.

129. Coppe JP, Desprez PY, Krtolica A, & Campisi J (2010) The senescence-associated secretory phenotype: the dark side of tumor suppression. *Annual review of pathology* 5:99-118.

130. Bernardes de Jesus B & Blasco MA (2012) Assessing cell and organ senescence biomarkers. *Circulation research* 111(1):97-109.

131. Benhamed M, Herbig U, Ye T, Dejean A, & Bischof O (2012) Senescence is an endogenous trigger for microRNA-directed transcriptional gene silencing in human cells. *Nature cell biology* 14(3):266-275.

132. Kuilman T & Peeper DS (2009) Senescence-messaging secretome: SMS-ing cellular stress. *Nature reviews. Cancer* 9(2):81-94.

133. Korhonen P, Helenius M, & Salminen A (1997) Age-related changes in the regulation of transcription factor NF-κB in rat brain. *Neuroscience letters* 225(1):61-64.

134. Brégégère F, Milner Y, & Friguet B (2006) The ubiquitin–proteasome system at the crossroads of stress-response and ageing pathways: A handle for skin care? *Ageing research reviews* 5(1):60-90.

135. Helenius M, Hanninen M, Lehtinen SK, & Salminen A (1996) Changes associated with aging and replicative senescence in the regulation of transcription factor nuclear factor-kappa B. *Biochem. J* 318:603-608.

136. Adler AS, *et al.* (2007) Motif module map reveals enforcement of aging by continual NF-κB activity. *Genes & development* 21(24):3244-3257.

137. Tilstra JS, *et al.* (2012) NF-kappaB inhibition delays DNA damage-induced senescence and aging in mice. *The Journal of clinical investigation* 122(7):2601-2612.

138. Osorio FG, *et al.* (2012) Nuclear lamina defects cause ATM-dependent NF-kappaB activation and link accelerated aging to a systemic inflammatory response. *Genes & development* 26(20):2311-2324.

139. Zhang G, *et al.* (2013) Hypothalamic programming of systemic ageing involving IKK-[bgr], NF-[kgr]B and GnRH. *Nature* 497(7448):211-216.

140. Tilstra JS, Clauson CL, Niedernhofer LJ, & Robbins PD (2011) NF-kappaB in Aging and Disease. *Aging and disease* 2(6):449-465.

141. Bernal GM, *et al.* (2014) Loss of Nfkb1 leads to early onset aging. *Aging* 6(11):931-943.

142. Oakley F, *et al.* (2005) Nuclear Factor-κB1 (p50) Limits the Inflammatory and Fibrogenic Responses to Chronic Injury. *The American journal of pathology* 166(3):695-708.

143. Jurk D, *et al.* (2014) Chronic inflammation induces telomere dysfunction and accelerates ageing in mice. *Nature communications* 2:4172.

144. Acosta JC, *et al.* (2008) Chemokine signaling via the CXCR2 receptor reinforces senescence. *Cell* 133(6):1006-1018.

145. Kuilman T, *et al.* (2008) Oncogene-induced senescence relayed by an interleukin-dependent inflammatory network. *Cell* 133(6):1019-1031.

146. Chien Y, *et al.* (2011) Control of the senescence-associated secretory phenotype by NF-kappaB promotes senescence and enhances chemosensitivity. *Genes & development* 25(20):2125-2136.

147. Krtolica A, Parrinello S, Lockett S, Desprez PY, & Campisi J (2001) Senescent fibroblasts promote epithelial cell growth and tumorigenesis: a link between cancer and aging. *Proceedings of the National Academy of Sciences of the United States of America* 98(21):12072-12077.

148. Helenius M, Kyrylenko S, Vehvilainen P, & Salminen A (2001) Characterization of aging-associated up-regulation of constitutive nuclear factor-kappa B binding activity. *Antioxidants & redox signaling* 3(1):147-156.

149. Salminen A, *et al.* (2008) Activation of innate immunity system during aging: NF-kB signaling is the molecular culprit of inflamm-aging. *Ageing Research Reviews* 7(2):83-105.

150. Gregg SQ, Robinson AR, & Niedernhofer LJ (2011) Physiological consequences of defects in ERCC1-XPF DNA repair endonuclease. *DNA repair* 10(7):781-791.

151. Niedernhofer LJ, *et al.* (2004) The structure-specific endonuclease Ercc1-Xpf is required to resolve DNA interstrand cross-link-induced double-strand breaks. *Molecular and cellular biology* 24(13):5776-5787.

152. Gurkar AU & Niedernhofer LJ (2015) Comparison of mice with accelerated aging caused by distinct mechanisms. *Experimental gerontology* 68:43-50.

153. Jaspers NG, *et al.* (2007) First reported patient with human ERCC1 deficiency has cerebro-oculo-facio-skeletal syndrome with a mild defect in nucleotide excision repair and severe developmental failure. *American journal of human genetics* 80(3):457-466.

154. Kashiyama K, *et al.* (Malfunction of Nuclease ERCC1-XPF Results in Diverse Clinical Manifestations and Causes Cockayne Syndrome, Xeroderma Pigmentosum, and Fanconi Anemia. *The American Journal of Human Genetics* 92(5):807-819.

155. McWhir I, Selfridgel I, Harrisonz DI, Squires S, & Melton DW (1993) Mice with DNA repair gene (ERCC-1) deficiency have elevated levels of. *Nature genetics* 5.

156. de Vries A, *et al.* (1995) Increased susceptibility to ultraviolet-B and carcinogens of mice lacking the DNA excision repair gene XPA.

157. Dollé MET, *et al.* (2006) Increased genomic instability is not a prerequisite for shortened lifespan in DNA repair deficient mice. *Mutation Research/Fundamental and Molecular Mechanisms of Mutagenesis* 596(1):22-35.

158. Paul C, *et al.* (2007) Deletion of genes implicated in protecting the integrity of male germ cells has differential effects on the incidence of DNA breaks and germ cell loss. *PloS one* 2(10):e989.

159. Hsia K-T, *et al.* (2003) DNA repair gene Ercc1 is essential for normal spermatogenesis and oogenesis and for functional integrity of germ cell DNA in the mouse. *Development* 130(2):369-378.

160. Lavasani M, *et al.* (2012) Muscle-derived stem/progenitor cell dysfunction limits healthspan and lifespan in a murine progeria model. *Nature communications* 3:608.

161. Dollé MET, *et al.* (2011) Broad segmental progeroid changes in short-lived Ercc1−/Δ7 mice. *Pathobiology of aging & age related diseases* 1.

162. Vo N, *et al.* (2010) Accelerated aging of intervertebral discs in a mouse model of progeria. *Journal of Orthopaedic Research* 28(12):1600-1607.

163. Chen Q, *et al.* (2013) DNA damage drives accelerated bone aging via an NF-κB–dependent mechanism. *Journal of Bone and Mineral Research* 28(5):1214-1228.

164. Kirkwood TB (2005) Understanding the odd science of aging. *Cell* 120(4):437-447.

165. Acosta JC, *et al.* (2013) A complex secretory program orchestrated by the inflammasome controls paracrine senescence. *Nature cell biology* 15(8):978-990.

166. Nelson G, *et al.* (2012) A senescent cell bystander effect: senescence-induced senescence. *Aging cell* 11(2):345-349.

167. Uziel T, *et al.* (2003) Requirement of the MRN complex for ATM activation by DNA damage. *The EMBO journal* 22(20):5612-5621.

168. Lee JH & Paull TT (2004) Direct activation of the ATM protein kinase by the Mre11/Rad50/Nbs1 complex. *Science* 304(5667):93-96.

169. Lee JH & Paull TT (2005) ATM activation by DNA double-strand breaks through the Mre11-Rad50-Nbs1 complex. *Science* 308(5721):551-554.

170. Soutoglou E & Misteli T (2008) Activation of the cellular DNA damage response in the absence of DNA lesions. *Science* 320(5882):1507-1510.

171. Lee SJ, Dimtchev A, Lavin MF, Dritschilo A, & Jung M (1998) A novel ionizing radiation-induced signaling pathway that activates the transcription factor NF-kappaB. *Oncogene* 17(14):1821-1826.

172. McCool KW & Miyamoto S (2012) DNA damage‐dependent NF‐κB activation: NEMO turns nuclear signaling inside out. *Immunological reviews* 246(1):311-326.

173. Oakley F, *et al.* (2005) Nuclear factor-kappaB1 (p50) limits the inflammatory and fibrogenic responses to chronic injury. *The American journal of pathology* 166(3):695-708.

174. Lu ZY, Yu SP, Wei JF, & Wei L (2006) Age-related neural degeneration in nuclear-factor kappaB p50 knockout mice. *Neuroscience* 139(3):965-978.

175. Chung HY, *et al.* (2009) Molecular inflammation: Underpinnings of aging and age-related diseases. *Ageing Research Reviews* 8(1):18-30.

176. Coppe JP, *et al.* (2011) Tumor suppressor and aging biomarker p16(INK4a) induces cellular senescence without the associated inflammatory secretory phenotype. *The Journal of biological chemistry* 286(42):36396-36403.

177. Karakasilioti I, *et al.* (2013) DNA damage triggers a chronic autoinflammatory response, leading to fat depletion in NER progeria. *Cell metabolism* 18(3):403-415.

178. Sedelnikova OA, *et al.* (2004) Senescing human cells and ageing mice accumulate DNA lesions with unrepairable double-strand breaks. *Nature cell biology* 6(2):168-170.

179. Hickson I, *et al.* (2004) Identification and characterization of a novel and specific inhibitor of the ataxia-telangiectasia mutated kinase ATM. *Cancer research* 64(24):9152-9159.

180. Beg AA, Sha WC, Bronson RT, Ghosh S, & Baltimore D (1995) Embryonic lethality and liver degeneration in mice lacking the RelA component of NF-kappa B. *Nature* 376(6536):167-170.

181. Hertlein E, Wang J, Ladner KJ, Bakkar N, & Guttridge DC (2005) RelA/p65 regulation of IkappaBbeta. *Molecular and cellular biology* 25(12):4956-4968.

182. Lieu CA, Chinta SJ, Rane A, & Andersen JK (2013) Age-related behavioral phenotype of an astrocytic monoamine oxidase-B transgenic mouse model of Parkinson's disease. *PloS one* 8(1):e54200.

183. Weinstein JR & Anderson S (2010) THE AGING KIDNEY: PHYSIOLOGICAL CHANGES. *Advances in chronic kidney disease* 17(4):302-307.

184. Sharpless NE & DePinho RA (2007) How stem cells age and why this makes us grow old. *Nature reviews. Molecular cell biology* 8(9):703-713.

185. Vo N, *et al.* (2010) Accelerated aging of intervertebral discs in a mouse model of progeria. *Journal of orthopaedic research : official publication of the Orthopaedic Research Society* 28(12):1600-1607.

186. Urban JP & Winlove CP (2007) Pathophysiology of the intervertebral disc and the challenges for MRI. *Journal of magnetic resonance imaging : JMRI* 25(2):419-432.

187. Saar G, *et al.* (2012) Assessment of glycosaminoglycan concentration changes in the intervertebral disc via chemical exchange saturation transfer. *NMR in biomedicine* 25(2):255-261.

188. Guerin HAL & Elliott DM (2006) Chapter 3 - Structure and Properties of Soft Tissues in the Spine. *Spine Technology Handbook*, eds Kurtz SM & Edidin AA (Academic Press, Burlington), pp 35-62.

189. Hasty P, Campisi J, Hoeijmakers J, van Steeg H, & Vijg J (2003) Aging and genome maintenance: lessons from the mouse? *Science* 299(5611):1355-1359.

190. Biton S & Ashkenazi A (2011) NEMO and RIP1 Control Cell Fate in Response to Extensive DNA Damage via TNF-α Feedforward Signaling. *Cell* 145(1):92-103.

191. Kang C, *et al.* (2015) The DNA damage response induces inflammation and senescence by inhibiting autophagy of GATA4. *Science* 349(6255):aaa5612.

192. Campisi J (2013) Aging, cellular senescence, and cancer. *Annual review of physiology* 75:685-705.

193. Hotamisligil GS, Shargill NS, & Spiegelman BM (1993) Adipose expression of tumor necrosis factor-alpha: direct role in obesity-linked insulin resistance. *Science* 259(5091):87-91.

194. Mackenzie IRA & Munoz DG (1998) Nonsteroidal anti-inflammatory drug use and Alzheimer-type pathology in aging. *Neurology* 50(4):986-990.

195. Bulckaen H, *et al.* (2008) Low-dose aspirin prevents age-related endothelial dysfunction in a mouse model of physiological aging. *American Journal of Physiology-Heart and Circulatory Physiology* 294(4):H1562-H1570.

196. Alarcón de la Lastra C & Villegas I (2005) Resveratrol as an anti‐inflammatory and anti‐aging agent: Mechanisms and clinical implications. *Molecular nutrition & food research* 49(5):405-430.

197. Anisimov VN, *et al.* (2008) Metformin slows down aging and extends life span of female SHR mice. *Cell cycle* 7(17):2769-2773.

198. Fontana L (2009) Neuroendocrine Factors in the Regulation of Inflammation: Excessive Adiposity and Calorie Restriction. *Experimental gerontology* 44(1-2):41-45.

199. Dixit VD (2008) Adipose-immune interactions during obesity and caloric restriction: reciprocal mechanisms regulating immunity and health span. *Journal of Leukocyte Biology* 84(4):882-892.

200. Kang TW, *et al.* (2011) Senescence surveillance of pre-malignant hepatocytes limits liver cancer development. *Nature* 479(7374):547-551.

201. Kirkland JL & Tchkonia T (2015) Clinical strategies and animal models for developing senolytic agents. *Experimental gerontology* 68:19-25.

202. Dalkilic I & Kunkel LM (2003) Muscular dystrophies: genes to pathogenesis. *Current Opinion in Genetics & Development* 13(3):231-238.

203. Mercuri E & Muntoni F (Muscular dystrophies. *The Lancet* 381(9869):845-860.

204. Cai D, *et al.* (2004) IKKβ/NF-κB Activation Causes Severe Muscle Wasting in Mice. *Cell* 119(2):285-298.

205. Kawai T & Akira S (2010) The role of pattern-recognition receptors in innate immunity: update on Toll-like receptors. *Nat Immunol* 11(5):373-384.

206. Ghosh S, Latimer RD, Gray BM, Harwood RJ, & Oduro A (1993) Endotoxin-induced organ injury. *Critical care medicine* 21(2 Suppl):S19-24.

207. Kabir K, *et al.* (2002) Characterization of a murine model of endotoxin-induced acute lung injury. *Shock* 17(4):300-303.

208. Jeyaseelan S, Chu HW, Young SK, & Worthen GS (2004) Transcriptional profiling of lipopolysaccharide-induced acute lung injury. *Infection and immunity* 72(12):7247-7256.

209. Reay DP, *et al.* (2011) Systemic delivery of NEMO binding domain/IKKgamma inhibitory peptide to young mdx mice improves dystrophic skeletal muscle histopathology. *Neurobiology of disease* 43(3):598-608.

210. Tas S, *et al.* (2006) Local treatment with the selective IkappaB kinase beta inhibitor NEMO-binding domain peptide ameliorates synovial inflammation. *Arthritis Research & Therapy* 8(4):R86.

211. Jimi E, *et al.* (2004) Selective inhibition of NF-kappa B blocks osteoclastogenesis and prevents inflammatory bone destruction in vivo. *Nature medicine* 10(6):617-624.

212. Oguiza A, *et al.* (2015) Peptide-based inhibition of IκB kinase/nuclear factor-κB pathway protects against diabetes-associated nephropathy and atherosclerosis in a mouse model of type 1 diabetes. *Diabetologia* 58(7):1656-1667.

213. Ankermann T, *et al.* (2005) Topical inhibition of nuclear factor-κB enhances reduction in lung edema by surfactant in a piglet model of airway lavage. *Critical Care Medicine* 33(6).

214. Mora AL, *et al.* (2005) Prevention of NF-κB activation in vivo by a cell-permeable NF-κB inhibitor peptide. *American Journal of Physiology - Lung Cellular and Molecular Physiology* 289(4):L536-L544.

215. Guttridge DC, Albanese C, Reuther JY, Pestell RG, & Baldwin AS (1999) NF-κB controls cell growth and differentiation through transcriptional regulation of cyclin D1. *Molecular and cellular biology* 19(8):5785-5799.

216. Chang MR, *et al.* (2015) Antiobesity Effect of a Small Molecule Repressor of RORγ. *Molecular Pharmacology* 88(1):48-56.

217. Wolber G, Dornhofer A, & Langer T (2006) Efficient overlay of small organic molecules using 3D pharmacophores. *J Comput Aided Mol Des* 20(12):773-788.

218. Wolber G & Langer T (2005) LigandScout: 3-D pharmacophores derived from protein-bound ligands and their use as virtual screening filters. *Journal of chemical information and modeling* 45(1):160-169.

219. Jain A (2000) Morphological similarity: A 3D molecular similarity method correlated with protein-ligand recognition. *J Comput Aided Mol Des* 14(2):199-213.

220. (ACD/Labs) (Advanced Chemistry Development, Inc. .

221. Wallqvist A, Huang R, Thanki N, & Covell DG (2006) Evaluating chemical structure similarity as an indicator of cellular growth inhibition. *Journal of chemical information and modeling* 46(1):430-437.

222. Martin YC, Kofron JL, & Traphagen LM (2002) Do structurally similar molecules have similar biological activity? *Journal of medicinal chemistry* 45(19):4350-4358.

223. Irwin JJ & Shoichet BK (2005) ZINC – A Free Database of Commercially Available Compounds for Virtual Screening. *Journal of chemical information and modeling* 45(1):177-182.

224. Reay DP, *et al.* (2011) Systemic delivery of NEMO binding domain/IKKγ inhibitory peptide to young mdx mice improves dystrophic skeletal muscle histopathology. *Neurobiology of Disease* 43(3):598-608.

225. Acharyya S, *et al.* (2007) Interplay of IKK/NF-κB signaling in macrophages and myofibers promotes muscle degeneration in Duchenne muscular dystrophy. *The Journal of clinical investigation* 117(4):889-901.

226. Baima ET, *et al.* (2010) Novel Insights into the Cellular Mechanisms of the Anti-inflammatory Effects of NF-κB Essential Modulator Binding Domain Peptides. *Journal of Biological Chemistry* 285(18):13498-13506.

227. Golden MS, *et al.* (2013) Comprehensive Experimental and Computational Analysis of Binding Energy Hot Spots at the NF-κB Essential Modulator/IKKβ Protein–Protein Interface. *Journal of the American Chemical Society* 135(16):6242-6256.

228. Chen L-W, *et al.* (2003) The two faces of IKK and NF-[kappa]B inhibition: prevention of systemic inflammation but increased local injury following intestinal ischemia-reperfusion. *Nature medicine* 9(5):575-581.

229. Trifilieff A, *et al.* (2000) Inducible Nitric Oxide Synthase Inhibitors Suppress Airway Inflammation in Mice Through Down-Regulation of Chemokine Expression. *The Journal of Immunology* 165(3):1526-1533.

230. Razavi HM, *et al.* (2004) Pulmonary Neutrophil Infiltration in Murine Sepsis. *American Journal of Respiratory and Critical Care Medicine* 170(3):227-233.

231. Xiong Y, Karupiah G, Hogan SP, Foster PS, & Ramsay AJ (1999) Inhibition of Allergic Airway Inflammation in Mice Lacking Nitric Oxide Synthase 2. *The Journal of Immunology* 162(1):445-452.

232. Karupiah G, Chen J-H, Mahalingam S, Nathan CF, & MacMicking JD (1998) Rapid Interferon γ–dependent Clearance of Influenza A Virus and Protection from Consolidating Pneumonitis in Nitric Oxide Synthase 2–deficient Mice. *The Journal of experimental medicine* 188(8):1541-1546.

233. Kristof AS, Goldberg P, Laubach V, & Hussain SNA (1998) Role of Inducible Nitric Oxide Synthase in Endotoxin-induced Acute Lung Injury. *American Journal of Respiratory and Critical Care Medicine* 158(6):1883-1889.

234. Okamoto T, *et al.* (2003) Multiple contributing roles for NOS2 in LPS-induced acute airway inflammation in mice. *American Journal of Physiology - Lung Cellular and Molecular Physiology* 286(1):L198-L209.

235. Freund A, Patil CK, & Campisi J (2011) p38MAPK is a novel DNA damage response-independent regulator of the senescence-associated secretory phenotype. *The EMBO journal* 30(8):1536-1548.

236. Peinado JR, *et al.* (2011) Proteomic Profiling of Adipose Tissue from Zmpste24−/− Mice, a Model of Lipodystrophy and Premature Aging, Reveals Major Changes in Mitochondrial Function and Vimentin Processing. *Molecular & Cellular Proteomics* 10(11).

237. Tinsley FC, Taicher GZ, & Heiman ML (2004) Evaluation of a Quantitative Magnetic Resonance Method for Mouse Whole Body Composition Analysis. *Obesity Research* 12(1):150-160.

238. El-Haschimi K, *et al.* (2003) Insulin Resistance and Lipodystrophy in Mice Lacking Ribosomal S6 Kinase 2. *Diabetes* 52(6):1340-1346.

239. Gavrilova O, Marcus-Samuels B, Leon LR, Vinson C, & Reitman ML (2000) Hormones: Leptin and diabetes in lipoatrophic mice. *Nature* 403(6772):850-850.

240. Shimomura I, Hammer RE, Ikemoto S, Brown MS, & Goldstein JL (1999) Leptin reverses insulin resistance and diabetes mellitus in mice with congenital lipodystrophy. *Nature* 401(6748):73-76.

241. Kawahara TLA, *et al.* (2009) SIRT6 links histone H3 lysine 9 deacetylation to control of NF-κB dependent gene expression and organismal lifespan. *Cell* 136(1):62-74.

242. Aggarwal BB & Harikumar KB (2009) Potential therapeutic effects of curcumin, the anti-inflammatory agent, against neurodegenerative, cardiovascular, pulmonary, metabolic, autoimmune and neoplastic diseases. *The international journal of biochemistry & cell biology* 41(1):40-59.

243. Hu MCT, *et al.* (IκB Kinase Promotes Tumorigenesis through Inhibition of Forkhead FOXO3a. *Cell* 117(2):225-237.

244. Lee D-F, *et al.* (2007) IKKβ Suppression of TSC1 Links Inflammation and Tumor Angiogenesis via the mTOR Pathway. *Cell* 130(3):440-455.

245. Selman C, *et al.* (2009) Ribosomal protein S6 kinase 1 signaling regulates mammalian life span. *Science* 326(5949):140-144.

246. Selman C, *et al.* (2008) Evidence for lifespan extension and delayed age-related biomarkers in insulin receptor substrate 1 null mice. *The FASEB Journal* 22(3):807-818.

247. Tchkonia T, *et al.* (2010) Fat tissue, aging, and cellular senescence. *Aging cell* 9(5):667-684.

248. Tsai W-B, Chung YM, Takahashi Y, Xu Z, & Hu MCT (2008) Functional interaction between FOXO3a and ATM regulates DNA damage response. *Nature cell biology* 10(4):460-467.

249. Tchkonia T, *et al.* (Cellular senescence and inflammation in obesity. (NATURE PUBLISHING GROUP 75 VARICK ST, 9TH FLR, NEW YORK, NY 10013-1917 USA), pp S57-S57.

250. Caron-Debarle M, Lagathu C, Boccara F, Vigouroux C, & Capeau J (2010) HIV-associated lipodystrophy: from fat injury to premature aging. *Trends in molecular medicine* 16(5):218-229.

251. Gregg SQ, *et al.* (2012) A mouse model of accelerated liver aging caused by a defect in DNA repair. *Hepatology* 55(2):609-621.

252. Kim JK (Fat uses a TOLL-road to connect inflammation and diabetes. *Cell metabolism* 4(6):417-419.

253. Spiegelman BM & Hotamisligil GS (Through thick and thin: Wasting, obesity, and TNFα. *Cell* 73(4):625-627.

254. Cai D, *et al.* (2005) Local and systemic insulin resistance resulting from hepatic activation of IKK-beta and NF-kappaB. *Nature medicine* 11(2):183-190.

255. Xu Y, Yang EM, Brugarolas J, Jacks T, & Baltimore D (1998) Involvement of p53 and p21 in cellular defects and tumorigenesis in Atm−/− mice. *Molecular and cellular biology* 18(7):4385-4390.

256. Barzilai A, Rotman G, & Shiloh Y (2002) ATM deficiency and oxidative stress: a new dimension of defective response to DNA damage. *DNA repair* 1(1):3-25.

257. Meredith MJ & Dodson ML (1987) Impaired glutathione biosynthesis in cultured human ataxia-telangiectasia cells. *Cancer research* 47(17):4576-4581.

258. Quick KL & Dugan LL (2001) Superoxide stress identifies neurons at risk in a model of ataxia‐telangiectasia. *Annals of neurology* 49(5):627-635.

259. Watters D, *et al.* (1999) Localization of a portion of extranuclear ATM to peroxisomes. *Journal of Biological Chemistry* 274(48):34277-34282.

260. Kamsler A, *et al.* (2001) Increased oxidative stress in ataxia telangiectasia evidenced by alterations in redox state of brains from Atm-deficient mice. *Cancer research* 61(5):1849-1854.

261. Palikaras K & Tavernarakis N (2012) Mitophagy in neurodegeneration and aging. *Frontiers in Genetics* 3:297.

262. Huang TT, Wuerzberger-Davis SM, Wu Z-H, & Miyamoto S (2003) Sequential Modification of NEMO/IKKγ by SUMO-1 and Ubiquitin Mediates NF-κB Activation by Genotoxic Stress. *Cell* 115(5):565-576.